Dendrimer based Chelating Agents for Removal of Radionuclides from Aqueous Medium

By

P. ILAIYARAJA
(CHEM02200804007)

Indira Gandhi Centre for Atomic Research
Kalpakkam

A thesis submitted to the
Board of Studies in Chemical Sciences
In partial fulfillment of requirements
For the Degree of

DOCTOR OF PHILOSOPHY
of
Homi Bhabha National Institute

November, 2013

Homi Bhabha National Institute

Recommendations of the Viva Voce Board

As members of the Viva Voce Board, we certify that we have read the dissertation prepared by **Mr. P. ILAIYARAJA** entitled **“Dendrimer based Chelating Agents for Removal of Radionuclides from Aqueous Medium”** and recommend that it may be accepted as fulfilling the dissertation requirement for the Degree of Doctor of Philosophy.

______________________ **Date:** 11.7.14

Chairman – **Dr. T. G. Srinivasan**

D. Po______________________ **Date:** 11.7.2014

Guide / Convener – **Dr. D. Ponraju**

______________________ **Date:** 11.7.14

External Examiner – **Prof. R.V. Jayaram**

______________________ **Date:** 11.07.2014

Member 1 – **Dr. B. Venkatraman**

______________________ **Date:** 11-7-14

Member 2 – **Dr. M. Saibaba**

CMallika______________________ **Date:** 11.07.14

Member 3 – **Dr. C. Mallika**

Final approval and acceptance of this dissertation is contingent upon the candidate’s submission of the final copies of the dissertation to HBNI.

I hereby certify that I have read this dissertation prepared under my direction and recommend that it may be accepted as fulfilling the dissertation requirement.

D. Po 11/7/14.

Guide/Convener- Dr. D. Ponraju

Date: 11.7.2014

Place: Kalpakkam

STATEMENT BY AUTHOR

This dissertation has been submitted in partial fulfillment of requirements for an advanced degree at Homi Bhabha National Institute (HBNI) and is deposited in the Library to be made available to borrowers under rules of the HBNI.

Brief quotations from this dissertation are allowable without special permission, provided that accurate acknowledgement of source is made. Requests for permission for extended quotation from or reproduction of this manuscript in whole or in part may be granted by the Competent Authority of HBNI when in his or her judgment the proposed use of the material is in the interests of scholarship. In all other instances, however, permission must be obtained from the author.

P. Ilaiyaraja

(P. Ilaiyaraja)

DECLARATION

I, hereby declare that the investigation presented in this thesis entitled "**Dendrimer based Chelating Agents for Removal of Radionuclides from Aqueous Medium**" submitted to **Homi Bhabha National Institute (HBNI)**, Mumbai, India for the award of **Doctor of Philosophy** in **Chemical Sciences** is the record of work has been carried out by me under the guidance of **Dr. D. Ponraju**. The work is original and has not been submitted earlier as a whole or in part for a degree /diploma at this or any other Institution/ University.

P. Ilaiyaraja

(P. Ilaiyaraja)

PUBLICATIONS

INTERNATIONAL JOURNAL PUBLICATIONS

1. Removal of thorium from aqueous solution by adsorption using PAMAM dendron-functionalized styrene divinyl benzene, **P. Ilaiyaraja,** Ashish Kumar Singha Deb, K. Siva Subramanian, D. Ponraju, B. Venkatraman, **J. Radioanal. Nucl. Chem. 2013, 297, 59–69**.
2. Adsorption of uranium from aqueous solution by PAMAM dendron functionalized styrene divinylbenzene, **P. Ilaiyaraja,** Ashish Kumar Singha Deb, K. Siva Subramanian, D. Ponraju, B. Venkatraman, **J. Hazard. Mater., 2013, 250– 251, 155– 166**.
3. Removal of cobalt from aqueous solution by chemical precipitation using Xanthate Functionalized Dendrimer, **P. Ilaiyaraja,** Ashish Kumar Singha Deb, D. Ponraju, B. Venkatraman **Desalin. Water Treat. doi: 10.1080/19443994.2013.808454 (2013) 1-8.**
4. Xanthate Functionalized Dendrimer Chelating Ligand for Decontamination of Radionuclides from Aqueous Waste, **P. Ilaiyaraja,** Ashish Kumar Singha Deb, A. Kumaresan, S. Bera, D. Ponraju, B. Venkatraman, P. Chellapandi, **J. Hazard. Mater.** (Communicated).
5. Removal of uranium and thorium from aqueous solution by Ultrafiltration and Dendrimer Assisted Ultrafiltration (DAUF), **P. Ilaiyaraja,** Ashish Kumar Singha Deb, D. Ponraju, **J. Radioanal. Nucl. Chem.** (Revised Manuscript under review).
6. DGA-functionalised PAMAM dendron- styrene divinyl benzene chelating resin for preconcentration of uranium and thorium from aqueous and nitric acid medium, **P. Ilaiyaraja,** Ashish Kumar Singha Deb, D. Ponraju, **Chem. Eng. J.** (communicated)

INTERNATIONAL/NATIONAL CONFERENCES

1. **P. Ilaiyaraja,** Ashish Kumar Singha Deb, D. Ponraju, Synthesis and characterization of PAMAM Dendrimer and its application in uranium extraction, International conference on Nanoscience and Nanotechnology (ICONN), p. 137, Feb. 24-26, 2010, Tamil Nadu, India.
2. **P. Ilaiyaraja,** Ashish Kumar Singha Deb, D. Ponraju, Recovery of uranium using polyamidoamine (PAMAM) dendrimer from aqueous solution, Symposium on Emerging Trends in Separation Science and Technology (SESTEC), March 1-4, 2010, Kalpakkam, India.
3. **P. Ilaiyaraja,** Ashish Kumar Singha Deb, D. Ponraju, Removal of europium from aqueous liquid waste by xanthate functionalized dendrimer, Nuclear and Radiochemistry Symposium (NUCAR), p. 497, February 22-26, 2011, Visakhapatnam, India.
4. **P. Ilaiyaraja,** Ashish Kumar Singha Deb, D. Ponraju, B. Venkatraman, Dendrimer as an extractant for removal of radioactive metal ion from aqueous solution, Chemistry Research Scholar meet (CRSM), July 14-15, 2011, IGCAR, Kalpakkam, India.
5. **P. Ilaiyaraja,** Ashish Kumar Singha Deb, D. Ponraju, Removal of Co^{2+} from aqueous solution by chemical precipitation using xanthate functionalized dendrimer, Symposium on Emerging Trends in Separation Science and Technology (SESTEC), p-140, February 27 – March 1, 2012, Mumbai, India.
6. **P. Ilaiyaraja,** Ashish Kumar Singha Deb, D. Ponraju and B. venkatraman, PAMAM dendrimer for removal of heavy metal ions from aqueous waste, Interdisciplinary Symposium on Materials Chemistry (ISMC), P. 507, Dec.11-15, 2012, Mumbai, India.
7. **P. Ilaiyaraja,** Ashish Kumar Singha Deb, D. Ponraju, B. Venkatraman, Adsorption of thorium form aqueous solution by PAMAM dendron grafted chelating resin, Nuclear and Radiochemistry Symposium (NUCAR), p-409, Feb.19-23, 2013, Madhya Pradesh, India.

8. **P. Ilaiyaraja**, Ashish Kumar Singha Deb, K. Siva Subramanian, D. Ponraju, Diglycolamic acid functionalized PAMAM-SDB chelating resin for removal of Th(IV) from aqueous and nitric acid medium, SESTEC-2014, February 25-28, BARC, Mumbai.

AWARDS

BEST POSTER PRESENTATION AWARD

P. Ilaiyaraja, Ashish Kumar Singha Deb, D. Ponraju, Recovery of uranium using polyamidoamine (PAMAM) dendrimer from aqueous solution, Symposium on Emerging Trends in Separation Science and Technology (SESTEC), March 1-4, 2010, Kalpakkam, India.

P. Ilaiyaraja

(P. Ilaiyaraja)

Dedicated to my Parents

ACKNOWLEDGEMENT

I wish to express my sincere gratitude to my guide **Dr. D. Ponraju** for his invaluable guidance, keen interest, motivation, continuous support and valuable suggestions during my research work. His patience, enthusiasm, and immense knowledge helped me throughout the time of my research and writing thesis.

Words would be inadequate to express my sincere gratitude to **Prof. C.T. Vijayakumar**, Kamaraj College of Engineering and Technology, Virudhunagar who suggested this problem and familiarized me into this field through valuable discussions and constant encouragement.

I am very much grateful to my mentors **G. Thirumal**, Govt. Higher Secondary School, Melmalayanur, **Dr. Sophia**, St. Joseph Art and Science college Cuddalore, **Prof. N.Srimannarayanan**, School of Analytical Chemistry, University of Madras, **Prof.K.S. Viswanathan,** IISER, Mohali, **Dr. T.Gnanasekaran**, **Dr. N. Sivaraman**, Chemistry Group, IGCAR and **Dr. V. Ganesan**, Dean, HBNI (Chemical Sciences), IGCAR for their encouragement, motivation and excellent teaching which induced me to pursue this thesis.

My sincere thanks to my lab members **Dr. K. Sivasubramaniam**, **Mr. H. Krishnan, Mr. Ashish Kumar Singha Deb**, **Mr. B.N. Mohanty**, **Mr. Shailesh Joshi**, **Mr. T.K. Srinivasan** and **Mrs. Ramani Yuvaraj** for their kind help and wholehearted support.

It is my great privilege to acknowledge members of the doctoral committee: **Dr. T. G. Srinivasan** (Chairman), **Dr. B. Venkatraman** (Member), **Dr. M. Sai Baba** (Member) and **Dr. C. Mallika** (Member) for their critical review and valuable comments.

I would like to express my sincere thanks to Sophisticated Analytical Instrumentation Facilities (**SAIF)**, Centre for Nanoscienece and Nanotechnology**, IIT-Madras** for the NMR and MALDI-MS analysis. It is with sincere gratitude that I wish to thank **Dr. Kamruddin**, Material Science Group and **Swapan Kumar Mahato**, Chemistry Group for SEM-EDS analysis. I also want to thanks **Mrs. Annapoorni**, **Dr. Shankaran**, **Mrs. Uma Maheshwari**, for ICP-AES and AAS analysis. **Dr. R. Kumaresan** for helping in handling of radioactive sample, **Dr. M. Joseph** for mass spectrum analysis and **Mrs. Snehalatha,** SED for TGA analysis. I am pleased to thank **Mr. Akhilesh Joshi** and **Mr. Abdul Nishad,** Water and Steam Chemistry Division, BARCF, for turbidity analysis and ICP-AES analysis. My special thanks to **Mr. Arul, Mrs Shyamla**, **Mrs. Bakkiam**, **Miss. Swetha**, **Dr. M.T. Jose**, **Dr. Madhsoodanan**, **Mrs. Annalakshmi** and all the **Radiological Safety Division** members of IGCAR for their moral support during this work.

I take this opportunity to sincerely acknowledge **Indira Gandhi Centre for Atomic Research**, for providing financial assistance in the form of Junior and Senior Research Fellowships which buttressed me to perform my work comfortably. I thank the former and present Directors of IGCAR, **Dr. Baldev Raj**, **Mr. C.S.Chetal** and **Dr. P.R. Vasudeva Rao** for providing me accommodation, necessary infrastructure and resources to accomplish my research work.

I am very fortunate to have beloved batch mates, juniors and other friends: **Mr. D. Sri Maha Vishnu**, **Mr. D. Sharath**, **Mr. Jagadeesh Sure**, **Mr. K. Siva Srinivas**, **Dr. Jammu Ravi**, **Mr. M. Bubathi**, **Mr. Mariyappan**, **Mr. Naveena**, **Mr. Laxmoji**, **Mr. Pradeep Kumar**, **Mr. Sudhanshu**, **Mr. Herojit, Mrs. Debasmita**, **Dr. Maneesha**, **Dr. Priyada**, **Miss. Pravati swain**, **Miss. Priyadarshini**, **Miss K. Akila, Mr. Mahendaran**, **Miss. Anbu mozhi**, **Mr. Srinivasan**, **Mr. Shaswat**, **Mr. Benadict Rakesh**, **Mr. Karthik**, **Mr. Manas** who made my life cheerful during my stay at Kalpakkam.

I would like to express my sincere thanks to my friends **R. Karthik Raj, Udhaya Sankar, A. Dhanasekaran, Gopala Krishnan, Senthil Kumar, Karunanithi, Arunagiri, Sateesh Kumar and Dhamodharan** for their constant support and encouragement.

My deepest gratitude goes to my Father **D. Perumal**, Mother **P. Dhesammal**, Brother **P. Sridhar**, Sister-in-law **R. Usha**, Sister **M. Priya** and Brother in law **G. Muthal** for their love, affection, encouragement and support throughout my life.

Finally, I thank one and all who have helped me during the research work.

P. Ilaiyaraja

November 2013 **P. Ilaiyaraja**

CONTENTS

Page No.

Synopsis i

List of Figures xiv

List of Tables xix

Glossary xx

CHAPTER 1

INTRODUCTION 1

1.1 Nuclear energy and nuclear fuel cycle 1

1.2 Sources of radioactive wastes 2

1.3 Classification of radioactive waste 4

- 1.3.1 High Level Waste (HLW) 4
- 1.3.2 Intermediate Level Waste (ILW) 4
- 1.3.3 Low Level Waste (LLW) 5

1.4 Radioactive waste management 5

- 1.4.1 Membrane separation process 5
  - 1.4.1.1 Reverse osmosis and Nanofiltration 6
  - 1.4.1.2 Ultrafiltration /microfiltration combined with sorption or precipitation or complexation 7
  - 1.4.1.3 Membrane distillation 8
  - 1.4.1.4 Polymer assisted Ultrafiltration 8
- 1.4.2 Solid phase extraction 9
  - 1.4.2.1 Amberlite XAD resin 10
  - 1.4.2.2 Merrifield resin 11
  - 1.4.2.3 Other chelating resin 12
- 1.4.3 Chemical precipitation 13

1.5 Thesis objective 14

1.6 Dendrimers 15

1.7 Motivation for the present study 18

1.8 Overview of thesis 18

CHAPTER 2

EXPERIMENTAL 21

2.1 Chemicals and preparation of solution 21

2.1.1 Chemicals 21

2.1.2 Standard solutions 21

2.1.3 Acid solutions 22

2.1.4 Simulated Nuclear Liquid Waste (SNLW) 22

2.1.5 Radioactive liquid waste (RLW) 22

2.1.6 Reagents 23

2.2 Instruments 24

2.2.1 Ultrafiltration device 24

2.3 Analytical Techniques 24

2.3.1 Thin layer chromatography (TLC) 24

2.3.2 Column chromatography 25

2.3.3 High Performance Liquid chromatography (HPLC) 25

2.3.4 FTIR spectrometer 26

2.3.5 Nuclear magnetic resonance (NMR) spectroscopy 26

2.3.6 Mass spectrometry (MS) 26

2.3.7 Dynamic Light Scattering (DLS) 27

2.3.8 Scanning Electron Microscope-Energy Dispersive Spectrometer 27

2.3.9 X-ray photoelectron spectroscopy (XPS) 27

2.3.10 Thermogravimetric Analysis (TGA) 27

2.3.11 Potentiometer 28

2.3.12 Fluorimeter 28

2.3.13 UV-Vis Spectrophotometer 28

2.3.14 Gamma counter 29

2.3.15 Inductive Coupled Plasma-Optical Emission Spectrometer (ICPOES) 29

2.3.16 Atomic Absorption Spectrometer (AAS) 29

2.4 Experimental setup for synthesis 29

2.5 General methods for dendrimers synthesis 30
2.6 Synthesis of Poly(amido)amine (PAMAM) dendrimer 31
    2.6.1 Ester terminated PAMAM dendrimer (G0.5) 31
    2.6.2 Amine terminated PAMAM dendrimer (G1) 32
    2.6.3 PAMAM dendrimer of higher generation 32
2.7 Characterization of PAMAM dendrimer 35
    2.7.1 High Performance liquid chromatography 35
    2.7.2 Size exclusion chromatography 35
    2.7.3 DLS 36
    2.7.4 Potentiometric tritration 37
    2.7.5 FTIR analysis 38
    2.7.6 Mass spectral analysis 39
    2.7.7 ^{1}H&^{13}C NMR spectral analysis 42
2.8 Synthesis of PAMAM dendron -SDB chelating resin 46
    2.8.1 Synthesis of amine terminated PAMAM dendron -SDB resin 46
    2.8.2 Synthesis of Diglycolic acid (DGA) functionalized PAMAM-SDB (DGA- PAMAM- SDB) resin 46
2.9 Characterization 51
    2.9.1 FTIR 51
    2.9.2 Morphology study 53
    2.9.3 Thermal degradation study 54
    2.9.4 Potentiometric titration 55
2.10 Synthesis of xanthate functionalized PAMAM dendrimer 56
    2.10.1 Ester terminated PAMAM Dendrimer 56
    2.10.2 Hydroxyl terminated PAMAM dendrimer 56
    2.10.3 Xanthate functionalization 56
2.11 Characterization 58
    2.11.1 UV absorption spectra 58
    2.11.2 FTIR spectra 58
    2.11.3 ^{1}H & ^{13}C NMR spectra 59
    2.11.4 MALDI-Mass spectrum 60

2.11.5 Determination of extent of xanthate functionalization in XFPD ligand 61

CHAPTER 3

REMOVAL OF ACTINIDES FROM AQUEOUS SOLUTION BY ULTRAFILTRATION (UF) AND DENDRIMER ASSISTED ULTRAFILTRATION (DAUF) 62

3.1 Introduction 62

3.2 Experiments 63

- 3.2.1 Ultrafiltration 63
- 3.2.2 PAMAM assisted ultrafiltration 64

3.3 Results and Discussion 65

- 3.3.1 Removal of U(VI) and Th(IV) ions by ultrafiltration 65
- 3.3.2 PAMAM dendrimer assisted UF removal of U(VI) and Th(IV) 68
- 3.3.3 Effect of pH on binding of U(VI) and Th(IV) with PAMAM dendrimer 68
  - 3.3.3.1 Fluorescence study 69
  - 3.3.3.2 Potentiometric titration 71
- 3.3.4 Effect of dendrimer concentration and generation 72
- 3.3.5 Effect of ionic strength on metal ion removal 73
- 3.3.6 Removal of Eu(III) and Co(II) metal ions by UF and DAUF 74
- 3.3.7 Selective and collective removal of U(VI) and Th(IV) metal ions 75

3.4 Conclusion 77

CHAPTER 4

ADSORPTION OF URANIUM AND THORIUM ON PAMAM DENDRON GRAFTED STYRENE DIVINYLBENZENE (PAMAM-SDB) CHELATING RESIN 79

4.1 Introduction 79

4.2 Experimental 80

- 4.2.1 Adsorption studies-Batch experiments 80
  - 4.2.1.1 Adsorption kinetics 81
  - 4.2.1.2 Adsorption isotherm 82

4.2.1.3 Adsorption thermodynamics 83
4.2.2 Desorption studies 84
4.3 Results and Discussion 84
4.3.1 Effect of pH on U(VI) and Th (IV) adsorption 84
4.3.2 Effect of contact time on adsorption 85
4.3.3 Effect of initial metal ion concentration 86
4.3.4 Adsorption kinetics 87
4.3.5 Adsorption isotherm 90
4.3.6 Effect of PAMAMG3-SDB dosage 92
4.3.7 Adsorption thermodynamics 93
4.3.8 Effect of Dendron generation 94
4.3.9 Effect of ionic strength 95
4.3.10 Desorption of U(VI) and Th(IV) from resin 96
4.3.11 Recovery of U(VI) and Th(IV) from SNLW 97
4.4. Conclusion 98

CHAPTER 5

STUDIES ON REMOVAL OF U(VI) AND Th(IV) FROM AQUEOUS AND NITRIC ACID MEDIUM USING DIGLYCOLAMIC ACID FUNCTIONALIZED PAMAM-SDB CHELATING RESIN (DGA-PAMAM-SDB) 100
5.1 Introduction 100
5.2 Experimental 101
5.2.1 Adsorption studies-Batch experiments 101
5.2.2 Desorption studies 102
5.3 Results and Discussion 103
5.3.1 Effect of pH on U(VI) and Th(IV) adsorption 103
5.3.2 Effect of nitric acid concentration on adsorption 104
5.3.3 Effect of contact time 105
5.3.4 Effect of initial metal ion concentration 106
5.3.5 Adsorption kinetics 107
5.3.6 Adsorption isotherm 109

5.3.7 Effect of DGA-PAMAMG_3-SDB dosage 111
5.3.8 Adsorption thermodynamics 111
5.3.9 Effect of dendron generation 113
5.3.10 Effect of ionic strength 114
5.3.11 Desorption of U(VI) and Th(IV) from resin 115
5.3.12 Removal of metal ions from SNLW 116
5.4 Conclusion 117

CHAPTER 6

DECONTAMINATION OF RADIOACTIVE WASTE BY PRECIPITATION USING XANTHATE FUNCTIONALIZED PAMAM DENDRIMER (XFPD) CHELATING AGENT 119
6.1 Introduction 119
6.2 Experimental 120
6.2.1 Removal of $Cu^{2+,}$ Co^{2+} and Eu^{3+} metal ions from aqueous solution 120
6.2.2 Extent of binding of metal ions 121
6.2.3 Leaching test of Co-XFPD precipitate 122
6.2.4 Removal of metal ions from liquid wastes 123
6.3 Results and Discussion 123
6.3.1 Complexation of Cu^{2+}, Co^{2+} and Eu^{3+} metal ions with XFPD 123
6.3.2 Effect of pH on complexation and metal ions removal efficiency 129
6.3.3 Settling time of suspended particle 130
6.3.4 Extent of binding of Eu^{3+} and Cu^{2+} metal ions 131
6.3.5 Effect of ionic strength on metal ions removal 132
6.3.6 TCLP and SDLT test 133
6.3.7 Removal of metal ions from liquid wastes 134
6.4 Conclusion 135

CHAPTER 7

SUMMARY AND FUTURE SCOPE 137
7.1 Summary 137
7.2 Scope for the future study 140
REFERENCES 142

Synopsis

Removal of radionuclides from liquid wastes has received increasing attention due to concerns over human health and environmental hazards. Radioactive wastes are being generated in various activities such as mining and milling of ore, operation of nuclear power reactor, reprocessing of nuclear spent fuel, decommissioning and decontamination of nuclear plants, use of radioactive materials in industry, research laboratories, medical, agricultural and environmental applications. Also, historical tests of nuclear weapons and nuclear accidents are major sources for this pollution [1]. Radioactive liquid wastes are classified into three categories as low level waste (LLW), intermediate level waste (ILW) and high level waste (HLW) based on their radioactivity [2]. Accumulation of large volume of these liquid radioactive wastes makes storage more risky and expensive. The risk and expenditure are directly proportional to volume of the waste. Therefore, these waste streams require treatment to reduce their activity to a level at which they are permitted to be discharged as per National Regulations. Radioactive decay is the only natural way of reducing radioactivity. Since radionuclides have half-lives ranging from seconds to millions of years, proper segregation of wastes based on their half-lives, suitable treatment and conditioning of these wastes are important factors in overall scheme of radioactive waste management.

HLW is managed by vitrification process in suitable matrices and safe disposal in deep geological repository. The strategy for management of LLW and ILW lies in development of innovative processes resulting in volume reduction as one of the important parameter. The selection of an appropriate technology for waste processing depends mainly on characteristics of the waste, scale of waste production and requirements for final waste form. In general, treatment of these wastes involves several processes such as solvent extraction, precipitation, coagulation, filtration, ion exchange, sorption, steam/solar evaporation and membrane separation [3, 4].

Among these processes, membrane separation, sorption and precipitation are best suited for treatment of large volume of liquid wastes containing relatively low concentration of radioactive elements. They also have advantages such as easy operation, providing better decontamination and possibility to combine with other separation processes.

Membrane- based processing of radioactive liquid waste from nuclear plant is rapidly gaining importance and is being adopted in nuclear industries. Various membrane processes for the collective and selective separation of radionuclides include Reverse Osmosis (RO), Nano-filtration (NF), Ultrafiltration (UF), Microfiltration (MF), Membrane Distillation (MD), Supported Liquid Membranes (SLM), Polymer Inclusion Membranes (PIM), Solid Polymer based Electrolysis (SPE), Polymer Assisted Ultrafiltration (PAUF) etc. [5].

RO membranes have pore sizes in the range of 0.1-1.0 nm and thus are very effective in retaining dissolved inorganic and organic solutes with molar mass below 1000 Da. NF membranes are very effective in removing hardness and organic solutes with molar mass between 1000–3000 Da. However, high pressure is required to operate both RO and NF membranes. Though UF and MF membranes require lower pressure (200–700 kPa), they are not very effective in removing dissolved organic and inorganic solutes with molar mass below 3000 Da. However, removal of radionuclides by UF membrane can be enhanced by employing PAUF. This technique combines ion exchange or chelating properties of water-soluble polymer with sieving power of an ultra filtration membrane. Invention of dendritic polymers provide unprecedented opportunity to develop effective UF process for purification of water contaminated with toxic metal ions, radionuclides, organic and inorganic solutes, bacteria and viruses [6].

Dendrimers are a new class of polymeric materials with tree-like architecture having a high degree of molecular uniformity, narrow molecular weight distribution, loosely packed interior pockets and highly functionalized terminal surface. The word dendrimer is derived from the Greek words dendri- (tree branch-like) and meros (part of) which was coined by Tomalia et al [7]. Dendrimers are constructed through a set of repeated chemical synthesis procedure that builds up from molecular level to nanoscale level. Its diameter increases linearly and the total external surface area rises dramatically. Size, shape and reactivity of dendrimers are determined by their generation (shell) and chemical composition of core, interior branching and surface functionalities. The control over size, shape and surface functionality makes dendrimers one of the “smartest’ or customizable nanomaterials. Due to their unique physical and chemical properties, dendrimers possess potential applications in the field of adhesives, coatings, medical diagnostics, drug-delivery systems, catalysts and separations [8, 9].

Studies have been carried out on the coordination behaviour of dendrimers such as Polypropyleneimine (PPI), Poly(amido)amine (PAMAM) dendrimers and their derivatives with metal ions. These ‘soft’ nanoparticles with size in the range of 1–20 nm can be used as recyclable and water soluble ligands with high capacity for removal of toxic metal ions, radionuclides and inorganic anions. The use of PAMAM dendrimer in combination with ultra filtration technique has shown potential applications in effective removal of metal ions such as Cu(II), Ni(II), Co(II), Pd(II), Pt(II), Zn(II), Fe(III), Ag(I), Au(I) and U(VI) from dilute aqueous solution [10, 11].

Separation methods based on solid phase adsorption are being developed considerably in the last decade due to their simplicity, rapidity, convenience, easy operation and cost effectiveness.Various adsorbents such as organic, inorganic, bio-sorbent and carbon based materials have been developed for metal ion recovery. The choice of adsorbent depends on its selectivity, efficiency, ease of preparation and cost effectiveness. Among the solid adsorbents, chelating resins are being increasingly used for the removal of metal ions due to their high adsorption capacity and selectivity. These chelating resins are prepared either by coating/impregnating the chelating agents on solid substrate or chemically bonding/grafting of same. The main disadvantage of impregnated chelating resin is leaching of chelating agent from solid support which results in gradual loss of capacity and useful lifetime. Generally, the adsorption efficiency depends mainly on the type of chelating group and to some extent on size and physiochemical properties of the resin. The choice of appropriate chelating group is a critical factor to obtain maximum recovery with high enrichment factor [12]. The solid-phase synthesis of PAMAM dendron on polystyrene-poly(ethylene glycol) resin bead has been reported [13]. PAMAM dendron grown on surface of silica particles are used for removal of various metal ions, organic dyes and surfactants from water [14, 15].

Chemical precipitation is the oldest technique employed for separation of radionuclides in a large-scale. This process concentrates the radionuclides present in a liquid waste stream into a small volume of wet solid that can be separated from the bulk. It is fairly versatile and may be used to treat a wide variety of waste streams containing large amount of particulates or high concentration of salts. A wide range of chemicals such as oxalates, carbonates, peroxides, fluorides, sulphides, thiols, hydroxides, dithiocarbamates, dithiophosphates and xanthates are useful precipitants for removal of heavy metal ions [16].

Among these chemical reagents, molecules with single and multiple xanthate groups are claimed to have high removal efficiency for heavy metals due to low solubility product and high stability constant of metal-xanthate complex [17]. Molecules with multiple xanthate groups exhibit excellent binding characteristics and better settling behaviour [18]. Hence, it is desirable to increase the number of xanthate functional groups in a molecule to enhance binding and precipitating abilities. PAMAM dendrimer macromolecule as described by *Tomalia* et al. [7] is relatively easy to synthesize with desired number of reactive functional groups.

The aim of the present study is to explore the use of dendrimer macromolecules for the removal of radionuclides from aqueous waste by using common treatment processes described above namely membrane separation, adsorption and chemical precipitation.

Studies on the removal of radionuclides from aqueous waste have been carried out using the following four indigenously developed compounds,

(i) PAMAM dendrimer chelating ligand by Dendrimer Assisted Ultrafiltration (DAUF),

(ii) PAMAM dendron grafted - styrene divinyl benzene (SDB) chelating resin by adsorption,

(iii) DGA functionalized-PAMAM dendron- styrene divinyl benzene chelating resin in both aqueous and nitric acid medium by adsorption and

(iv) Xanthate Functionalized PAMAM Dendrimer (XFPD) by precipitation.

Chapter 1

This chapter gives an introduction to the research problem dealt in the present study. The sources of radioactive waste in various steps of nuclear fuel cycle and handling of radioactive materials in industry, research laboratories, medicine and agriculture have been briefed. Classification of radioactive wastes from safety as well as process consideration point of view is described. Main objective of radioactive waste management is to separate long lived alpha emitting radionuclides which belong to actinide series in the periodic table. The most common treatment processes such as membrane separation, sorption and precipitation are also described in this chapter. A brief introduction about dendrimer macromolecules and their applications in various fields is given. The development of dendrimer macromolecules for the treatment of aqueous wastes has been briefed in this chapter. Finally, the scope of the present work is highlighted.

Chapter 2

This chapter describes preparation of standard reagents, experimental setup, synthesis of chelating agents and their characterization. Major part of this chapter is devoted to synthesis, purification and characterisation of dendrimer chelating ligand and solid supported dendron chelating resin. Detailed procedures for the synthesis of PAMAM dendrimer, Xanthate Functionalized Dendrimer (XFPD) and amine/DGA functionalized-Styrene Divinyl Benzene (SDB) chelating resins are described. The description of following instruments Liquid Chromatography (HPLC and SEC), Fourier Transform Infra Red (FT-IR), Matrix Assisted Laser Desorption Ionisation – Mass Spectroscopy (MALDI-MS), Nuclear Magnetic Resonance (NMR), Dynamic Light Scattering (DLS), Fluorimeter, Potentiometer, Scanning Electron Microscope with Energy Dispersive Spectrometer (SEM-EDS), X-ray Photoelectron Spectroscopy (XPS), Thermo Gravimetric Analysis (TGA), Inductively Coupled Plasma-Optical Emission Spectrometer (ICP-OES) and UV-Vis Spectrometer used in the study is presented. The method of purification of synthesized dendrimers and their purity conformation using chromatographic techniques such as Thin Layer Chromatography (TLC) and High Performance Liquid Chromatography (HPLC) are briefed. Liquid chromatographic techniques were used to monitor the growth of dendrimer generation. The functional group and structural characterisation of PAMAM and hydroxy terminated dendrimer ($PAMAMG_1OH$) were carried out using spectroscopic techniques such as FTIR, NMR and MALDI-MS. Potentiometric titration was carried out to determine pKa of functional groups and confirm ideal growth of dendron/dendrimer. Particle size of PAMAM dendrimer was measured by using DLS technique. The procedure for the determination of the extent of xanthate functionalization in XFPD chelating ligand is described. The difference in morphology of dendron functionalized-SDB and SDB was examined using SEM. Thermal stability of dendron functionalized-SDB was determined using TGA.

Chapter 3

This chapter describes studies on the removal of radionuclides from aqueous solution by Ultrafiltration (UF) and Dendrimer Assisted Ultrafiltration (DAUF). UF and DAUF experiments were carried out using regenerated cellulose acetate membrane and PAMAM [poly(amido)amine] dendrimer complexing agent. The effect of metal ion speciation on removal of U(VI) and Th(IV) by ultrafiltration and PAMAM dendrimer assisted ultrafiltration has been discussed. Potentiometric and fluorimetric experiments were carried out to investigate speciation of U(VI) and Th(IV) metal ions in the presence of PAMAM dendrimer complexing agent. Effect of pH, ionic strength, PAMAM dendrimer concentration and dendrimer generation on metal ion retention is discussed. The metal ion recovery and reusability of PAMAM dendrimer is discussed. Studies on selective and collective removal of U(VI) and Th(IV) metal ions from simulated industrial nuclear effluent by UF and DAUF methods were also carried out and the results are discussed in this chapter.

Chapter 4

This chapter deals with adsorptive removal of uranium and thorium from aqueous solution using PAMAM dendron grafted Styrene Divinyl Benzene (SDB) chelating resin. The PAMAM dendron up to generation 5 was grown on the surface of SDB resin (PAMAMG_{1-5}-SDB) by a divergent method. Adsorption of U(VI) and Th(IV) on PAMAMG_3-SDB chelating resin was investigated in a series of batch experiments. Effect of contact time, pH, ionic strength, adsorbent dose, initial metal ion concentration, dendron generation and temperature on adsorption of U(VI) and Th(IV) were investigated and the results are discussed in detail. Regeneration of chelating resin was carried out by altering the acidity of equilibration solution. Adsorption kinetics was studied using pseudo-first-order, pseudo-second-order, Elovich and intraparticle diffusion models. The adsorption isotherm was analysed in terms of Langmuir and Freundlich equations and thermodynamic constants (ΔG^o, ΔH^o and ΔS^o) were evaluated from temperature dependency data.

Chapter 5

This chapter describes removal of U(VI) and Th(IV) from both aqueous and acidic media using diglycolic acid functionalized PAMAM dendron polymeric chelating resin (DGA-PAMAM-SDB). DGA-PAMAMG_{1-5}-SDB was prepared by reacting PAMAMG_{1-5} dendron styrene divinylbenzene (SDB) with diglycolic anhydride. Adsorption of U(VI) and Th(IV) on DGA-PAMAMG_3-SDB chelating resin from aqueous and nitric acid medium was investigated by conducting a series of batch experiments. Effect of contact time, pH, ionic strength, adsorbent dose, initial metal ion concentration, dendron generation and temperature on adsorption of U(VI) and Th(IV) were investigated and the results are discussed in detail. Adsorption kinetics was studied using pseudo-first-order, pseudo-second-order, Elovich and intraparticle diffusion models. The adsorption isotherm was analysed in terms of Langmuir and Freundlich equations and thermodynamic constants (ΔG^o, ΔH^o and ΔS^o) were evaluated from temperature dependent data. Desorption of U(VI) and Th(IV) from DGA-PAMAMG$_3$-SDB chelating resin was carried out by altering the acidity of equilibration solution.

Chapter 6

This chapter describes removal of radionuclides from aqueous waste by xanthate precipitation process. Xanthate Functionalized PAMAM Dendrimer (XFPD) chelating ligand, first of its kind, has been synthesized from first generation hydroxyl terminated PAMAM dendrimer. Studies on the removal of copper, cobalt (representative of radioactive transition metal ions) and europium (representative of lanthanide ions & surrogate for americium) from aqueous solution by precipitation was carried out using XFPD. Experimental results on (i) effect of pH, (ii) ionic strength and (iii) settling behaviour of precipitate are discussed. Toxicity Characteristics Leaching Procedure (TCLP) and Semi-Dynamic Leaching Test (SDLT) were conducted to investigate metal leachability and stability characteristics of metal-XFPD complexes. The indigenously developed XFPD chelating ligand was deployed for treatment of radioactive liquid waste and results are highlighted.

Chapter 7

This chapter summarizes highlights of the results described in the thesis. The potential application of dendrimer based chelating agent for removal of actinides and other radionuclides from aqueous medium are demonstrated.

Studies on UF of uranium and thorium through regenerated cellulose acetate membrane reveal that about 76-97% of U(VI) and Th(IV) are removed from aqueous solution at pH 5-7. Removal of U(VI) and Th(IV) is due to adsorption/mass deposition on the membrane surface. The continuous use of membrane results in decrease of membrane flux due to membrane fouling. In-situ acid rinsing of the membrane proved to be effective for removing the floc build-upon the membrane surface and flux recovery. The water soluble PAMAM dendrimer chelating ligand has shown greater ability to bind with U(VI) and Th(IV) metal ions. The presence of PAMAM dendrimer chelating ligand does not prevent hydrolysis of actinides whereas the hydrolyzed actinide species are effectively binding with PAMAM dendrimer. About 3 mg of G_4-NH_2 dendrimer is required to retain 5 mg of U(VI) /Th(IV) in the retentate at pH 6. Increase in dendrimer generation reduces the quantity of PAMAM chelating ligand requirement. It is estimated that about 1.1, 0.6 and 0.45 g of PAMAM$G_{3,}$ PAMAMG_4 and PAMAMG_5 dendrimers are required to retain1g of (VI) /Th(IV) in the retentate at pH 6. At acidic pH (≤ 3), the binding of metal ions with PAMAM dendrimer is observed to be very less and hence PAMAM can be regenerated.

Studies on the adsorption of U(VI) and Th(IV) on indigenously developed PAMAMG_3-SDB chelating resin reveals that adsorption capacity of PAMAMG_3-SDB is dependent on contact time, pH and initial concentration of U(VI) and Th(IV). Kinetic study shows that the adsorption process is fast and equilibrium is reached within 60 minutes. Adsorption follows pseudo-second order kinetics and Langmuir isotherm model suggesting chemical adsorption. Adsorption capacity of the chelating resin increases exponentially with increase in dendron generation. PAMAMG_5-SDB has adsorption capacity (q_e) of 493 and 261.5 mg g^{-1} for U(VI) and Th(IV) respectively. The adsorbed U(VI) and Th(IV) could be easily desorbed from resin by decreasing the pH of the solution and maximum of ~ 99 % desorption was observed at pH 1 which indicates regenerability/reusability of the resin.

Diglycolic acid functionalized PAMAM dendron- styrene divinylbenzene chelating resin can remove metal ions from aqueous and nitric acid medium. The adsorption capacity of DGA-PAMAMG_5-SDB for U(VI) and Th(IV) are 682 and 544.2 mg g^{-1} respectively.

Xanthate Functionalized PAMAM Dendrimer (XFPD) ligand is effective in removal of various metal ions from aqueous solution by precipitation. XFPD form water insoluble complexes with copper, cobalt and europium metal ions. The pH of aqueous solution plays an important role on both complexation and settling of suspended metal-xanthate. XFPD ligand effectively remove metal ions in the pH range of 4-8 and settling of suspended metal-xanthate complexes at pH > 6 requires the addition of aluminium sulphate as coagulating agent. The loading capacity of XFPD for copper, cobalt and europium metal ions are determined to be 0.355 g, 0.48 g and 0.94 g per gram of XFPD respectively. Actinides (U & Th) are precipitated as metal hydroxides along with other metal ions during the xanthate precipitation at pH 5 - 7. Studies with radioactive liquid waste (RLW) show that percentage removal of radionuclides are observed to be in the following order; Zr(IV) ≈ Eu(III) ≈ Co(II) (> 99.8) > Ce(III) (98.84) > Sb(III) (83.31) > Ru(III) (79.44) > Mn(II) (54.29) > Cs(I) (24.02). Hence, XFPD ligand possesses potential application in effective removal of radionuclides from radioactive wastes.

The present study, establish the conditions for efficient removal of radionuclides from aqueous wastes using various classes of dendrimer/dendron chelating agents. Removal of radionuclides by ultrafiltration requires adjustment of pH of the aqueous solution. Dendrimer assisted ultrafiltration is more effective in concentrating the radionuclides in the retentate than UF. High decontamination factor were achieved for actinides using PAMAM dendron grafted-SDB chelating resin. Selective removal of actinides was achieved using PAMAM dendrimers and dendron grafted chelating resin at weakly acidic to neutral medium. DGA functionalized PAMAM dendron-SDB chaleting resin is effective in removal of radionuclides from both aqueous and acidic medium. PAMAM dendrimer and dendron grafted chelating resin could be regenerated and reusable. Xanthate functional group introduced on dendrimer surface effectively precipitates various metal ions over the pH range of 4-8. This xanthate process is very effective in total decontamination of radioactive wastes. The overall objective of the research described here is to develop a potential removal process using dendrimer based chelating agents for treatment of radioactive waste streams in nuclear facilities.

References

(1) R. O. Abdel Rahman (2012) Planning and Implementation of Radioactive Waste Management System, Radioactive Waste, ISBN: 978-953-51-0551-0.

(2) P. A. Baisden, G. R. Choppin (2007) Nuclear waste management and the nuclear fuel cycle, Radiochemistry and Nuclear chemistry.

(3) K. Raj, K.K. Prasad, N.K. Bansal, Nucl. Eng. Des. 236 (2006) 914–930.

(4) R. O. Abdel Rahman, H. A. Ibrahium and Yung-Tse Hung, Water 3 (2011) 551-565.

(5) D. Rana, T. Matsuura, M.A. Kassim, A.F. Ismail, Desalination 321 (2013) 77-92.

(6) N. Savage and M. S. Diallo, J. Nanopart. Res. 7 (2005) 331–342.

(7) D.A. Tomalia, H. Baker, J. Dewald, M. Hall, G. Kallos, S. Martin, J. Roeck, J. Ryder, P. Smith, Polymer Journal 17 (1985) 117-132.

(8) B. Klajnert and M. Bryszewska, Acta Biochim. Pol. 48(1) (2001) 199-208.

(9) R. Touzani, J. Mater. Environ. Sci. 2 (3) (2011) 201-214.

(10) Diallo, M.S.: US2006021938 (2006).

(11) Diallo MS, Arasho W, Johnson JH, Goddard WA., Environ. Sci. Technol. 42 (2008) 1572-1579.

(12) P. Ilaiyaraja, A K Singha Deb, K. Siva Subramanian, D. Ponraju and B. Venkatraman, J. Hazard. Mater. 250– 251 (2013) 155– 166.

(13) V. Swali, N.J. wells, G.J. Langley and M. Bradley, J. Org. Chem. 62 (1997) 4902-4903.

(14) R. Qu, Y. Niu, C. Sun, C. Ji, C. wang, G. Cheng, Micropor. Mesopor. Mat. 97 (2006) 58-65.

(15) C.C. Chu, N. Ueno and T. Imae, Chem. Mater. 20 (2008) 2669-2676.

(16) NEA/NSC/DOC(97)19, Actinide separation chemistry in nuclear waste streams and materials, December 1997.

(17) Y.K. Chang, J.E. Chang, T.T. Lin, Y.M. Hsu, J. Hazard. Mater. B94 (2002) 89–99.

(18) L Liu, J. Wu, X Li, Y Ling, Sep. Purif. Tech.103 (2013) 92-100.

List of Figures

Figure No.	Caption	Page No.
Fig.1.1	Schematic of membrane separation process	7
Fig.1.2	Schematic of a generalized 2D and 3D view of dendrimer structure	17
Fig.2.1	Experimental setup used for dendrimer synthesis is	32
Fig 2.2	Scheme of divergent and convergent dendrimer synthesis	33
Fig.2.3	Synthesis scheme of PAMAM dendrimer	34
Fig.2.4	Structure of G_3, G_4 and G_5 PAMAM dendrimer	36
Fig.2.5	HPLC chromatogram of (a) ester and (b) amine terminated PAMAM dendrimers	37
Fig.2.6	SEC chromatograms of (a) ester and (b) amine terminated PAMAM dendrimer	38
Fig.2.7	Mean size of amine terminated PAMAM as a function of dendrimer generation	39
Fig.2.8	FTIR spectra of (a) ester and (b) amine terminated PAMAM dendrimer	41
Fig.2.9	Unsymmetrical structure of G_1 PAMAM dendrimer (A) incomplete addition (B) Intramolecular cyclization (C) dimerization	42
Fig.2.10	MALDI-Mass spectra of full generation amine terminated PAMAM dendrimer	43
Fig.2.11	^{1}H&^{13}C NMR of ester terminated $G_{0.5}$ PAMAM dendrimer	44
Fig.2.12	^{1}H&^{13}C NMR of amine terminated G_1 PAMAM dendrimer	45
Fig.2.13	Synthesis scheme of PAMAM dendron-SDB chelating resin	49
Fig.2.14	Structure of PAMAMG_4,G_5-SDB chelating resin	50
Fig.2.15	Synthesis scheme of DGA-PAMAM-SDB chelating resin	51
Fig.2.16	Structure of DGA-PAMAMG_2,G_3,G_4,G_5-SDB	52

Fig.2.17 FTIR spectra of (a) CSDB (b) ester terminated PAMAMG$_{2.5}$-SDB (c) Amine terminated PAMAMG$_3$-SDB (d) DGA-PAMAM-SDB resin 53

Fig.2.18 FE-SEM image of (a) CSDB and (b) PAMAMG$_3$-SDB (C) DGA-PAMAM-SDB 55

Fig.2.19 TG curve of CSDB, PAMAMG$_3$-SDB and DGA-PAMAMG$_3$-SDB 56

Fig.2.20 Synthesis of xanthate functionalized PAMAM dendrimer 59

Fig.2.21 UV-Visible spectra of PAMG$_1$OH & XFPD 60

Fig.2.22 FTIR Spectra of (a) PAMAMG$_1$OH, (b) XFPD 61

Fig.2.23 ^{1}H & ^{13}C spectra of PAMAMG$_1$OH 62

Fig.2.24 Mass spectrum of PAMAMG$_1$OH 66

Fig.3.1 Speciation diagram of (a) U(VI) and (b) Th(IV) ions as a function of pH in aqueous solution at atmospheric condition 69

Fig.3.2 Effect of pH on (a) U(VI) deposition and (b) uranium removal 70

Fig.3.3. Effect of pH on (a) Th(IV) deposition and (b) thorium removal 71

Fig.3.4. Fluorescence emission spectra of U(VI) solution as a function of pH 73

Fig.3.5. Fluorescence emission spectra of U(VI) as a function of PAMAMG$_2$ 73

Fig.3.6 Potentiometric titration of PAMAMG$_3$ with UO_2^{2+} and Th^{4+} ions 75

Fig.3.7 Effect of PAMAMG$_4$ concentration on retention and mass deposition of (a) U(VI) and (b) Th(IV) 76

Fig.3.8 Effect of $Ca(NO_3)_2$ concentration on removal of (a) U(VI) and (b) Th(IV) 77

Fig.3.9 Effect of NaCl concentration on removal of (a) U(VI) and (b) Th(IV) 78

Fig.3.10 Effect of pH on removal of (a) Eu(III) and (b) Co(II) by UF and DAUF 79

Fig.3.11 Potentiometric titration curve of PAMAMG$_3$ with Eu^{3+} and Co^{2+} metal ions 79

Fig. 4.1 Effect of pH on adsorption of U(VI) and Th(IV) onto PAMAMG$_3$-SDB 89

Fig. 4.2. Effect of contact time on adsorption of U(VI) and Th(IV) onto PAMAMG$_3$-SDB 90

Fig. 4.3 Effect of initial concentration of U(VI) and Th(IV) on adsorption capacity 91

Fig. 4.4 Kinetic models for U(VI) and Th(IV) adsorption on PAMAMG$_3$-SDB (a) pseudo-first-order, (b) pseudo-second-order, (c) Elovich and (d) intra-particle kinetic models 92

Fig. 4.5 (a) Langmuir and (b) Freundlich adsorption isotherm for U(VI) and Th(IV) adsorption on PAMAMG$_3$-SDB 94

Fig. 4.6 Langmuir separation factor (R_L) as a function of initial metal ion concentration 96

Fig. 4.7 Effect of PAMAMG$_3$-SDB dosage on adsorption of U(VI) and Th(IV) 97

Fig. 4.8 Effect of temperature on U(IV) and Th(IV) adsorption onto PAMAMG$_3$-SDB 98

Fig. 4.9 Effect of PAMAM dendron generation on uranium adsorption capacity 99

Fig. 4.10 Effect of ionic strength on (a) U(VI) and (b) Th(IV) adsorption 100

Fig. 4.11 Desorption of U(VI) and Th(IV) from adsorbent as a function of pH 101

Fig. 5.1 Effect of pH on adsorption of U(VI) and Th(IV) onto DGA-PAMAMG$_3$-SDB 109

Fig. 5.2 Effect of HNO_3 concentration on adsorption of U(VI) and Th(IV) onto DGA-PAMAMG$_3$-SDB 110

Fig. 5.3 Effect of contact time on adsorption of U(VI) and Th(IV) onto DGA-PAMAMG$_3$-SDB 111

Fig. 5.4 Effect of initial U(VI) and Th(IV) concentrations on adsorption capacity 112

Fig. 5.5 Kinetic models for U(VI) and Th(IV) adsorption on DGA-PAMAMG$_3$-SDB (a) pseudo-first-order, (b) pseudo-second-order, (c) Elovich and (d) intra-particle kinetic models 113

Fig. 5.6 (a) Langmuir and (b) Freundlich adsorption isotherm for U(VI) and Th(IV) adsorption on DGA-PAMAMG$_3$-SDB 115

Fig.5.7 Langmuir separation factor (R_L) as a function of metal ion concentration (C_0) 115

Fig. 5.8 Effect of DGA-PAMAMG$_3$-SDB dosage on U(VI) and Th(IV) adsorption 116

Fig. 5.9 Effect of temperature on adsorption of U(VI) and Th(IV) onto DGA-PAMAMG$_3$-SDB 117

Fig. 5.10 Effect of DGA-PAMAM dendron generation on adsorption capacity 119

Fig. 5.11 Effe Effect of ionic strength on U(VI) and Th(IV) adsorption onto DGA-PAMAMG$_3$-SDB 120

Fig. 5.12 Desorption of U(VI) and Th(IV) from DGA-PAMAMG$_3$-SDB adsorbent 120

Fig.6.1 FTIR Spectra of (a) Cu-XFPD, (b) Co-XFPD and (c) Eu-XFPD complexes 129

Fig.6.2 Coordination pattern of xanthate ligand (a) unidentate (b) anisobidentate (c) coordination with two hetero atom (d) anisotetradentate 129

Fig.6.3 SEM-EDS spectra of Cu-XFPD, Co-XFPD and Eu-XFPD complexes 130

Fig.6.4 XPS spectra of Cu2p & Co2p from Cu-XFPD and Co-XFPD complexes 131

Fig. 6.5 XPS spectra of O1s and Eu4d from Eu-XFPD complex 133

Fig.6.6 Fluorescence emission spectra of Eu^{3+} and Eu-XFPD complex 134

Fig.6.7 Effect of pH on removal of Cu, Co and Eu metal ions 135

Fig.6.8 Residual turbidity of complexes as a function of time 136

Fig.6.9 Extent of binding of Cu^{2+}, Co^{2+} and Eu^{3+} metal ions with XFPD ligand 137

Fig.6.10 Effect of $NaNO_3$ and $Ca(NO_3)_2$ concentration on removal of Cu^{2+}, Co^{2+} and Eu^{3+} ions 138

Fig.6.11 Removal of metal ions from (a) SNLW and (b) RLW 140

List of Tables

Table No.	Caption	Page No.
Table 1.1	Precipitant process for specific decontamination	15
Table 2.1	Composition of SNLW and RLW	25
Table 2.2	Theoretical and determined number of amine groups and molar mass of amine and ester terminated PAMAM dendrimer	40
Table 2.3	^{1}H and ^{13}C chemical shift of ester terminated PAMAM dendrimers	46
Table 2.4	^{1}H and ^{13}C chemical shift of amine terminated PAMAM dendrimer	47
Table 2.5	Interpretation of vibrational frequencies for CSDB and ester, amine and DGA terminated PAMAM-SDB resin	54
Table 2.6	Theoretical and experimental determined number of primary (1°), tertiary (3°) amines and DGA functional groups in the PAMAM-SDB and DGA-PAMAM-SDB chelating resins.	57
Table 3.1	Percentage of metal ions from SNLW in UF and DAUF at pH 5.5 and pH 12.5	80
Table 4.1	Kinetic parameters for U(VI) and Th(IV) adsorption on PAMAMG$_3$-SDB	93
Table 4.2	Adsorption isotherm parameters for U(VI) and Th(IV) on PAMAMG$_3$-SDB	95
Table 4.3	Thermodynamic parameters of U(VI) and Th(IV) adsorption on PAMAMG$_3$-SDB	99
Table 4.4	Percentage removal of metal ions from simulated nuclear waste	102
Table 5.1	Kinetic parameters for U(VI) and Th(IV) adsorption on DGA-PAMAMG$_3$-SDB	114
Table 5.2	Isotherm parameters of U(VI) and Th(IV) adsorption on DGA-PAMAMG$_3$-SDB	116
Table 5.3	Thermodynamic parameters of U(VI) and Th(IV) adsorption on DGA-PAMAMG$_3$-SDB	118
Table 5.4	Removal of U(VI) and Th(IV) from SNLW at pH 5.5 and 12.5	121
Table 6.1	SDLT test of Cu-XFPD, Co-XFPD and Eu-XFPD complexes	139

Glossary

MWe	Mega Watt electric
PHWR	Pressurized Heavy Water Reactors
FBRs	Fast Breeder Reactors
MOX	Mixed Oxide
PUREX	Plutonium Uranium Reductive Extraction
TBP	Tributyl Phosphate
HLW	High Level Waste
EDTA	Ethylenediamine Tetra Acetic Acid
ILW	Intermediate Level Waste
LLW	Low Level Waste
RO	Reverse Osmosis
NF	Nanofiltration
UF	Ultrafiltration
MF	Microfiltration
MD	Membrane Distillation
PAUF	Polymer Assisted Ultrafiltration
SLM	Supported Liquid Membrane
PIM	Polymer Inclusion Membrane
SUF	Seeded Ultrafiltration
SMF	Seeded Microfiltration
DF	Decontamination Factor
CPMF	Co-Precipitation followed by Microfiltration
SDS	Sodium Dodecyl Sulfate
PEI	Polyethyleneimine
PAA	Polyacrylic Acid
PVA	Polyvinyl Alcohol
PVSA	Polyvinyl Sulfonic Acid
DADMAC	Dially Dimethyl Ammonium Chloride
PB	Polybrene

SPE	Solid Phase Extraction
CMP	(Carbamoylmethy1) Phosphonates
CMPO	Carbamoylmethylphosphine Oxide
EDHBA	4-Ethoxy-N,N-Dihexyl-Butamide
DADPA	(Dimethyl Amino Phosphonomethyl)Phosphoric Acid
MCM	Chloromethylated Merifield resin
DMDBMA	N,N'-Dimethyl-N,N'-Dibutylmalonamide
DB2EHM	Di-bis (2-Ethylhexylmalonamide)
DMDOHEMA	2-(2-Hexyloxy-Ethyl)N,N′-Dimethyl- N,N′-Dioctylmalonamide
TODGA	N,N,N′,N′-Tetraoctyl-3-Oxapentane-1,5-Diamide
PAMAM	Poly(amido) amine
DAUF	Dendrimer Assisted Ultrafiltration
EDA	EthyleneDiamine
MA	Methyl Acrylate
SDB	Styrene Divinyl Benzene
XFPD	Xanthate Functionalized PAMAM Dendrimer
CSDB	Chloromethylated Styrene Divinyl Benzene
SNLW	Simulated Nuclear Liquid Waste
RLW	Radioactive Liquid Waste
DEUF	Dendrimer-Enhanced Ultrafiltration
PAMAM-SDB	PAMAM dendron functionalized Styrene Divinyl Benzene
DGA-PAMAM-SDB	Diglycolamic Acid functionalized PAMAM-SDB
K_d	Distribution Coefficient
HSAB	Hard Soft Acid Base
TCLP	Toxicity Characteristics Leaching Procedure
SDLT	Semi-Dynamic Leaching Test

Chapter-1

INTRODUCTION

1.1 Nuclear Energy and Nuclear Fuel Cycle

Nuclear energy has been proposed as a viable alternative to meet ever-growing demand for energy with less impact on the environment. Presently, nuclear energy provides over 17 % of the world's total electricity. As of July 2013, there are 434 nuclear reactors in 31 countries with a total installed capacity of 3,70,543 megawatt electric (MWe) all over the world [1]. In India, currently about 3 % of total energy production is coming from nuclear energy. Though, the uranium resource (78,000 tonnes) in India is limited, we have vast resources of thorium (5,18,000 tonnes) [2]. In order to exploit the nuclear fuel resources for energy production, a sequential three-stage programme was envisaged in India based on a closed fuel cycle, where the spent fuel of one stage is reprocessed to produce fuel for the next stage. The first stage of Indian Nuclear Programme involves deployment of Pressurized Heavy Water Reactors (PHWRs), where natural uranium (^{238}U) is used as fuel. It produces energy as well as another fissile element i.e., ^{239}Pu.

In the second stage, Fast Breeder Reactors (FBRs) employ mixed oxide (MOX) fuel made from ^{239}Pu (recovered by reprocessing of spent fuel from the first stage) and natural uranium. In FBRs, ^{239}Pu undergoes fission to produce energy as well as ^{239}Pu by transmutation of ^{238}U. FBRs produce more fuel than they consume and hence termed Breeders. Over a period of time, plutonium inventory can be built up by feeding ^{238}U. ^{232}Th, which constitutes world's largest reserves in India, is not fissile therefore it is converted to a fissile material (^{233}U) by transmutation in FBRs. The third stage of the programme will be based on advanced nuclear power programme involving a self-sustaining series of ^{232}Th and ^{233}U fuelled reactors [3].

The overall nuclear fuel cycle operation involves mining, enrichment, fuel fabrication, reactor operation, spent fuel reprocessing, vitrification and waste disposal. The generation of radioactive waste is inevitable during nuclear fuel cycle and must be managed with care due to very long half lifes of radionuclides (few hundreds to millions of years) pose long term radiological risk to human health and ecology. Hence, safe and efficient management of radioactive waste is of utmost importance for acceptance of nuclear power to common man. It indeed requires knowledge of the source and composition of various wastes generated in nuclear industries.

1.2 Sources of radioactive waste

- Mine tailings from mining of U and Th ores generally contain elevated levels of naturally occurring radionuclides and their daughter products (e.g. Ra, Po, Bi and Pb).
- Radioactive wastes also arise during the extraction or processing of other minerals such as phosphate, gold-bearing rocks, coal etc. that happen to be rich with naturally occurring radioactive materials [4].
- The front end of nuclear fuel cycle includes fuel fabrication through various steps such as mining, milling, chemical processing and enrichment (if required) etc. Solid wastes and sludges formed in the above steps contain fluoride compounds of uranium (UF_4 and UO_2F_2) [5].
- Majority of the radioactive wastes originate from nuclear reactors. At first, the fuel from reactor core is removed before it is fully consumed, primarily because of buildup of fission products, which capture neutrons that are essential for sustaining chain reaction. The spent fuel is then stored in special water pools (at least for initial few years) where water is continuously circulated to remove decay heat. If the water is contaminated with radionuclides released from the defective spent fuel, then it has to be treated as radioactive waste stream. Almost the entire radioactivity produced in a

nuclear power plant is contained within the spent fuel. After sufficient years of cooling, spent fuel is reprocessed for recovery of Pu and U.

One of the most widely used extraction process for fuel reprocessing is the PUREX (Plutonium – Uranium Reductive Extraction) process.

- The reprocessing step involves chopping of fuel pins and dissolution in 12 M nitric acid. The hulls are separated as solid waste.
- U and Pu are separated/recovered by using an organic extractant which is typically 30% tributyl phosphate (TBP) in purified kerosene or n-dodecane diluent.
- The raffinate is stored as high level waste (HLW) which contains unextracted U, Pu, fission products (Sr, Zr, Mo, Tc, Ru, Pd, Cs, Ba and lanthanides), structural materials, activation products and minor actinides [6].

- ➢ Though TBP possesses chemical and radiation stabilities, it undergoes slow degradation by radiolysis and acid hydrolysis. The resultant acid phosphates that are routinely removed by alkaline wash retain some U, Pu and other actinides.
- ➢ Similarly, diluents and ion-exchange resins used in reprocessing also form an organic waste retaining some fraction of actinides [5].
- ➢ The small amount of activation products produced during the reactor operation and/or the activity leaking out from the defective spent fuel (very rare) enters the coolant system and produces a waste stream. Other types of wastes are personal showers and washes, chemical waste from laboratories, evaporator condensates etc [6].
- ➢ Various liquids such as dilute nitric acid, sometimes with added fluorides, mixtures with organic complexing agents (citric acid or ethylenediamine tetraacetic acid (EDTA)) used for removal of contaminants from equipment during refurbishment or decommissioning often contain radionuclides [5].

- Historical tests of nuclear weapons, nuclear and radioactive accidents are representing major sources for radioactive pollution in water [7].
- Production of isotopes such as ^{238}Pu from ^{237}Np [8] and ^{252}Cf [9] for various applications also generates radioactive wastes.
- Radioisotopes used in research, medical and industries also generate radioactive waste other than nuclear industry [10].

1.3 Classification of Radioactive Waste

For safe handling and waste management, radioactive wastes are classified as high level, intermediate level and low level depending upon the level of radioactivity [11-13].

1.3.1 High Level Waste (HLW)

The radioactive waste containing radioactivity above 3.7×10^{11} Bq/L is referred as HLW. It is emanating from nuclear power generation, (i.e. reprocessing waste streams) or nuclear weapons production. The aqueous waste stream (HLW) generated during the chemical processing of spent fuel contains radionuclides such as U, Pu, alpha emitting minor actinides and fission products. As a result, HLW is highly radioactive, producing a significant amount of heat and containing long-lived radionuclides with half lives ranging from few hundred to millions of years. Relative to the total volume of waste generated in nuclear power production, HLW constitutes only a small fraction (about 3 %) by volume, whereas majority of the radioactivity (> 95 %) resides in HLW.

1.3.2 Intermediate Level Waste (ILW)

The waste containing radioactivity ranging from 3.7×10^{6} to 3.7×10^{11} Bq/L is referred as ILW. The used resins, chemical sludge, reactor components as well as reprocessing equipments generally come under this category. ILW comprises about 7 % of the total volume of the radioactive waste, whereas in terms of radioactivity it is < 4 %.

1.3.3 Low Level Waste (LLW)

The waste containing radioactivity ranging from 37 to 3.7×10^6 Bq/L is referred as LLW. It is mostly generated in liquid form during (i) the decontamination of equipment, (ii) handling of radioactivity in laboratories and hospitals and (iii) various processes in nuclear fuel cycle. LLW comprises about 90 % of the total volume of the radioactive waste generated, but contains only < 1 % radioactivity.

1.4 Radioactive waste management

Accumulation of large volume of radioactive waste makes storage more risky and expensive. The risk and expenditure are directly proportional to volume of the waste. Therefore, these waste streams are treated to reduce their activity to a level at which they are permitted to be discharged as per national regulations. Solvent extraction, precipitation, ion exchange, sorption, membrane separation, electrodeposition, steam/solar evaporation and phyto remediation are conventional and recently developed methods reported for treatment of radioactive waste [13,14]. The selection of an appropriate technology for waste processing depends mainly on the characteristics of the waste, the scale of waste production and the final form of the waste. Among the above processes, we mainly focus our attention towards membrane separation, adsorption and chemical precipitation by considering their advantages such as easy operation, better decontamination and its possibility to form a hybrid system by combining with other separation processes.

1.4.1 Membrane Separation Process

During the past few decades, membrane separation process using semipermeable membrane has become one of the emerging technologies with a rapid growth. It has drawn the attention of researchers in the field of separation technology with its better performance compared to conventional separation processes. The basic process of the membrane separation (Fig.1.1) involves separation of feed mixture into a retentate (part of the feed that does not pass through the membrane) and a permeate (part of the feed that passes through the membrane) [15].

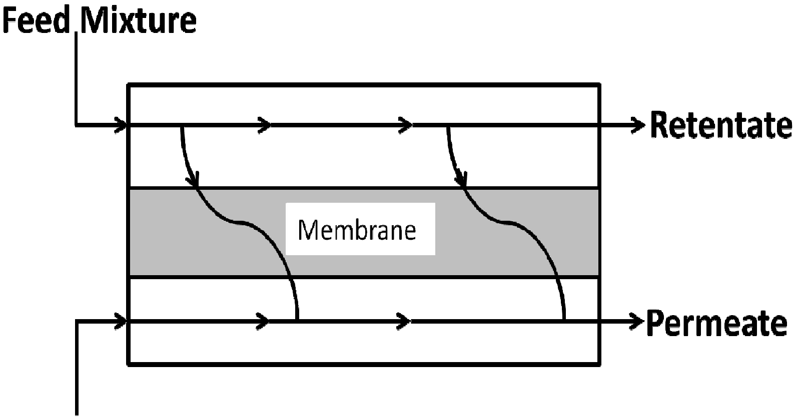

Fig.1.1 Schematic of membrane separation process

There are number of membrane processes such as Reverse Osmosis (RO), Nano-filtration(NF), Ultrafiltration (UF), Microfiltration (MF), Membrane Distillation (MD), Polymer Assisted Ultrafiltration (PAUF), Supported Liquid Membranes (SLM), Polymer Inclusion Membranes (PIM), etc. reported for decontamination of radionuclides [16].

Among the various membrane separation processes, reverse osmosis, nanofiltration, ultrafiltration and microfiltration are proven to be most versatile methods that are used for the treatment of radioactive waste. These filtration methods involve applying of pressure to the solution loaded on one side of selective membrane for removal of colloids, large molecules or ions.

1.4.1.1 Reverse Osmosis (RO) and Nanofiltration (NF)

RO process is applied for the treatment of effluents containing uranium. In this process, uranium content in permeate is reduced to less than 1 mg L^{-1}, where the removal of uranium is 99.5 % or higher [17,18]. Prabhakar et al. [19] used polyamide based RO, NF and UF membranes and conducted experiments with real effluents containing specific activity levels in 10 kBq/L. It is reported that the level of radioactive contaminants could be reduced from 10 kBq /L to few Bq/L by RO and NF whereas UF failed to remove the radioactive contaminants. Garrett [20] conducted experiments on RO to remove uranium, technetium, tritium, strontium and cesium from liquid effluents and groundwater. It was demonstrated that all of above contaminants could be removed to less than the regulated limits, except tritium. RO process was also applied for decontamination of radionuclides such as ^{137}Cs, ^{90}Sr, ^{103}Ru, ^{60}Co and ^{131}I using volcanic tuff, a natural zeolite and cellulose acetate membrane [21, 22].

Studies on selective removal of uranium from aqueous solution using various nanofiltration membranes showed relatively high selectivity, despite of high concentration of other divalent and monovalent cations [23, 24]. It is also reported that selective removal of cobalt species from simulated nuclear liquid waste was achieved along with partial separation of monovalent ionic species using various NF membranes [25, 26].

1.4.1.2 Ultrafiltration (UF) /microfiltration (MF) combined with sorption/precipitation/ complexation

UF and MF membranes have large pore size and they are not effective in retaining radioactive metal ions. Hence, in order to remove the radioactive ions, size enhancement of radioactive species by means of sorption/precipitation/ complexation before they are subjected to UF/MF known as seeded UF/MF process (SUF or SMF). SUF experiments conducted with ^{239,240}Pu and pseudo-colloids of iron in water having dissolved organic carbon (DOC) in the range of 10-60 mg/L revealed that in the presence of DOC, the colloidal size of Fe increases and acts as a matrix for high sorption of plutonium [27]. Studies on ferric hydroxide precipitation followed by micro-filtration (MF) for the treatment of LLW containing ^{241}Am showed that the removal of ^{241}Am is > 99.9 % and decontamination factor (DF) is >1651[28].

Studies on precipitation of cesium and strontium using copper ferrocyanide and calcium phosphate followed by filtration showed that the DF is in the range of 200–300 for cesium and 200 for strontium [29]. Co-precipitation followed by microfiltration (CPMF) process employed for removal of Sr from low level liquid waste showed that DF increases with increase in dosage of sodium carbonate [30]. Adsorption of Cs from liquid waste using $K_2Zn_3[Fe(CN)_6]_2$ adsorbent followed by microfiltration showed that the removal is 99.4 % [31]. Nickel hexacyanoferrate effectively bound cesium to help its removal by a membrane. The removal of cesium could be further enhanced by the addition of surfactant, sodium dodecyl sulfate (SDS). DF for Cs increased from 100 to 300 (with 400 mg/L surfactant) [32]. It is also reported that recovery of ^{241}Am is accomplished using SDS micellar solution at pH > 3 [33].

1.4.1.3 Membrane Distillation (MD)

Membrane Distillation (MD) is based on the relative volatility of various components in the feed solution. Separation occurs when solvent vapor passes through the membrane pores by a convective or diffusive mechanism [34]. The advantage of MD is the possibility of concentrating the solute in single stage process, avoiding sorption of ions such as ^{60}Co, ^{137,134}Cs inside the membrane pores and hence, elimination of fouling and minimization of secondary waste generation [35]. MD is best suited for treatment of low and intermediate level radioactive wastes. The application to high level liquid waste is limited owing to radiation instability of polymer based membranes.

1.4.1.4 Polymer assisted Ultrafiltration (PAUF)

The water soluble metal chelating polymers coupled with UF is a technology under development for selective concentration and recovery of valuable metal ions from wastewater. PAUF is a combination of ion exchange or chelating property of a functionalized water soluble polymer and sieving power of an ultra filtration membrane. Since, molecular weight of metal polymer complex is larger than the molecular weight cut-off of the membrane, they are concentrated in the retentate and the permeate is free from the metal ions. The polymers could be regenerated by changing pH of the solution. The water soluble polymers especially polyethyleneimine (PEI) and its derivatives, polyacrylic acid (PAA), polyallylamine, polyvinyl alcohol (PVA), polyvinylsulfonic acid (PVSA), copolymer of acrylic and maleic acid, polydiallydimethyl ammonium chloride (poly DADMAC), polybrene (PB), phosphonic acid polymer, chitosan, carboxymethyl cellulose and naturally available humic acid were shown to be effective for enrichment and removal of radionuclides from aqueous waste [36-51].

1.4.2 Solid Phase Extraction (SPE)

Separation based on solid phase extraction (SPE) also known as solid–liquid extraction is developed considerably in the last few decades due to their simplicity, rapidity, easy operation and cost effectiveness. The basic principle of SPE is transfer of metal ions from aqueous phase to the active sites of adjacent solid phase. The mechanism involves in SPE depends on the nature of the sorbent and metal ions. SPE is carried out by means of adsorption, ion exchange, chelation, ion-pair formation, etc. The metal ions sorbed on the solid phase shall be desorbed by changing the condition or using a suitable eluate and thus recovered.

Various types of sorbents such as organic [52,53], inorganic [54-57], bio-sorbent [58], composites [59] and carbon based material [60,61] have been developed for the recovery of radionuclides. The choice of sorbent material depends on its selectivity, efficiency, ease of preparation and cost effectiveness. Among the solid sorbents, chelating resins are being increasingly used due to their high adsorption capacity and selectivity. These chelating resins are prepared either by coating/impregnating or chemically bonding/grafting the chelating agents on solid substrate. Generally, the adsorption efficiency depends on the type of chelating agent and to some extent on the size and physiochemical properties of the resin. The choice of appropriate chelating agent is a critical factor to obtain maximum recovery. The classification of chelating resins based on the solid supports and their performance on removal of radionuclides are summarized below.

1.4.2.1 Amberlite XAD Resin

Carboxymethyl-1-methylcalix[4]resorcinarene [62], p-*tert*butylcalix[8]arene [63], *o*-vanillin semicarbazone [64] and bicine [65] chelating functional groups impregnated/grafted into Amberlite XAD-4 resin have been studied for removal/preconcentration of U(VI) and Th(IV) from aqueous solution. TBP impregnated on amberlite XAD-4 and XAD-7 polymeric supports are reported to be efficient for separation of U and Pu from Am and fission products in nitric acid medium. It is also reported that this resin is capable of separating traces of U and Pu from aqueous solutions [66-69]. CMP, CMPO and bifunctional organophosphorus (TBP+CMP, TBP+CMPO) compounds have been impregnated in XAD-4 and studied for selective extraction of actinides and lanthanides in nitric acid medium [70,71]. CMPO-TBP/XAD-7 system for the sequential separation of actinides (U, Pu, Am) and lanthanides (Eu, Ce) have been studied and it is reported that 98 % of U, Pu, Am, Eu and Ce were removed from solution in 4M nitric acid medium [72]. Grafting of 4-ethoxy-N,N-dihexyl-butamide (EDHBA) on AXAD-16 support was studied for selective separation of U(VI), Th(IV), La(III) and Nd(III) from high acidic matrices [73]. This amide grafted polymeric matrix is reported to possess high distribution ratio with maximum metal sorption capacities in 6M nitric acid. Chemical modification of Amberlite XAD-16 polymeric matrix with

[(2-dihydroxyarsinoylphenylamino)-methyl] phosphonic acid [74] is reported to possess impressive enrichment factors, viz. 365 and 300 for U(VI) and Th(IV) respectively.

1.4.2.2 Merrifield Resin

Selective extraction and sequential separation of lanthanides, Th and U from both acidic waste and environmental samples were studied using (dimethyl aminophosphonomethyl)phosphoric acid (DADPA) and CMPO grafted on Merrifield chloromethylated styrene-divinylbenzene resin (MCM) [75, 76]. The DADPA-MCM polymeric resin has the ability to extract both actinides and lanthanides in both acidic and near neutral conditions. CMPO/MCM resin has been successfully applied for the extraction of Th(IV) from high matrix monazite sand, U(VI) from sea water and both U(VI) and Th(IV) from nuclear wastes at high acid medium. Chemical anchoring of N,N’-dimethyl-N,N'-dibutylmalonamide (DMDBMA) with MCM resin appears promising for the separation of Am, Pu and U from their mixtures. The grafted resin is reported to possess superior binding for hexavalent and tetravalent metal ions such as U(VI) and Pu(IV) over trivalent metal ions viz. Am(III) and Pu(III). This resin could be used for pre-concentration of U and Pu from environmental and waste effluent [77,78]. MCM resin anchored with di-bis(2-ethylhexylmalonamide) (DB2EHM) [79] showed high binding affinity for U(VI) over Th(IV) and other diverse ions even under high acidity. Thenoyl trifluoroacetone [80], 11,23-disemicarbazono-26,28-*n*-dipropoxy-25,27-dihydroxy calix[4]arene semicarbazone [81] and quinoline-8-ol [82] crosslinked onto MCM resin offer quantitative extraction of U(VI) and Th(IV) in both aqueous and nitric acid medium. DB2EHM anchored resin has been tested for extraction of above actinides from a synthetic nuclear spent fuel solution. Calix[4]arene semicarbazone derivative of MCM resin [83] showed reasonably good extraction behavior for U(VI) and Th(IV) and is applied to monazite sand and some standard geological materials. Anchoring of a simple molecule like quinoline-8-ol to MCM resin offers 100-fold enrichment of uranium (VI) with maximum sorption capacity of 120.3 mg g^{-1} of resin [82].

1.4.2.3 Other Chelating Resin

TRU (Transuranium elements) resin consists of bifunctional organophosphorous extractant (TBP + CMPO) sorbed on an inert polymeric substrate known as Amberchrom CG 71ms [84]. This resin permits rapid and selective sorption of tri-, tetra- and hexavalent actinides from nitric acid media and their sequential elution by a choice of conditions [84-86]. The feasibility of using TRU resin for recovery of minor actinides from a Hanford tank waste has been reported [87]. Selective separation of U(VI) and Th(IV) with high recoveries using TRU-spec resin is also reported [88]. TEVA (TEtraVAlent actinides) resin consists of Aliquat™ • 336 (a mixture of trioctyl and tridecyl methyl ammonium chlorides) extractant impregnated in Amberchrom CG-71ms (Supelco) by means of dry impregnation method [86]. The TEVA resin is reported to be highly selective for tetravalent actinides in a wide range of nitric acid and hydrochloric acid concentrations. It is also reported that using solutions containing 1 M ammonium thiocyanate and 0.1 M formic acid as eluent, it is also possible to achieve a separation of trivalent actinides from lanthanides [86,89]. Sorption of several actinides [U(VI), Th(IV), Am(III), Cm(III)] and fission products from nitric acid solution on two novel chromatographic sorbents such as 2-(2-hexyloxy-ethyl)N,N′-dimethyl-N,N′-dioctylmalonamide (DMDOHEMA) and N,N,N′,N′-tetraoctyl-3-oxapentane-1,5-diamide (TODGA) impregnated on the Amberchrom®CG-71C have been reported [90,91]. TODGA resin exhibit large weight distribution ratio than that of DMDOHEMA resin for actinides as well as lanthanides.

A new poly(styrene-hydroxylamine) supported calix[6]arene hydroxamic acid resin has been used for chromatographic separation of U(VI), Th(IV) and Ce(IV) from monazite sand and environmental samples [92]. Extraction chromatography with TBP impregnated on a polystyrene support (Lewatit OC 1023) has been used for general actinide separation [93]. Chromatographic extraction with CMPO showed effective separation of minor actinides from PUREX high-level waste. A system comprising CMPO sorbed on chromosorb-102 has shown high uptake of both actinides and lanthanides from 0.5 to 6.0 M nitric acid [70].

1.4.3 Chemical Precipitation

Chemical precipitation is the oldest large-scale technique employed for the separation of radionuclides. It is a physio–chemical process in which soluble metal ions are converted into insoluble metal salts (precipitates) by the addition of a precipitating agent. Precipitates, which are small or colloidal, are then coagulated, flocculated, settled or filtered out of solution. Precipitation process is best suitable for the treatment of large volume of liquid waste containing relatively low concentration of radioactive elements. This process concentrates the radioactive ions present in a liquid waste stream into a small volume of wet solid that can be separated from the bulk. The process is fairly versatile and used to treat a wide variety of waste streams, including those containing large amount of particulates or high concentration of salts.

Generally, radionuclides are removed from solution by one or more of the following mechanisms (i) co-precipitation with the carrier, (ii) sorption into particulates present in the waste streams and (iii) sorption onto the floc [94]. Effective removal of metal ions depends on the following parameters which include (i) maintenance of proper pH throughout the precipitation process and subsequent settling time, (ii) excess addition of precipitating agent to drive the process towards completion and (iii) effective removal of precipitated solids. During precipitation, non-radioactive contaminations are also getting removed along with radioactive metal ions. A wide range of chemical reagents are now in use and mixtures of precipitants are also employed for improving overall decontamination [95]. The required quantities of precipitating agent depend on the chemical composition of the liquid waste.

Several precipitants are reported for removal of various radionuclides. The most efficient precipitants for each type of radionuclides are mentioned in Table 1.1 [96].

Table 1.1. Precipitant process for specific decontamination

Nuclides	Precipitant	pH	DF
α emitter	Ferric hydroxide	7-12	>1000
^{51}Cr	Ferrous hydroxide	≥ 8.5	>100
^{54}Mn	Mangenese hydroxide Manganese dioxide	≥ 8.5	>100
$^{58+60}$Co ^{59}Fe	Ferrous or Ferric hydroxides	≥ 8.5	>100
^{90}Sr	Calcium or iron phosphate	>11	>100
	Calcium carbonate	10.5	>100
	Barium sulphate	≥ 8.5	>100
	Manganese dioxide	>11	>100
^{95}Zr ^{95}Nb $^{141+144}$Ce	Ferric hydroxide	>8.5	>1000
$^{103+106}$Ru	Ferrous hydroxide	8.5	5-10
	Copper + ferrous hydroxides	8.5	10-25
	Cobalt sulphide	5-8.5	50-150
$^{124+125}$Sb	Ferrous hydroxide	8.5	5-10
	Titanium hydroxide	5-8.5	10-100
$^{134+137}$Cs	Ferrocyanide (Ni-Cu-Co-Zn)	6-10	>100
	Zeolites	7-11	10

1.5 Thesis objective

Safe management of radioactive waste with minimum impact to environment is emerging as one of the major challenges in separation science. Decay is the only natural way of reducing radioactivity. Since radionuclides have decay rates ranging from days to thousands of years, proper segregation of wastes depending on their half-lives and conditioning are important factors in the overall scheme of radioactive waste management. HLW is managed by using vitrification procedure in suitable matrices and safe disposal in deep geological repository. The strategy for management of LLW and ILW lies in development of innovative processes resulting volume reduction as one of the important criteria.

The major aim of radioactive waste management is to separate long lived alpha emitting radionuclides which belong to the actinide series of the periodic table. Being “hard” Lewis acids, actinide ions in aqueous solution show strong tendency to form complexes with “hard” donor-ligands (‘O’ or ‘F’ as donor atoms) rather than “soft” donor-ligands (‘N’, ‘S’ or ‘P’ as donor atoms). Binding in aqueous solution to soft donor atoms occurs via chelation with multidentate ligands, which contain bonds to both the soft donor and hard oxygen donor [97]. Recovery of actinides from aqueous waste using chelating agent containing >P=O, >C=O or other functional groups of desired basicity and stereochemistry have been extensively studied in recent years [77]. Amide based chelating agents are particularly interesting because of their innocuous degradation products and high radiolytic stability than those of traditionally used organophosphorous compounds in actinide separation. Also, stripping of actinides from amide containing ligands is relatively easy. In addition, the amide ligands are completely incinerable so that the amount of secondary wastes generated in nuclear waste treatment could be significantly reduced [77-79].

Advances in macromolecular chemistry such as invention of dendritic polymers are providing unprecedented opportunities to develop effective separation processes for treatment of waste water. A brief introduction about dendrimers and their potential application in separation science is described below.

1.6 Dendrimer

Dendrimer macromolecules are a new class of polymeric material with tree-like architecture (after linear, cross-linked and branched polymers) having unique properties such as high degree of branching unit, high density of surface functional group and narrow molecular weight distribution. Unlike other polymers (where atom-by-atom control is not feasible and polydispersity is an inherent character), dendrimers are characterized by monodispersity (i.e., all dendrimer molecules are of uniform and controllable size) [98,99]. The word dendrimer is derived from the Greek words dendri- (tree branch like) and meros (part of) and was coined by Tomalia et al [100]. Dendrimers comprise of three covalently bonded components: a core, interior branch cells, and terminal branch cells (Fig.1.2). Dendrimers are constructed through a sequence of iterative chemical reaction procedure that builds up from the molecular level to the nanoscale level. The each iteration is known as a generation (G_1, G_2…..) and has twice the complexity of the prior generation. The size of dendrimers ranges between 1 and 20 nanometers. Both architecture and composition can be highly controlled in these monodisperse polymers. Synthesis techniques allow molecular design parameters, including size, shape, surface/interior chemistry, flexibility, and topology to be almost completely ordered. Fig.1.2 provides a schematic of a generalized dendrimer structure.

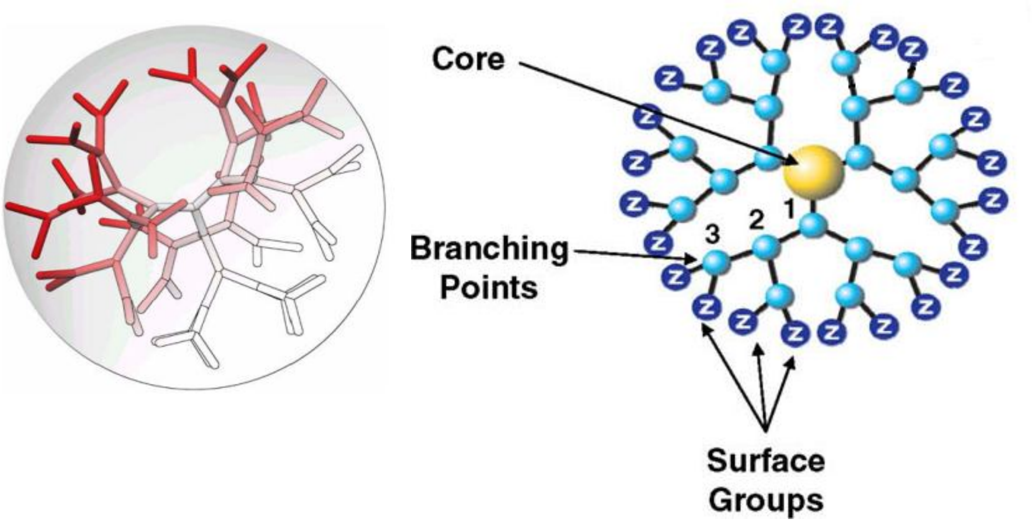

Fig.1.2 Schematic of a generalized 3D and 2D view of dendrimer structure [101]

As the dendrimer branches in a predictable manner, large voids can exist within the dendrimer. Both size and physical nature (e.g., hydrophobic or hydrophilic characteristics) of these voids can be controlled during synthesis by judicious selection of both length and composition of branch backbone. These voids can be used for trapping materials such as metals, molecules (organic and inorganic) and even other nanoparticles. Dendrimers can easily move across biological membranes and hence they are used as (i) carriers of genetic material into cells [102], (ii) drug delivery agents [103] and (iii) diagnostic imaging agents [104].

As the number of generations of the dendrimer increases, the total surface area increases dramatically. Current expertise in dendrimer synthesis also allows for attaching more than one type of functional group in the dendrimer, thus offering the possibility of synthesizing multifunctional molecules. Terminal groups can be chemically modified to alter solubility, binding capacity and specificity of the dendrimer. It has been suggested that amphipathic dendrimers could be synthesized by covering one half of the molecule (or one hemisphere) with hydrophobic groups and the other half with hydrophilic groups. It can also be used as (i) recyclable unimolecular micelles for recovering organic solutes from water [105] and (ii) scaffolds and templates for the preparation of redox and catalytically active nanoparticles [106]. Currently, dendrimers are also under investigation as metal sequestering agents for waste remediation technologies [107] and for the removal of metal ions from aqueous waste streams [108]. The highly branched molecules with numerous functional groups can be formulated to provide the required properties of water solubility, selectivity and high loading capacity and so on. The control over size, shape and surface functionality makes dendrimers one of the “smartest’ or customizable nanomaterial. The use of poly(amido)amine (PAMAM) and poly(propylene)imine (PPI) dendrimers and their derivatives in combination with ultra filtration technique have shown potential applications in removal of metal ions such as Cu(II), Ni(II), Co(II), Pd(II), Pt(II), Zn(II), Fe(III), Ag(I), Au(I) and U(VI) from dilute aqueous solution [108-110]. The modified PAMAM and poly(propyleneimine) dendrimers also described as "nanosponges" for the removal of polycyclic aromatic hydrocarbons [111].

1.7 Motivation for the present study

Three architectural components in dendrimer such as core, interior branching and peripheral groups essentially determine the physical and chemical properties, as well as the overall size, shape and flexibility of the dendrimer. The water soluble PAMAM dendrimer chelating agent has been extensively studied for removal of metal ions from aqueous solution. The strength of metal-ligand interaction is influenced by factors such as nature of functional group and density of the chelating agent, ionic potential of the metal, stereochemistry, steric constraints as well as electrostatic interactions. In PAMAM dendrimers, functional groups such as amide, tertiary, and primary amines are arranged in regular "branched upon branched" patterns showing strong chelating action with metal ions. Also, the ability to introduce various terminal functional groups in dendrimer affords development of versatile metal chelators. Hence the significance of dendrimers as an effective chelating ligand for removal of radionuclides from aqueous wastes constitutes the primary motive of the present work.

1.8 Over view of thesis

The aim of the present study is to explore the use of dendrimer macromolecules for the removal of radionuclides from aqueous waste by using common treatment processes such as membrane separation, adsorption and chemical precipitation.

Removal of radionuclides from aqueous waste have been studied by using the following four indigenously developed compounds, (i) PAMAM dendrimer chelating ligand, (ii) PAMAM dendron grafted - styrene divinyl benzene (PAMAM-SDB) chelating resin, (iii) Diglycolamic acid functionalized -PAMAM dendron- styrene divinyl benzene (DGA-PAMAM-SDB) chelating resin and (iv) Xanthate Functionalized Dendrimer (XFPD).

Chapter 2 comprises the synthesis, purification and characterisation of the above four chelating agents. Removal of U(VI) and Th(IV) metal ions from aqueous solution by Ultrafiltration (UF) and Dendrimer Assisted Ultrafiltration (DAUF) were studied using regenerated cellulose acetate membrane and PAMAM [poly(amido)amine] dendrimer. Studies were carried out to understand the effect of metal ion speciation on removal of U(VI) and Th(IV) by UF and PAMAM dendrimer assisted UF. Effect of pH, ionic strength, PAMAM dendrimer concentration and dendrimer generation on metal ion retention was investigated. Selectivity of PAMAM dendrimers towards U(VI) and Th(IV) ions and their recovery and regeneration were examined. The comprehensive compilation of results from these studies forms **chapter 3**.

Adsorption behaviour of U(VI) and Th(IV) metal ions from aqueous medium on poly(amido)amine dendron grown on the surface of styrene divinylbenzene (PAMAM-SDB) was investigated. The effect of contact time, pH, ionic strength, adsorbent dose, initial metal ion concentration, dendron generation and temperature on adsorption capacity of U(VI) and Th(IV) metal ions were also studied. The results from these studies are summarized in **chapter 4**.

PAMAM-SDB chelating resin surface was modified with diglycolamic acid functional group (DGA-PAMAM-SDB). Adsorption of U(VI) and Th(IV) metal ions on DGA-PAMAM-SDB chelating resin from aqueous and nitric acid medium was studied. The effect of contact time, pH, ionic strength, adsorbent dose, initial U(VI) concentration, dendron generation and temperature on adsorption capacity of U(VI) and Th(IV) metal ions were investigated. The results from these studies are discussed in **chapter 5**.

Chapter 6 focuses on decontamination of radioactive waste by using XFPD. It also addresses coordination behaviour of XFPD chelating agent with copper, cobalt (representative of radioactive transition metal ions) and europium (representative of lanthanide ions and surrogate of americium) metal ions in aqueous solution. The effect of pH and ionic strength on metal ion removal was investigated. The metal leachability and stability characteristics of metal-XFPD complexes were also investigated. Summary of the present work and scope for further development are consolidated in **chapter 7**.

Chapter-2

EXPERIMENTAL

This chapter describes the synthesis, purification and characterization of compounds such as poly(amido)amine (PAMAM), xanthate functionalized PAMAM dendrimer (XFPD), PAMAM-styrene divinyl benzene (PAMAM-SDB - solid supported PAMAM dendron) and diglycolamic acid functionalized PAMAM-SDB (DGA-PAMAM-SDB). The characterization of chelating agents using UV-Vis, FTIR, NMR, MALDI-MS, HPLC, SEC, DLS, SEM, TGA and potentiometric titration are presented. The details of various analytical techniques used in the present study are briefed. The preparation procedure of standard solutions, reagents and analytical methods used for the estimation of metal ions are described.

2.1 Chemicals and preparation of solution

2.1.1 Chemicals

Ethylenediamine (EDA) used for the synthesis was purified by vacuum distillation over calcium hydride. Analytical grade methyl acrylate (MA), tris(hydroxymethyl)amino methane (tris buffer), potassium carbonate, carbon disulphide (CS_2) and diglycolic anhydride (90 %) were used as such for synthesis. Dry methanol and dry dimethyl sulfoxide solvents were used for synthesis. Analytical grade toluene and methanol were used to remove EDA from reaction mixture by azeotropic vacuum distillation.

Merrifield resin-chloromethylated (1-1.3 mmol/g) styrene divinyl benzene (CSDB) with size in the range of 200-400 mesh was used as a solid support for the synthesis of chelating resin.

2.1.2 Standard solutions

Uranyl nitrate hexa hydrate (Analar, BDH, England), Thorium nitrate tetra hydrate (Fisons Philadelphia, USA), $Eu(NO_3)_3.5H_2O$ (99.9 %) (Sigma Aldrich), $CuCl_2.2H_2O$ (98 %) (Loba Chemi), $Co(NO_3)_2.6H_2O$ (98 %) (Sigma Aldrich), $Cs(NO_3)_2$

(> 99 %) (Aldrich), $Sr(NO_3)_2$ (>99 %) (Sigma Aldrich), $La(NO_3)_3.6H_2O$ (99.99 %) (Spectrochem), $Zn(NO_3)_2.6H_2O$ (98 %) (Acros), $Ni(NO_3)_2.6H_2O$ (> 98.5 %) (Sigma-Aldrich), $Ba(NO_3)_2$ (> 99 %) (Sigma-Aldrich) and $MnCl_2$ (97 %) (Aldrich) was used to prepare standard solutions by dissolving the required quantity in Millipore water (resistivity 18.2 MΩ.cm). Stock solutions of Ce, Nd, Sm, Gd metal ions were prepared from their oxides. These metal oxides were converted into nitrates by dissolving in concentrated nitric acid, evaporated to dryness and then diluted with water.

2.1.3 Acid solutions

Acid solutions (Nitric, phosphoric, hydrochloric and acetic acid) of various concentrations were prepared from AR grade of concentrated acids by suitable dilution. The acidity of the solutions were determined by titrating with standardized NaOH using phenolphthalein as indicator. Sodium hydroxide solution was standardized against potassium hydrogen phthalate.

2.1.4 Simulated Nuclear Liquid Waste (SNLW)

Simulated nuclear liquid waste was prepared by mixing required volume of standard solutions of various metal ions. The composition of SNLW is given in Table 2.1.

2.1.5 Radioactive liquid waste (RLW)

RLW was prepared by spiking high level waste (HLW) arising from reprocessing of mixed carbide fuel, $(U_{0.3}Pu_{0.7})C$, irradiated to the burn-up of 155 GWd/Te in Fast Breeder Test Reactor (FBTR) situated at Kalpakkam in India. The activity of each element in RLW is given in Table 2.1.

Table 2.1 Composition of SNLW and RLW

SNLW		RLW	
Metal ion	**Conc. (mg L^{-1})**	**Metal ion**	**Activity (dps)**
La	68	^{54}Mn	21.30
Ce	66	^{144}Ce	1.14×10^{4}
Nd	64	^{106}Ru	1.05×10^{3}
Gd	78	^{154}Eu	45.30
Sm	72	Nd	-
Mn	25	^{95}Zr	21.39
Co	30	^{60}Co	2.46
Ni	42	Ni	-
Zn	37	Zn	-
U	103	U	-
Th	104	Th	-
Ba	70	^{125}Sb	3.95×10^{2}
Sr	66	^{90}Sr	-
Cs	70	^{137}Cs	1.13×10^{4}

2.1.6 Reagents

Phenolphthalein: About 500 mg of phenolphthalein was dissolved in 100 mL of 1:1 mixture of ethanol and water.

Arsenano (III): About 200 mg of arsenazo (III) [2,2'-(1,8-dihydroxy-3,6-disulfonaphthalene-2,7-bisazo)bisbenzenearsonic acid] was dissolved in 200 mL of 9:1 mixture of water and ethanol.

Methyl Red: About 100 mg of methyl red (2-(N,N-dimethyl-4-aminophenyl) azobenzenecarboxylic acid) was dissolved in 30 mL of ethanol and then diluted to 100 mL using millipore water.

Nitroso R–salt: About 1 g of nitroso R-salt (sodium 1-nitroso-2-hydroxynaphthalene-3,6-disulfonate) was dissolved in 100 mL of Millipore water.

Sodium acetate buffer: About 125 g of sodium acetate was dissolved in 150 mL of water and after filtering thorough whatmann-40 filter paper, the solution was diluted to 250 mL with water.

2.2 Instruments

Solution pH was measured using cyberscam 100 pH meter (Eutech). Distillation was carried out using a rotary evaporator (Equitron). Turbidity meter (Hach) working in the range of 0-1000 NTU was used to measure turbidity of the solutions. Vacuum oven (SEMCO) was used for drying the samples. KS 4000i control-incubator shaker (IKA make) was used for equilibration studies. Refrigerated centrifuge machine (REMI-C-24 BL) was used for centrifugation. Ultrasonic bath (Life-care-EN 50US) was used for preparing uniform suspension of chelating resin in the solution. Mettler AE240 single panel balance was used for weighing the samples.

2.2.1 Ultrafiltration device

Centrifugal ultrafiltration device (Amicon Ultra-15) with molecular weight cutoff of 3000 Dalton (purchased from Millipore) was used for UF and DAUF. Filter unit is made of co-polymer of styrene and butadiene and the membrane is made of regenerated cellulose with active surface area of 7.60 cm^2.

2.3 Analytical techniques

2.3.1 Thin layer chromatography (TLC)

The progress of PAMAM dendrimer synthesis reaction and its purity after column chromatographic separation were monitored by TLC. Experiments were performed using Silica Gel 60 F_{254} Merck TLC plate (an aluminium sheet coated with a thin layer of silica-0.2 mm) in a mixture of dichloromethane and methanol (9:1-7:3) solvent. The spots on the TLC plate were visualized by placing in iodine vapour.

2.3.2 Column chromatography

The reaction products were purified by using silica gel and size exclusion column chromatography. The 5 × 50 cm column was packed with silica gel (200-400 mesh; Merck) and mixture of dichloromethane and methanol as eluent. In size exclusion chromatography, the column was packed with Sephadex LH-20 (25-200µ) (Sigma-Sephadex$^{@}$ Amersham Bioscience Limited) and methanol as chromatographic eluent [112].

2.3.3 High Performance Liquid chromatography (HPLC)

JASCO PU-1580 module HPLC system with UV-VIS detector (model UV-1570) was used for chromatographic separation studies.

Reverse phase-HPLC: Both purity and growth of dendrimer generations were analyzed using RP-HPLC. A Reprosil Gold 300 × BD silica based C_{18} RP-HPLC column (250 × 4.6 mm, 5µm) supplied by Merck Specialties Private Limited, India was used for separation. Mobile phase for elution of PAMAM dendrimer of various generations was a linear gradient beginning with 100:0 (v/v) water/acetonitrile (ACN) mixture at a flow rate of 1 mL/min reaching 50:50 after 30 min. Trifluoroacetic acid (TFA) at 0.1% (v/v) concentration in water as well as in ACN were used to modify the dendrimer surface [113]. The detection of eluted samples was performed at 210 nm.

Size exclusion chromatography (SEC): SEC was used to monitor the growth of dendrimer generation and determining the molar mass of the synthesized PAMAM dendrimer. SEC experiments were performed using Yarra 3u SEC-2000 column (300 × 7.8 mm) purchased from Phenomenex, Hydrebad, India. Phosphate buffer (0.05M Na_2HPO_4, 0.05M NaH_2PO_4, and 0.15M NaCl) in water was used as a mobile phase. The pH of the mobile phase was adjusted to 6.8 using HCl and the flow rate was maintained at

1mL/min. Molecular mass of the PAMAM dendrimers was determined by comparing with SEC standards (catalogue No: 151-1901) purchased from BIO-RAD, India.

2.3.4 FTIR spectrometer

FTIR spectra were recorded in between 500 cm^{-1} and 4000 cm^{-1} with 16 cm^{-1} resolution using ABB-MB3000 FTIR instrument. Based on the physical state of compounds, various techniques such as transmission, Attenuated Total Reflectance (ATR) and Diffuse Reflectance Infrared Fourier Transform Spectroscopy (DRIFTS) were used to record the IR spectra.

Transmission: This technique involves transmission of infrared energy through the sample and detecting that portion of the beam that is transmitted, i.e. not absorbed. IR spectra of metal-XFPD complexes were recorded using this technique.

ATR: Attenuated Total Reflectance (ATR) technique measures the changes that occur in a totally internally reflected infrared beam when the beam is in contact with the sample. IR spectra of dendrimers were recorded using this technique.

DRIFTS: This technique collects and analyzes scattered IR radiation. IR spectra of dendron chelating resins were recorded using this technique.

2.3.5 Nuclear magnetic resonance (NMR) spectroscopy

^{1}H and ^{13}C-NMR spectra of dendrimers were recorded using Bruker 400/500 MHz spectrometer. $CDCl_3$, DMSO and D_2O were used as solvents.

2.3.6 Mass spectrometry (MS)

Mass spectra of synthesized dendrimers were recorded using Voyager-DE™ PRO Matrix Assisted Laser Desorption Ionization-Time of Flight (MALDI-TOF) Biospectrometry. In this technique, single charged ions are being produced predominantly allowing for determination of direct mass number of dendrimer [114]. In MALDI analysis, 10mg/mL of 2,5-dihydroxybenzoic acid (DHB) or α-cyano-4-hydroxycinnamic acid (CHCA) in acetonitrile/water (50:50) was used as the matrix. A dendrimer solution was prepared by dissolving 1 mg of dendrimer syrup in 1 mL of water. The analytical sample for the MALDI analysis was prepared by mixing the dendrimer solution (1 µL) with the matrix solution (1 µL) on a stainless steel probe tip and this mixture was allowed to dry at room temperature. Nitrogen pulsed laser of 337 nm was used for desorption.

2.3.7 Dynamic Light Scattering (DLS)

Mean size of PAMAM as a function of dendrimer generation was measured by using a Zetasizer-Nano (Malvern Instrument, UK). It uses a He-Ne laser (4 mW, $\lambda = 633$ nm) and avalanche photodiode detector and measures the scattering information at an angle close to 180^o (the detector position is at 173^o).

2.3.8 Scanning Electron Microscope-Energy Dispersive Spectrometry (SEM-EDS)

Surface morphology, porous structure of chelating resins and particle size of the metal-XFPD precipitates were studied by using scanning electron microscope (FE-SEM-ZEISS make). Energy dispersive spectra (EDS) were used for in-situ chemical analysis of the metal-XFPD precipitate.

2.3.9 X-ray photoelectron spectroscopy (XPS)

XPS technique was used to examine the oxidation state of metal ions in metal-XFPD complexes. Experiments were carried out using a VGEscalab MKII spectrometer using Al Kα ($h\nu = 1486.6$ eV) radiation as the X-ray source. The source characteristics were 15 kV and 20 mA. The base vacuum of the analysis chamber was 10^{-10} mbar. The binding energies (BE) were calibrated with C1s level of carbon at 285.1 eV in each sample.

2.3.10 Thermogravimetric Analysis (TGA)

Metler Toledo Star TG analyzer was used to study the thermal stability of chelating resins.

2.3.11 Potentiometer

Number of amino and DGA groups present in dendrimer/dendron chelating agents and their pKa values were determined by acid-base titration using PHM 100M digital potentiometer (Elixir electronic, Chennai).

2.3.12 Fluorimeter

Jobin Yvow-Spex Fluorolog fluorimeter was used to study the formation of europium–XFPD complex, the speciation of uranium in aqueous solution and its binding with PAMAM dendrimer.

2.3.13 UV-Vis Spectrophotometer

Concentrations of uranium, thorium and cobalt ions in aqueous solution were estimated by absorbance measurements using UV-Vis spectrophotometer (Hitachi 330). The procedures for estimation of above metal ions are described below.

Uranium estimation [115]**:** Uranium standard solution of 0.5 mL was taken in a 5 mL of glass tube followed by addition of 0.4 mL of 0.01M HCl, 0.4 mL of 0.1 % arsenazo(III) reagent and then diluted to 2 mL with 0.7 mL of water. The absorbance was measured at 655 nm after 10 minutes of colour development. The calibration graph was plotted for uranium concentration ranging between 4.2×10^{-6} M and 4.2×10^{-5} M. The unknown concentration of the analyte sample was estimated from the calibration curve.

Thorium estimation [115]**:** An aliquot of thorium standard solution was taken in a 10 mL standard flask followed by addition of 6 mL of concentrated 10 M nitric acid, 0.5 mL of 10 wt % sulphamic acid and then addition of 0.5 mL of 0.1 % Arsenazo-III after 5 minutes. The final volume was made up to 10 mL with water and absorbance was recorded at 660 nm after 15 minutes of colour development. The calibration graph was constructed for thorium concentration range between 2×10^{-6} M and 3.5×10^{-5} M. The unknown concentration of samples was estimated from the calibration curve.

Cobalt estimation [116]**:** An aliquot of cobalt standard solution was diluted with 7.5 mL of water in a 50 mL boiling tube followed by addition of 5 mL of sodium acetate buffer and 1 mL of Nitroso-R-salt. After 5 minutes, the solution was heated to boil for 1 minute following addition of 1 mL of conc.HNO_3 and then boiled for one more minute. After cooling in dark place the final solution was diluted with water in 25 mL standard flask. The calibration graph was plotted for cobalt concentration ranges between 1×10^{-5} M and 1×10^{-4} M by measuring the absorbance at 520 nm.

2.3.14 Gamma counter

Well type NaI (Tl) scintillation detector with single channel analyzer was used for counting gamma rays.

2.3.15 Inductively Coupled Plasma - Optical Emission Spectrometer (ICP-OES)

John Yvon Inductively Coupled Plasma - Optical Emission Spectrometer (ICP-OES) was used for determining the concentration of lanthanides and transition metal ions.

2.3.16 Atomic Absorption Spectrometer (AAS)

Analytica Janan NovAA300 Atomic Absorption Spectrometer (AAS) was used for determining the concentration of alkali and alkaline earth metal ions.

2.4 Experimental setup for synthesis

Dendrimers synthesis was carried out in four-necked cylindrical glass vessel. The four necks were used for addition of reagents, argon purging, fitting the water condenser and sampling of reaction mixture at various time intervals for monitoring the progress of the reaction (Fig.2.1). REMI magnetic stirrer was used for stirring the reaction mixture.

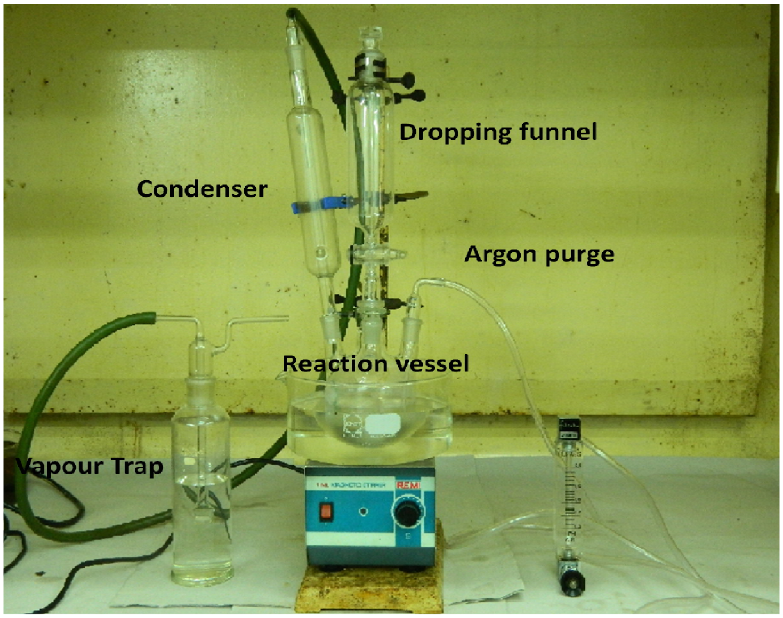

Fig.2.1 Experimental setup used for dendrimer synthesis

2.5 General methods for dendrimer synthesis

Dendrimers are generally synthesized either by divergent method or convergent method [117]. In **divergent method,** the dendrimer grows outwards from a multifunctional core molecule (Fig.2.2). The divergent approach is successful for the synthesis of symmetrical higher generation dendrimers. The difficulty in this approach is purification of the products.

In **Convergent method**, the dendrimer is constructed stepwise, starting from the end group and progressing inwards. When the growing branched polymeric arms, called dendrons, are large enough, they are attached to a multifunctional core molecule (Fig.2.2). In convergent growth method, the purification of desired product is comparatively easy. This approach does not allow the formation of high generations due to steric hindrance occurring during the reaction between dendrons and core molecule.

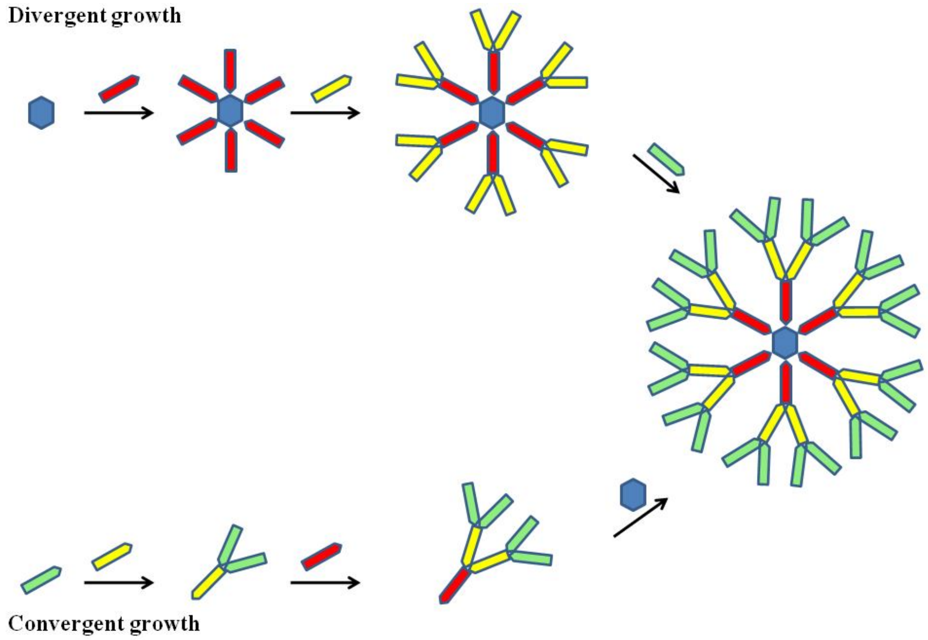

Fig.2.2 Scheme of divergent and convergent dendrimer synthesis

2.6 Synthesis of Poly(amido)amine (PAMAM) dendrimer

PAMAM dendrimer was synthesized by divergent method and it consists of two consecutive steps: Michael addition of primary amine to methyl acrylate followed by amidation of formed multiester with ethylenediamine (EDA). Michael addition of methyl acrylate leads to ester terminated half generation dendrimer, whereas amidation step gives amine terminated full generation PAMAM dendrimer [100].

2.6.1 Ester terminated PAMAM dendrimer ($G_{0.5}$)

A solution of freshly distilled ethylene diamine (EDA) in methanol was added drop wise into a magnetically stirred solution of methyl acrylate (MA) in methanol, under argon atmosphere, over a period of 2 h at 283 K. The mixture was allowed to warm to room temperature and stirred for further 24 h. The solvent and excess MA were removed from the reaction mixture by vacuum distillation and the resulting ester terminated

PAMAM dendrimer ($G_{0.5}$) was dried in vacuum oven for 12 h. The product was further purified using column chromatography.

2.6.2 Amine terminated PAMAM dendrimer (G_1)

The purified ester terminated PAMAM dendrimer ($G_{-0.5}$) was dissolved in methanol and then, slowly added to a magnetically stirred methanolic solution of EDA at 283 K. After complete addition, the mixture was stirred for 96 h at room temperature. The solvent was removed by vacuum distillation at 313 K. The excess EDA was removed by distillation with an azeotropic mixture of toluene and methanol (9:1) at 343 K. Amine terminated PAMAM dendrimer (G_1) was dried in vacuum oven for 12 h.

2.6.3 PAMAM dendrimer of higher generation

By repeating the above two steps, PAMAM dendrimer upto generation-5 (G_5) were synthesized. Overall chemical reactions involved in the synthesis of PAMAM dendrimer is given in Fig.2.3.

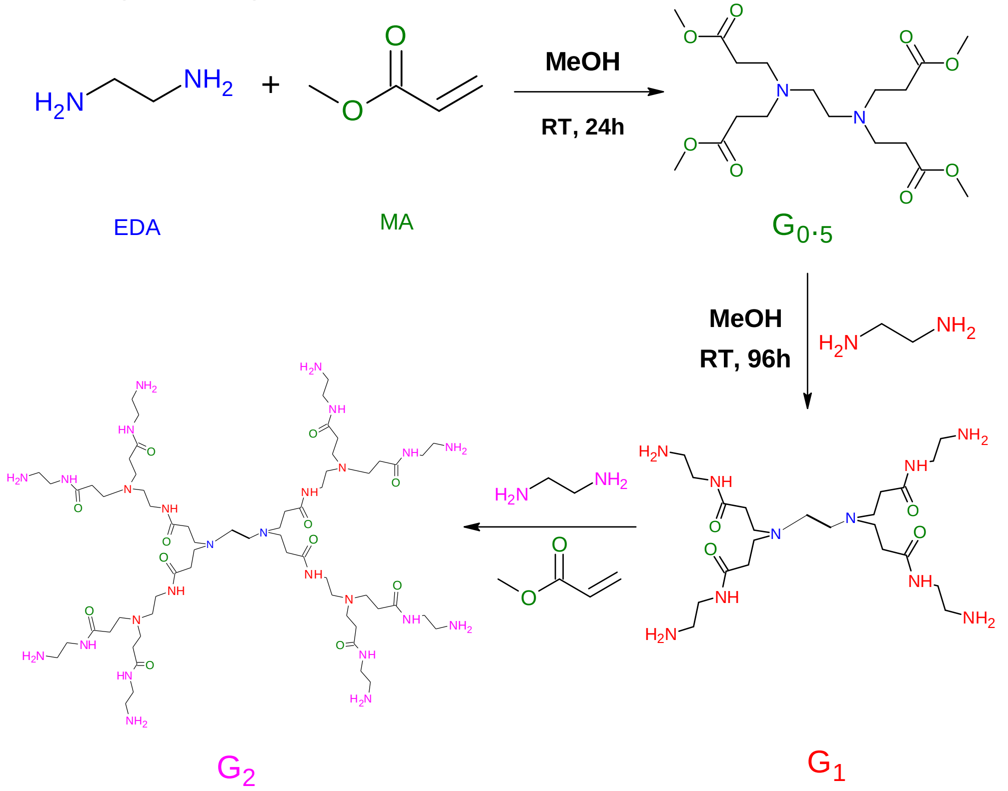

Fig.2.3 Synthesis scheme of PAMAM dendrimer

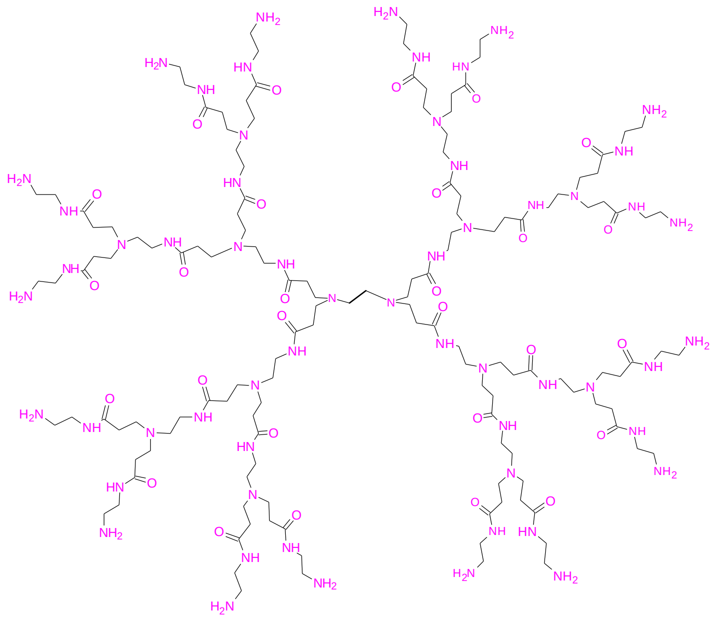

G_3

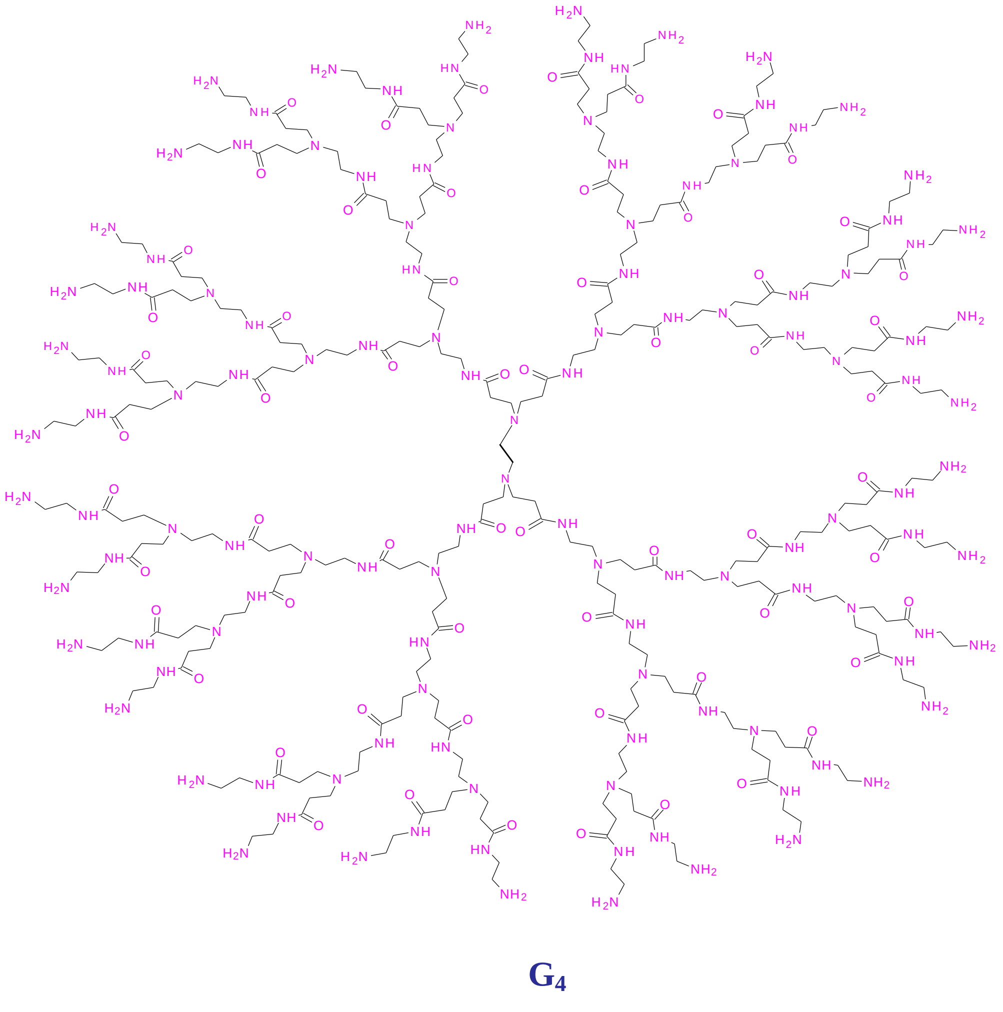

G_4

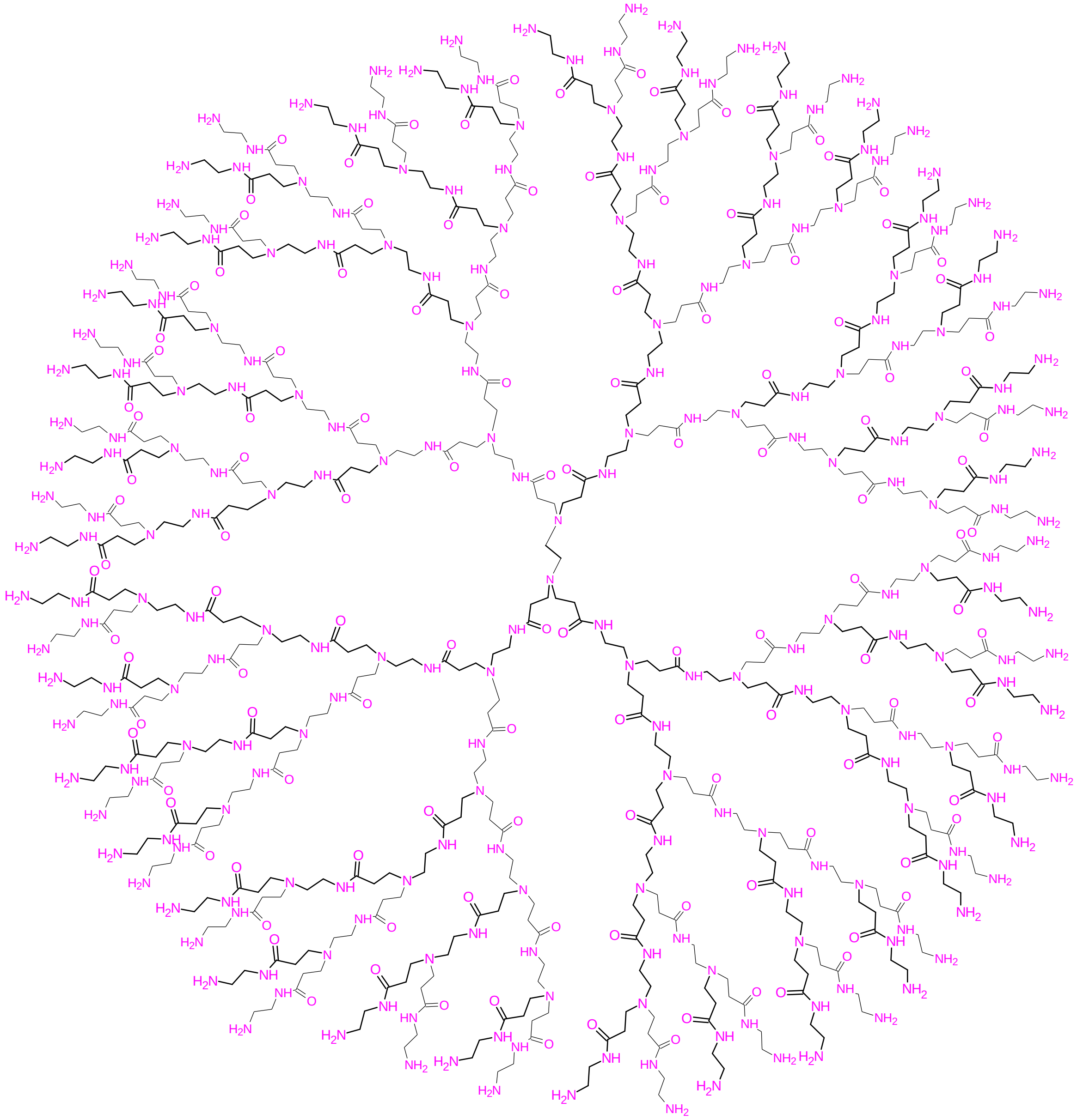

G5

Fig.2.4 Structure of G_3, G_4 and G_5 PAMAM dendrimer

2.7 Characterization of PAMAM dendrimer

2.7.1 High Performance liquid chromatography

HPLC chromatogram of ester and amine terminated PAMAM dendrimers are shown in Fig.2.5. The primary factor governing the elution of dendrimers through a hydrophobic column is the density of dendrimer-TFA ion pairs, which increases as a function of dendrimer generation.

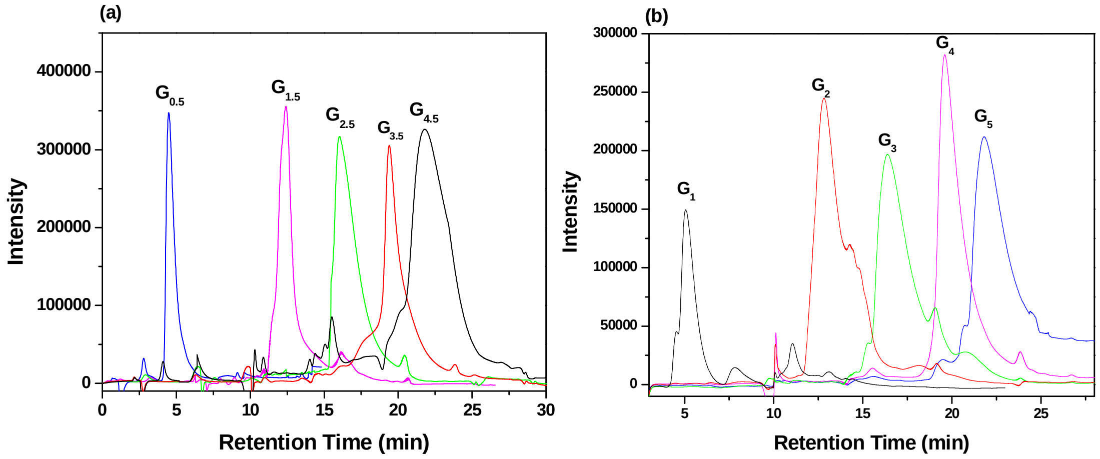

Fig.2.5 HPLC chromatogram of (a) ester and (b) amine terminated PAMAM dendrimers

The chromatogram shows that increase in retention time (t_R) as a function of dendrimer generation. Besides the main peak, both trailing generation and dimer peaks are observed. At each generation, the dimer peak overlaps very closely with the next higher generation, while the trailing generation overlaps with the next lower generation (Fig.2.4). Occurrence of undesirable side reactions during successive iterations of alkylation and amidation steps result in macromolecular polydispersity.

2.7.2 Size exclusion chromatography

Size exclusion chromatogram of ester and amine terminated PAMAM dendrimers are shown in Fig.2.6. The molar mass of PAMAM dendrimers measured using SEC deviates from theoretical ones (Table 2.2).

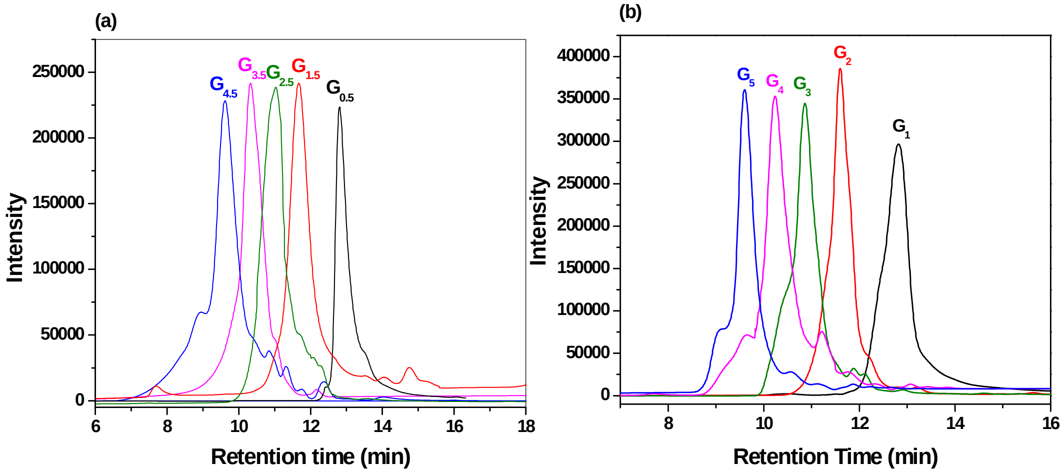

Fig.2.6 SEC chromatograms of (a) ester and (b) amine terminated PAMAM dendrimer

It is generally known that the performance of SEC technique is based on the difference in molecular volumes of macromolecules. The molar mass of PAMAM dendrimers were determined by comparing its retention time with protein standards. Though, protein standards and PAMAM dendrimers have nearby mass, they differ in their molecular volume due to difference in intramolecular attraction leading to deviation in measured molar mass of PAMAM dendrimer. The appearance of hump and peak tailing in the main peak suggest existence of few structural imperfection dendrimers composed of both generational (trailing generations and dimers) and skeletal (missing arms and intramolecular loops).

2.7.3 DLS

The mean size of PAMAM dendrimers (G_2-G_5) was directly measured by using DLS at 25°C. Fig. 2.7 shows the increase in mean size of ester and amine terminated PAMAM as a function of dendrimer generation.

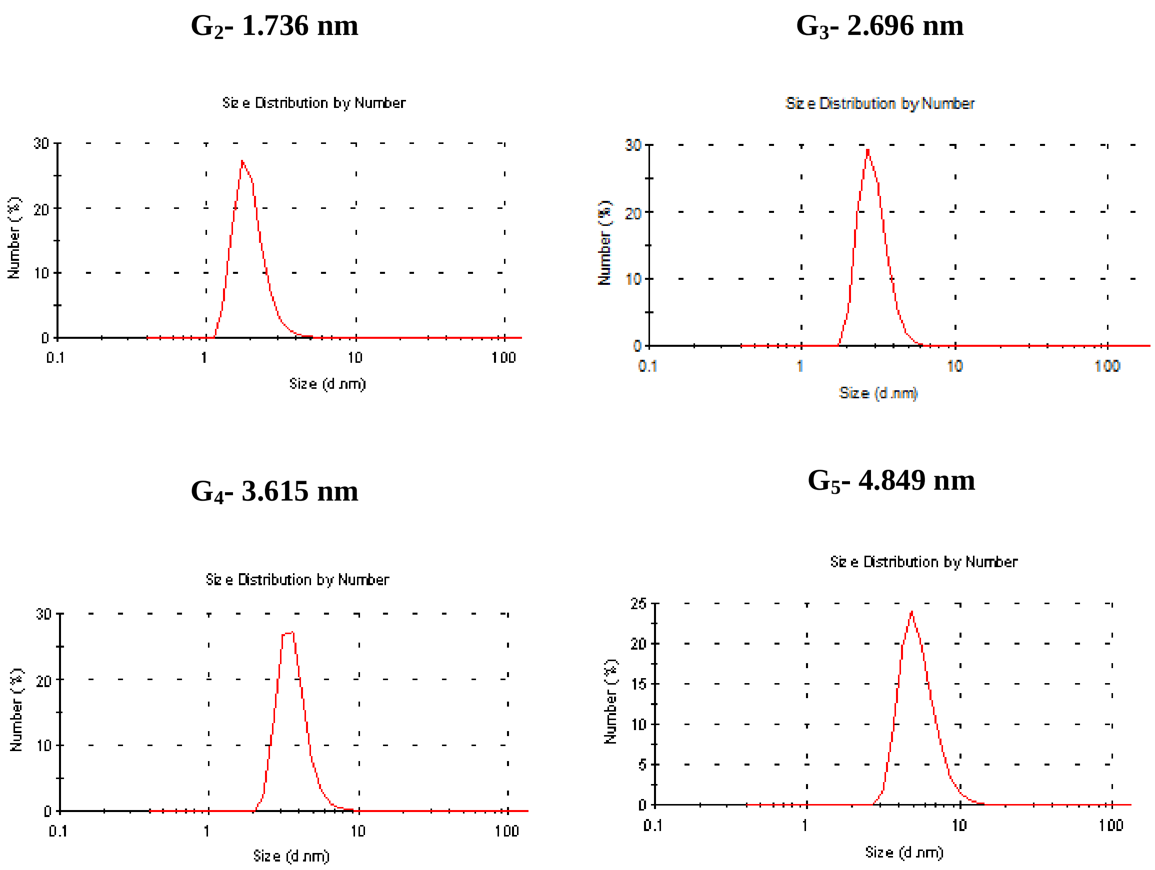

G_2- 1.736 nm

G_3- 2.696 nm

G_4- 3.615 nm

G_5- 4.849 nm

Fig.2.7 Mean size of amine terminated PAMAM as a function of dendrimer generation

2.7.4 Potentiometric tritration

Potentiometric titrations were performed for determination of total number of amine groups in PAMAM dendrimer (G_1-G_5) [118]. A known quantity of the dendrimer was dissolved in 20 mL of water containing 0.1 M KCl. This solution was acidified with known quantity of standard HCl solution (0.0951 N) for complete protonation and then back titrated against a standardized KOH (0.0912 N) solution. The titration was continued till completion of de-protonation in the dendrimer. During potentiometric titration, the solution was purged with argon gas to eliminate the influence of atmospheric carbon dioxide on pH of the solution. The number of tertiary and primary amino groups present in the PAMAM dendrimer was determined from respective neutralization points.

The experimental data was compared with theoretical values (Table 2.2) and the results indicate that there is a deviation in number of amine groups (primary and tertiary) suggesting defects in few dendrimer structure.

Table 2.2 Theoritical and determined number of amine groups and molar mass of amine and ester terminated PAMAM dendrimer

Amine terminated PAMAM dendrimer					
Generation	**1**	**2**	**3**	**4**	**5**
Theoretical molar mass (g/mol)	517	1430	3256	6909	14215
molar mass by SEC (g/mol)	499	1629	3715	7227	13803
Theoretical number of amine groups	1°- 4, 3°- 2	1°- 8, 3°- 6	1°-16, 3°-14	1°- 32, 3°- 30	1°- 64, 3°- 62
Number of amine groups by Potentiometric titration	1°- 4, 3°-2	1°- 7±1, 3°- 5±1	1°-13±2, 3°-12±1	1°-28±3, 3°-26±2	1°-58±4, 3°-56±2
Ester terminated PAMAM dendrimer					
Generation	**0.5**	**1.5**	**2.5**	**3.5**	**4.5**
Theoretical molar mass (g/mol)	404	1204	2804	6004	12404
molar mass by SEC (g/mol)	489	1545	2951	6683	12882

2.7.5 FTIR analysis

FTIR spectra of ester and amine terminated PAMAM dendrimers are shown in Fig.2.8 (a & b). The characteristic C=O stretching vibration of ester is observed at 1736 cm^{-1}. The appearance of peaks at 2945 and 2848 cm^{-1} are due to C–H stretching vibration.

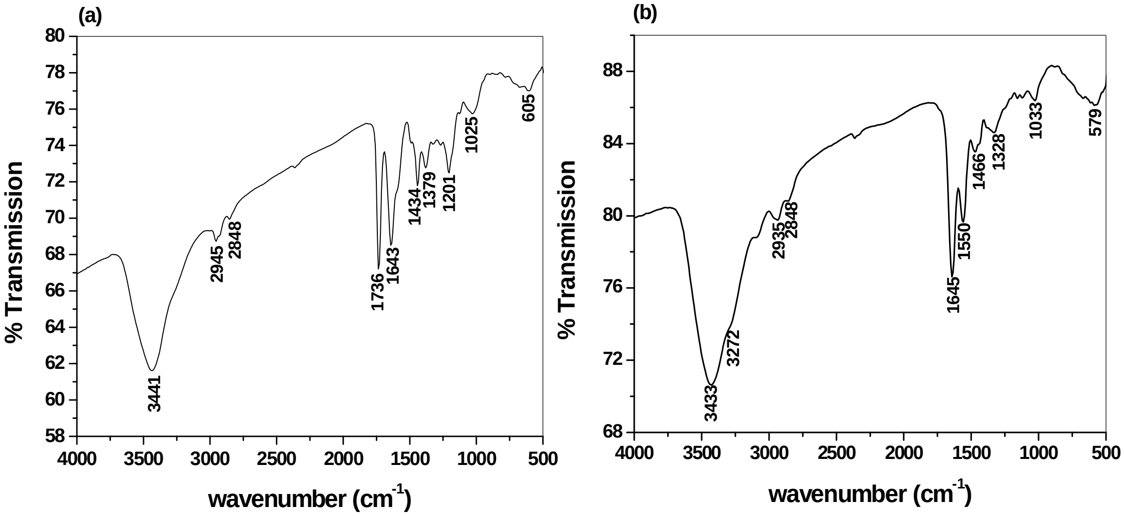

Fig.2.8 FTIR spectra of (a) ester and (b) amine terminated PAMAM dendrimer

The peaks at 1434 cm^{-1} and 1379 cm^{-1} are due to bending vibration of methylene (-CH_2) and methyl (-CH_3) groups respectively. The peaks at 1201 cm^{-1} and 1025 cm^{-1} are due to stretching vibration of C–O group. In case of amine terminated dendrimer, the peaks at 1650 cm^{-1} and 1550 cm^{-1} are characteristic C=O stretching and N–H bending vibration of amide group. In addition, the appearance of peaks at 3433 cm^{-1} and 3272 cm-^{1} correspond to N–H stretching vibration of primary amine and amide groups respectively. The peaks at 1328 cm^{-1} and 1033 cm^{-1} correspond to stretching vibration of C–N and C–O groups. The progress of dendrimer generation was also monitored from the vibration peak at 1736 cm^{-1}. The absence of this peak in each full generation amine terminated dendrimer (Fig.2.8 (b)) confirms completion of amidation reaction.

2.7.6 Mass spectral analysis

MALDI-TOF MS spectra of full generation PAMAM dendrimer (G_1-G_5) are shown in Fig.2.10. MALDI spectrum consists of sharp lines upto generation-2(G_2) whereas from generation G_3 to G_5, line structure in the mass spectra was not observed.

Though the line spectrum was lost, the mean molecular weight distribution could be observed in the spectra. Similar spectra are reported in the literature [114,119].

In generation-1 (G_1), the peaks at 517.35 and 258.26 are due to molecular ion and half fragmentation of the ideally branched dendrimer. The weak lines at 540 and 555 are corresponding to $M+Na^+$ and $M+K^+$ lines. Appearance of additional peaks in the spectrum indicates the presence of structural defective dendrimers.

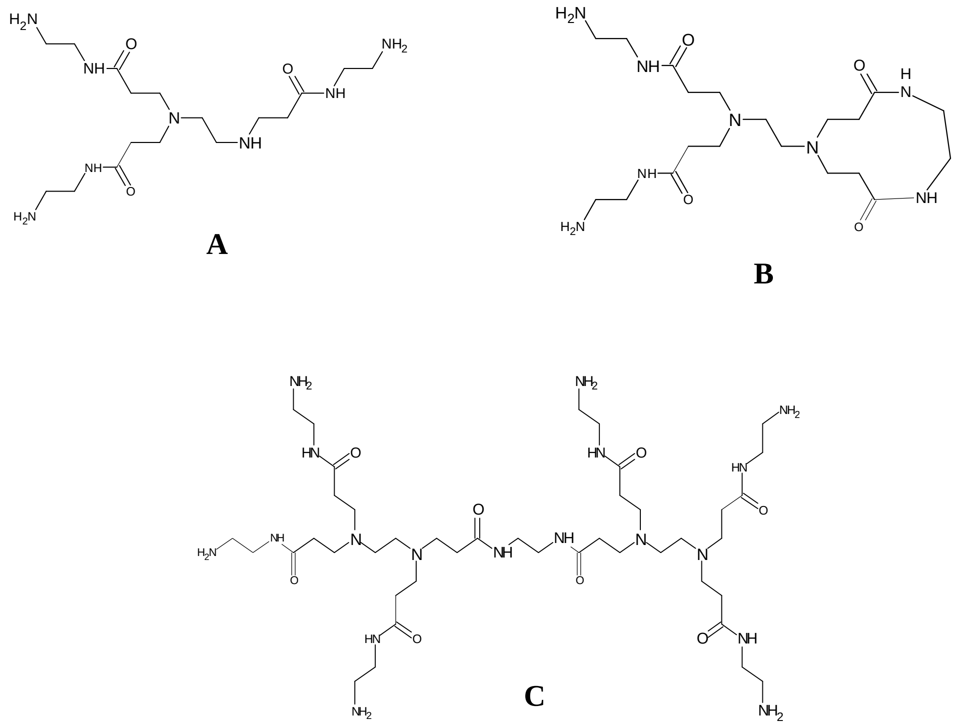

Fig.2.9 Unsymmetrical structure of G_1 PAMAM dendrimer (A) incomplete addition (B) Intramolecular cyclization (C) dimerization

The structural defects in dendrimers are caused due to the following side reactions: (i) incomplete Michael addition is the primary side-reaction causing the appearance of unsymmetrical dendrimeric structure (Fig.2.9A), (ii) intramolecular cyclization results in formation of cyclic products (Fig.2.9 B), (iii) *retro*-Michael reaction leading to structural defect (Fig.2.9 A) and (iv) dendrimer dimer formation (Fig.2.9 C).

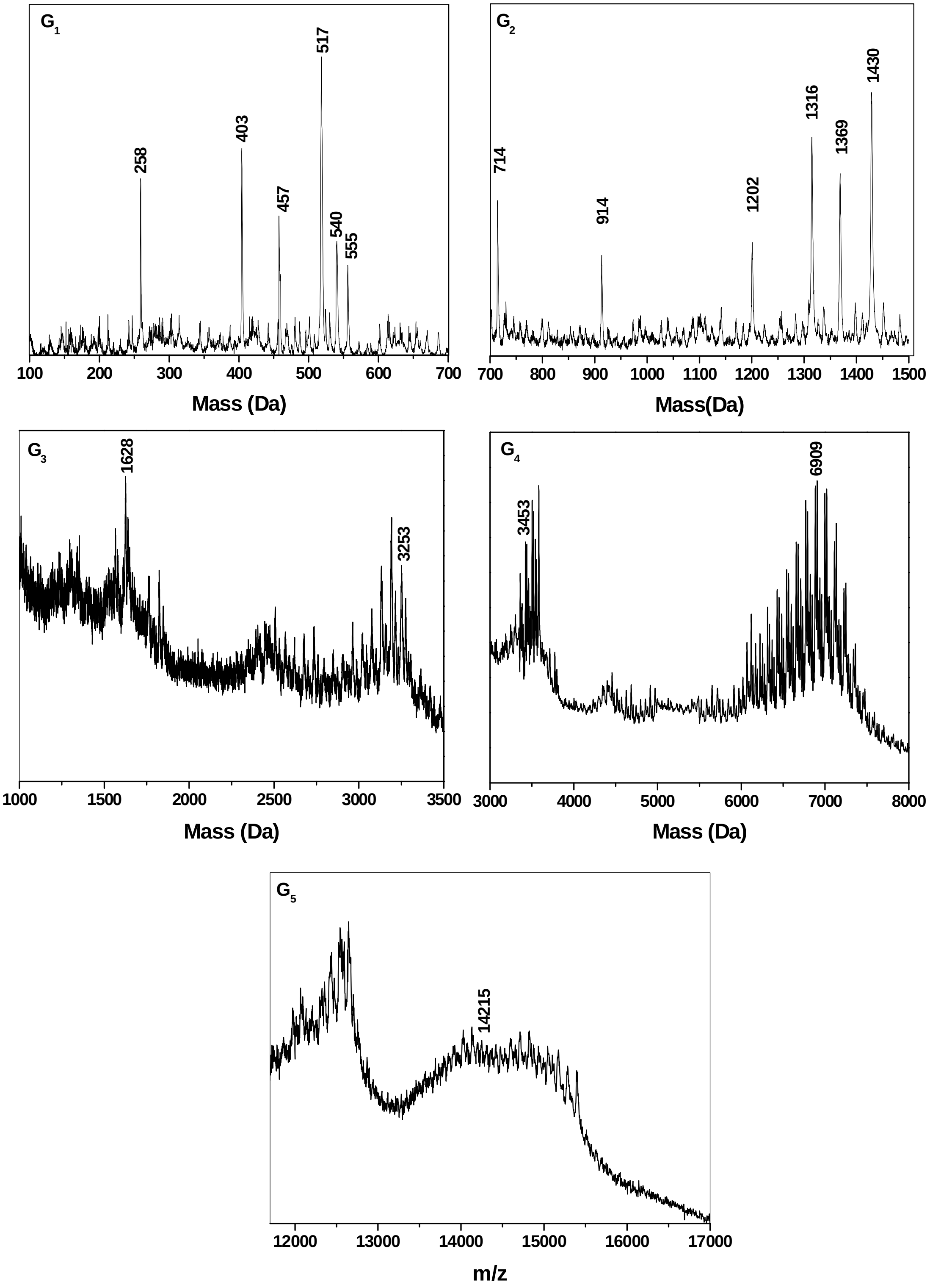

Fig.2.10 MALDI-Mass spectra of full generation amine terminated PAMAM dendrimer.

2.7.7 ^{1}H&^{13}C NMR spectral analysis

^{1}H&^{13}C NMR spectra of $G_{0.5}$ester and G_1 amine terminated PAMAM dendrimer is shown in Fig. 2.11 & 2.12 respectively and the chemical shifts of remaining generations $G_{1.5}$-G_5 are given in Table 2.3 & 2.4. It was observed that as the PAMAM generation increases, NMR peak becomes broader and multiples are not getting resolved due to repetition of same structural units.

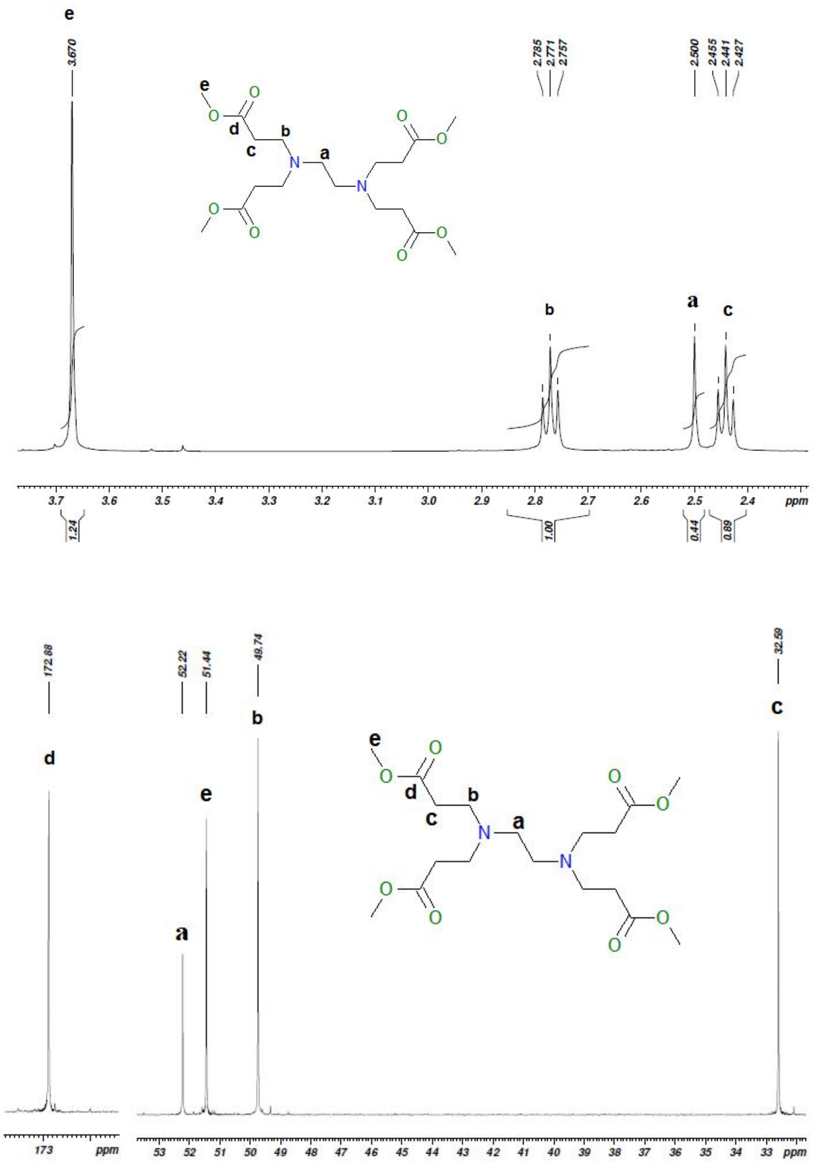

Fig.2.11 ^{1}H&^{13}C NMR of ester terminated $G_{0.5}$ PAMAM dendrimer

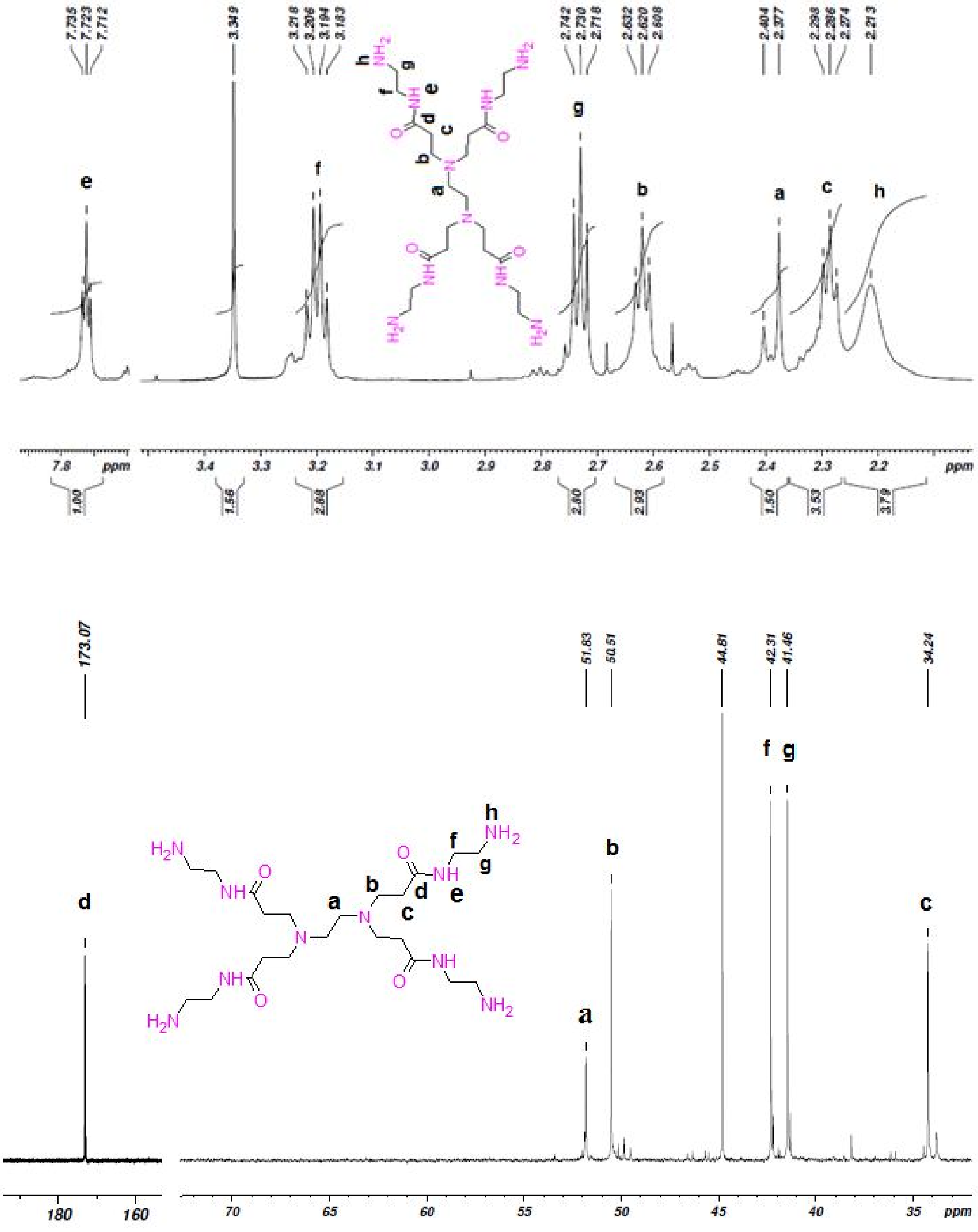

Fig.2.12 ^{1}H&^{13}C NMR of amine terminated G$_1$ PAMAM dendrimer

Table 2.3 ^{1}H and ^{13}C chemical shift of ester terminated PAMAM dendrimers

PAMAM generation	^{1}H and ^{13}C NMR Chemical shift	
	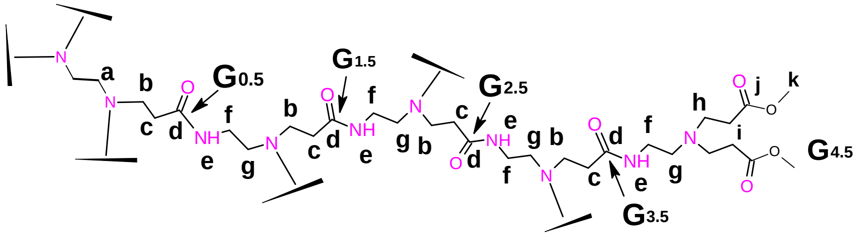	
G$_{0.5}$	^{1}H	e-3.67, b-2.77, a-2.50, c-2.44
	^{13}C	d-172.88, a-52.22, e-51.44, b- 49.74, c-32.59
G$_{1.5}$	^{1}H	e-7.28, k-3.62, f-3.23, g-2.85, b-2.72, h-2.72, a-2.44, i-2.49, c-2.39
	^{13}C	j-172.89, d-172.74, a-52.71, k -51.34, g-51.30, b-49.91, h-49.09, f-37.22, c-32.69, i-32.31
G$_{2.5}$	^{1}H	e-7.29, k-3.69, f-3.34-3.24, g-2.88-2.8, b,h-2.79-2.71, a-2.63, i-2.59-2.51, c-2.48-2.4
	^{13}C	j-173.12,d-172.43, a-52.84, k-52.34, g-51.73,51.65, b-50.49,49.84, h-49.23, f-37.22, i-32.66
G$_{3.5}$	^{1}H	e-7.29, k-3.66, f-3.31-3.22, g-2.86-2.78, b, h-2.78-2.71, a-2.61, i-2.56-2.5, c-2.46-2.39
	^{13}C	j-173.14, d-172.46, a-52.82, k-52.20, g -51.73,50.34, b-49.78, h-49.18, f-37.50, 37.17, c-33.65, 32.62, i-31.98
G$_{4.5}$	^{1}H	e-7.64-7.46, k-3.64, f-3.27-3.12, g,b,h-2.79-2.61, a-2.55, i-2.51-2.41, c-2.39-2.32
	^{13}C	-

Table 2.4 ^{1}H and ^{13}C chemical shift of amine terminated PAMAM dendrimer

PAMAM generation	^{1}H and ^{13}C NMR Chemical shift	
	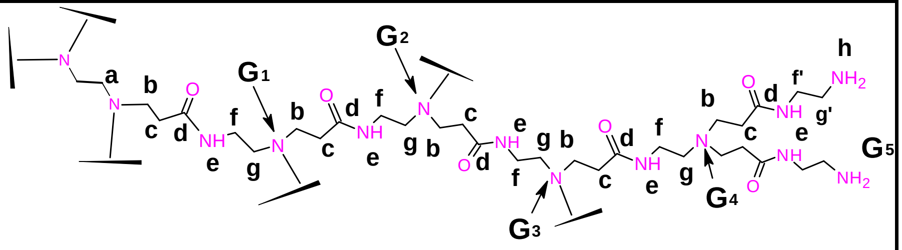	
G$_1$	^{1}H	a-2.37, b-2.73, c-2.28, e-7.72, f-3.19, g-2.62, h-2.21
	^{13}C	a-51.83, b- 50.51, c-34.24, d-173.07, f-42.31, g-41.46
G$_2$	^{1}H	e- 8-7.7, f,f'-3.17-3.04, g,g'-2.69-2.62, b-2.61-2.54, a-2.39-2.36, c-2.23-2.15
	^{13}C	d-173.07, 173.45, a-52.57 g-50.27, b-50.30, f'-42.13, g'-41.29, f-37.61, c-33.81, 34.06
G$_3$	^{1}H	e-8.28-7.94, f,f'3.12-3, g,g'-2.69-2.6, b-2.6-2.53, a-2.39-3.37, c-2.26-2.13
	^{13}C	d-171.52,171.44,171.32, a-52.16, g-50.89, b-49.65,48.53, f'-42.03, g'-41.16, f-36.88,38.8, c-33.27,33.14
G$_4$	^{1}H	e-7.99-7.83, f,f'-3.11-3.02, g,g'-2.7-2.59, b-2.44-2.38, a-2.38-2.35, c-2.25-2.11, h-1.25-1.2
	^{13}C	-
G$_5$	^{1}H	e-8-7.8, f,f'-3.12-2.99, g,g'-2.7-2.59, b -2.43-2.35, a-2.34-2.31, c-2.23-2.11,
	^{13}C	-

2.8 Synthesis of PAMAM dendron-SDB chelating resin

2.8.1 Synthesis of amine terminated PAMAM dendron-SDB resin

Chloromethylated styrene divinyl benzene was treated with excess ethylene diamine (EDA) at 323 K and the product (PAMAMG_0-SDB) was washed with methanol to remove unreacted EDA. This PAMAMG_0-SDB resin was further treated with excess methyl acrylate in methanol (50/50 by weight) at room temperature and left under stirring for overnight. The final product was washed with methanol to remove unreacted methyl acrylate. The ester terminated dendron (PAMAM$G_{0.5}$-SDB) was dried at 323 K in vacuum oven. The first generation amine terminated PAMAM dendron (PAMAMG_1-SDB) was prepared by treating PAMAM$G_{0.5}$-SDB with excess EDA at 323 K (Fig.2.13). The above steps were repeated for synthesis of higher generation dendron PAMAM$G_{2\text{-}5}$-SDB chelating resin [120].

2.8.2 Synthesis of diglycolamic acid (DGA) functionalized PAMAM-SDB (DGA-PAMAM-SDB) resin

DGA functionalized PAMAM-SDB chelating resin was prepared by the addition of diglycolic anhydride to amine terminated full generation dendrons ($G_{1\text{-}5}$) in DMSO and this reaction mixture was stirred for 24 h at 298 K (Fig.2.15). At the end of the reaction, DMSO and excess diglycolic anhydride were removed by washing with methanol and then the product (DGA-PAMAM-SDB) was dried in vacuum oven.

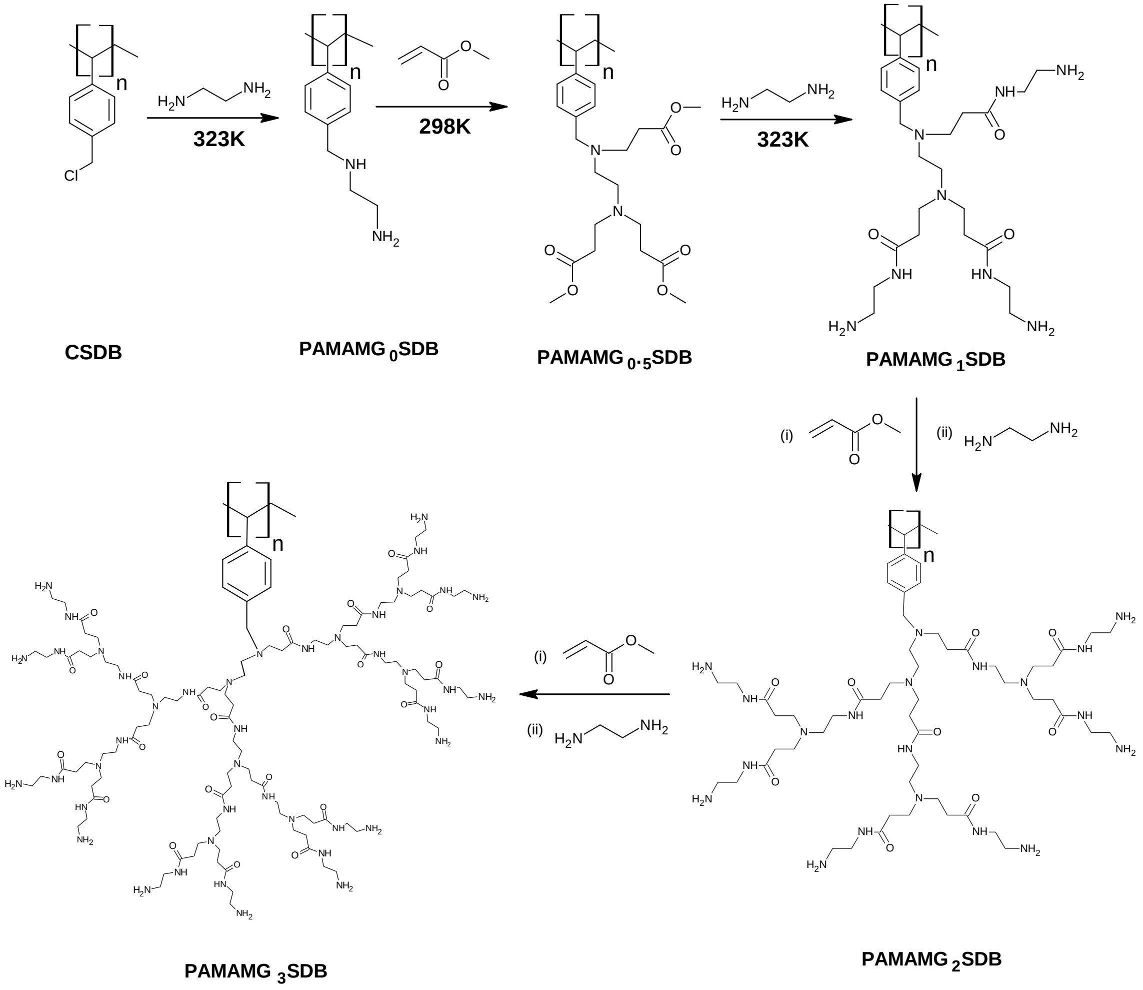

Fig.2.13 Synthesis scheme of PAMAM dendron-SDB chelating resin

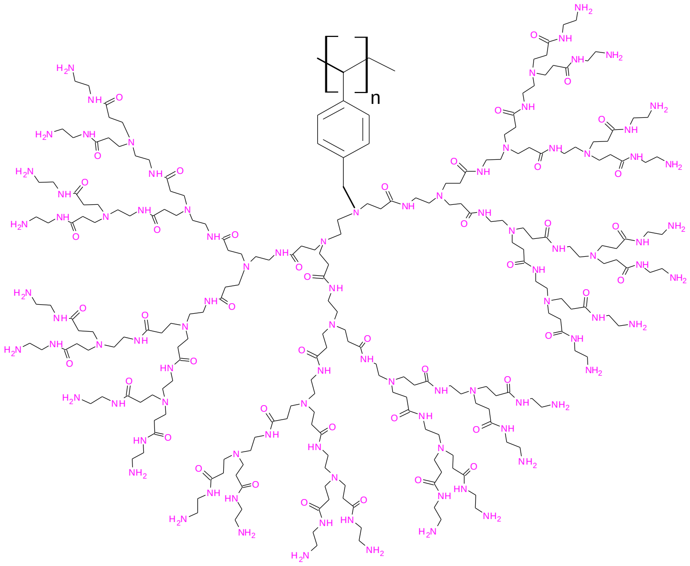

PAMAMG$_4$SDB

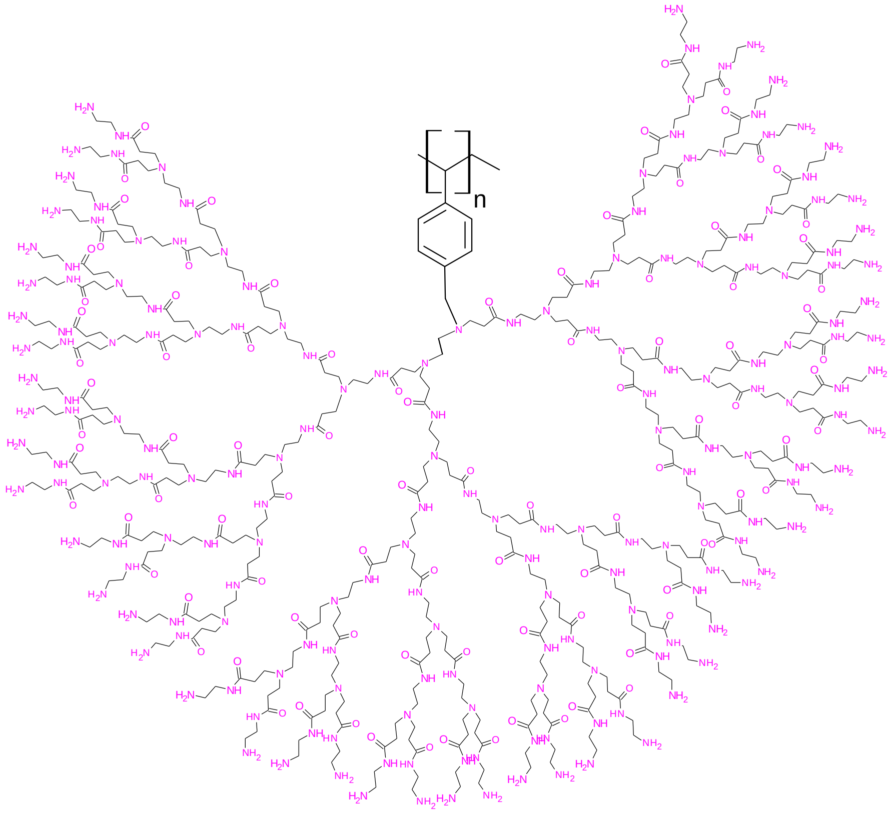

PAMAMG$_5$SDB

Fig.2.14 Structure of PAMAMG$_4$,G$_5$-SDB chelating resin

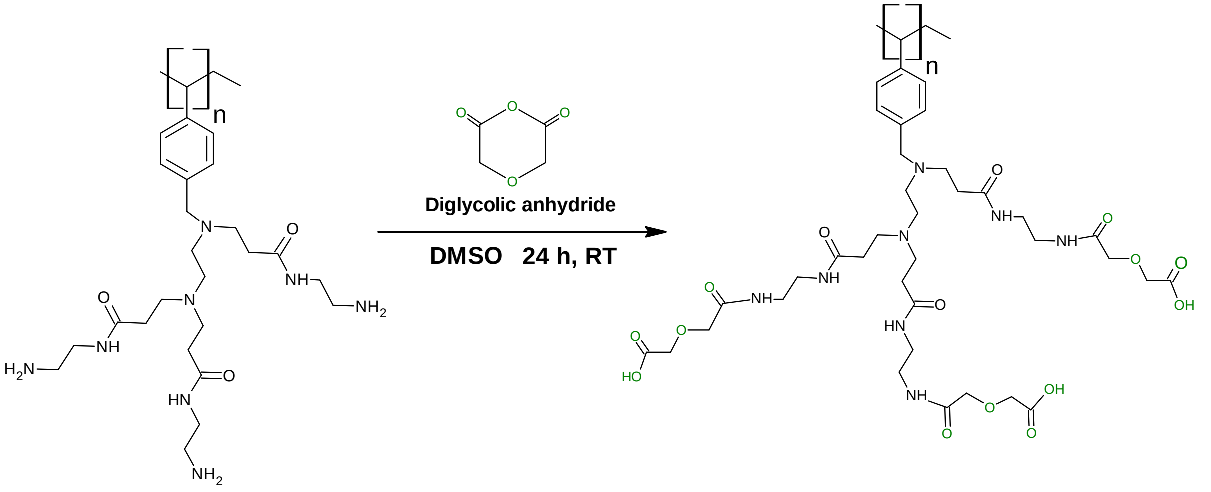

PAMAMG$_1$SDB

DGA-PAMAMG $_1$-SDB

Fig.2.15 Synthesis scheme of DGA-PAMAM-SDB chelating resin

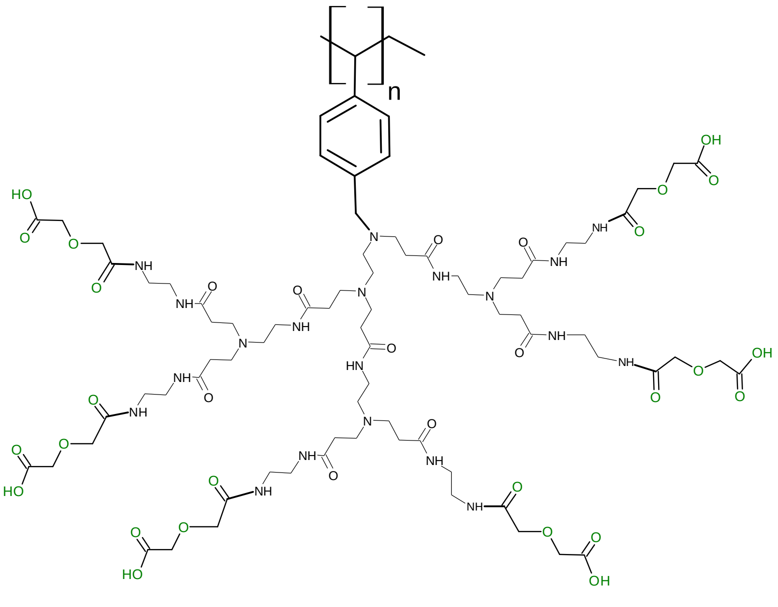

DGA-PAMAMG $_2$-SDB

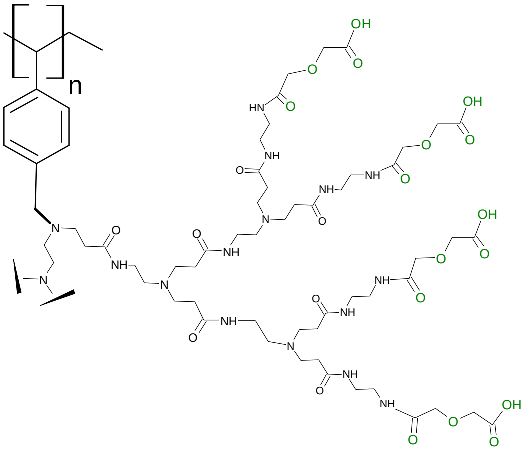

DGA-PAMAMG$_3$-SDB

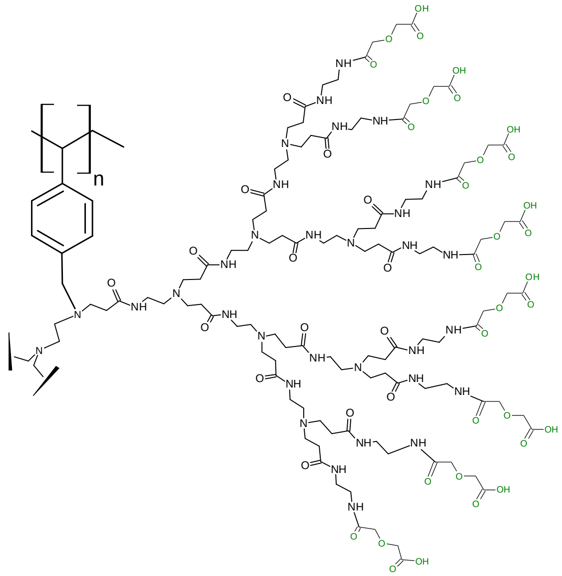

DGA-PAMAMG$_4$-SDB

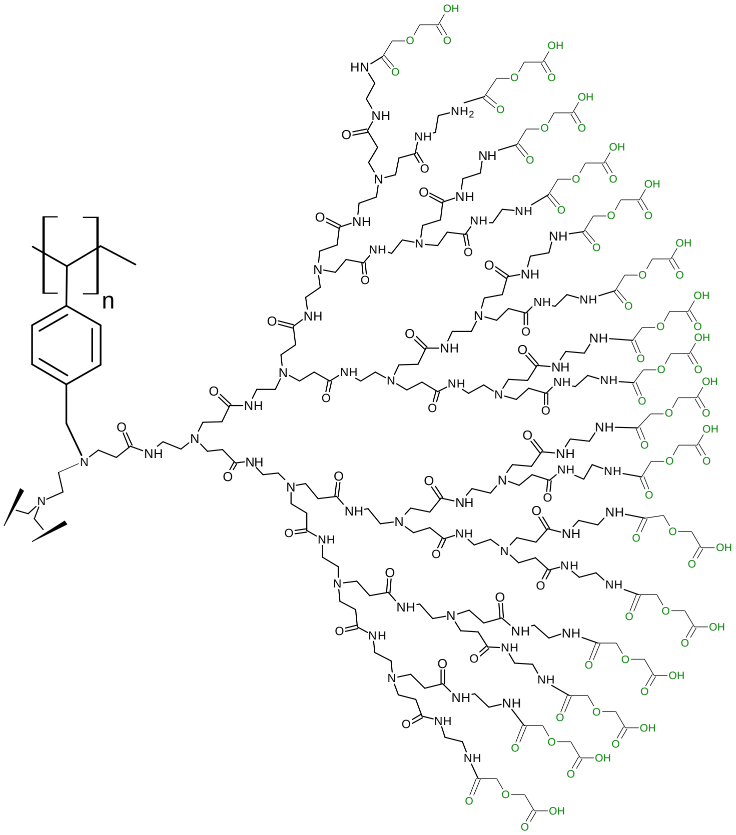

DGA-PAMAMG$_5$-SDB

Fig.2.16 Structure of DGA-PAMAMG$_2$,G$_3$,G$_4$,G$_5$-SDB

2.9 Characterization

2.9.1 FTIR

FTIR spectra of CSDB and PAMAM-SDB (ester, amine and DGA terminated) recorded using DRIFTS are shown in Fig.2.17 (a-d) and their corresponding vibrational frequencies are given in Table 2.5. The presence of ester group in ester terminated PAMAM dendron was confirmed by the appearance of characteristic vibrational peaks at 1726 cm^{-1} (ester C=O stretch) and 1050-1300 cm^{-1} (C-O stretch).

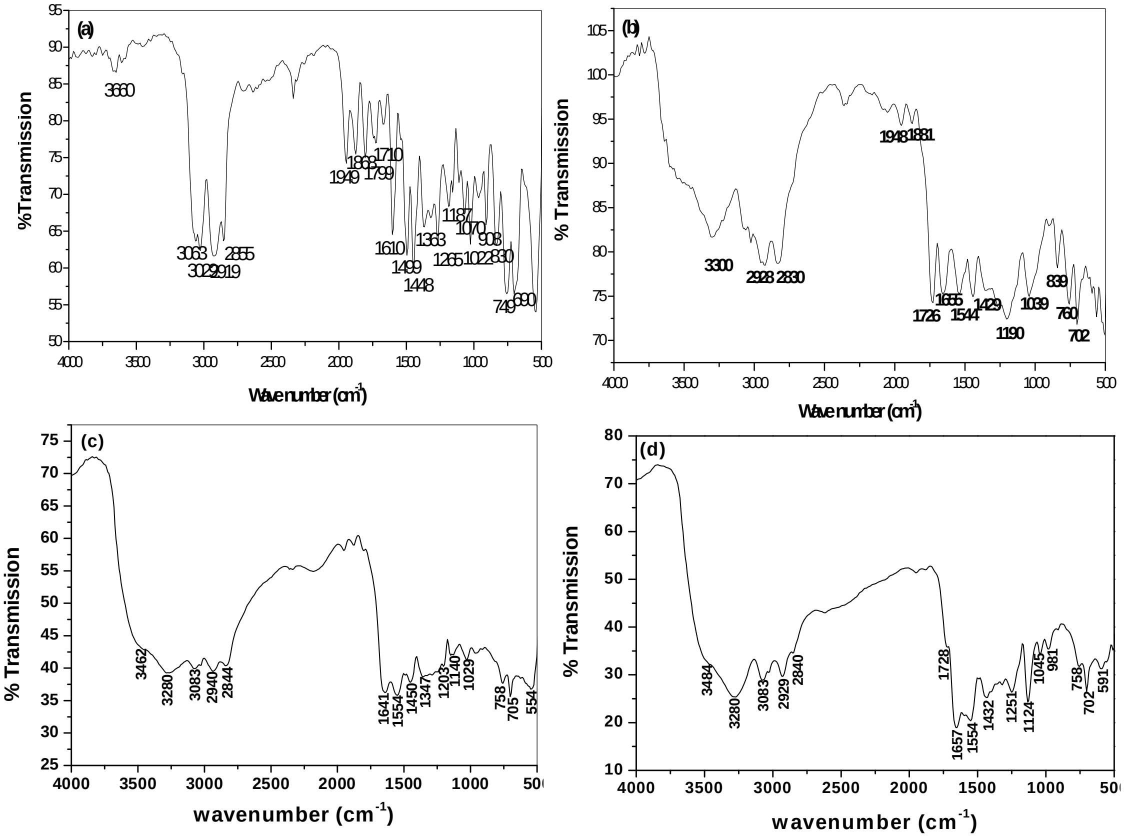

Fig.2.17 FTIR spectra of (a) CSDB (b) ester terminated PAMAMG$_{2.5}$-SDB (c) Amine terminated PAMAMG$_3$-SDB (d) DGA-PAMAM-SDB resin

Table 2.5 Interpretation of vibrational frequencies for CSDB and ester, amine and DGA terminated PAMAM-SDB resin

Compound	**Peak (cm^{-1})**	**Interpretation**
Chloro methylated resin	2840-3100	sp^2, sp^3 C-H stretching
	900 - 675	Aromatic C-H out-of-plane bending
	1610 & 1499	aromatic C=C
	1448	Methylene $-CH_2$ bend
	1363-1230	$-CH_2$ wagging (CH_2- Cl)
	749	C-Cl stretch
Ester terminated resin	3300	N-H stretch of amide
	1726, 1655	C=O stretch of ester, amide
	1544	–NH bend
	1429	Methylene $-CH_2$ bend
	1190	C-O stretch of ester
	850-650	C-H bending of aromatic ring
Amine terminated resin	3462, 3282	N-H stretch of amine, amide
	1641	C=O stretch of amide
	1554	–NH bend
	1450	Methylene $-CH_2$ bend
	1347	C-N stretch
	850-650	Aromatic C-H out-of-plane bending
DGA terminated resin	3484,3280	O-H, N-H stretch of acid and amide
	1728, 1657	C=O stretch of acid, amide
	1554	–NH bend
	1432	Methylene $-CH_2$ bend
	1124	C-O-C stretch of DGA
	1251,1045	C-O stretch
	850-650	Aromatic C-H out-of-plane bending

The completion of amidation reaction in each full generation was confirmed by the disappearance of the peak at 1726 cm^{-1} and presence of a characteristic single C=O vibrational amide stretch at 1650 cm^{-1}. The gradual disappearance of CSDB vibrational peaks were observed with increasing PAMAM dendron generation. Thus, the step by step growth of PAMAM dendron on SDB surface was monitored by using FTIR. In case of DGA terminated PAMAM-SDB resin, a strong peak at 1124 cm^{-1} corresponds to C-O-C stretching in addition to the standard signatures of full generation dendrimer (peaks at1643 and 1554 cm^{-1}) confirms the DGA functionalization. Besides this, the presence of carbonyl peak at 1728 cm^{-1} and OH stretching at around 3484 cm^{-1} attribute to acid group ensuring the formation of DGA functionalized PAMAM dendron.

2.9.2 Morphology study

Field emission scanning electron microscopy (FE-SEM) image of CSDB, PAMAMG$_3$ -SDB and DGA-PAMAMG$_3$ -SDB resin are shown in Fig.2.18 (a-c). The images clearly indicate the morphological change from spherical to distinct flakes due to growth of PAMAM dendron on SDB surface.

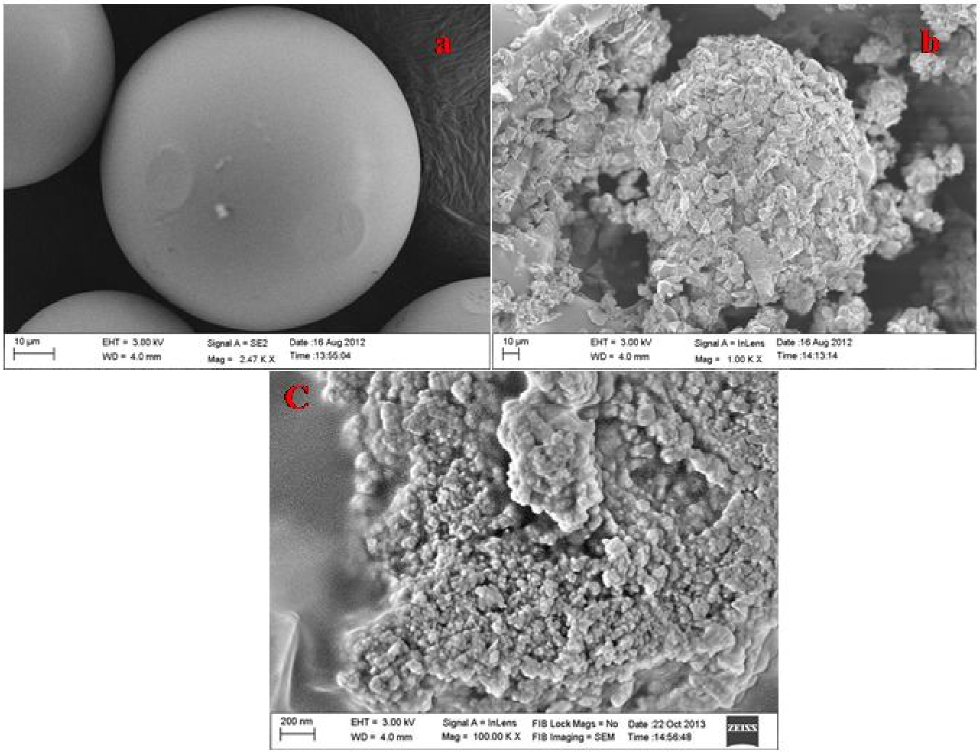

Fig.2.18 FE-SEM image of (a) CSDB and (b) PAMAMG$_3$-SDB (C) DGA-PAMAM-SDB

2.9.3 Thermal degradation study

Thermal stability of CSDB and chelating resins (PAMAMG_3-SDB and DGA-PAMAMG_3-SDB) were studied upto 1023 K by TGA. Percentage weight loss as a function of temperature for CSDB, PAMAMG_3-SDB and DGA-PAMAMG_3-SDB are shown in Fig.2.19. Thermal decomposition of CSDB occurred in two stages: (i) 553–723 K and (ii) 723–823 K. In the first stage, nearly 53% of weight loss was due to pyrolysis and in the next stage, further 35 % of weight loss was due to carbonization. Thermogravimetric curve of the chelating resin PAMAMG_3-SDB indicates weight loss in four stages; (i) 336-354 K (ii) 481-560 K (iii) 569-671 K and (iv) 686-850 K. In the first stage, 5.6 % weight loss was observed due to loss of adsorbed water and in the second stage, 14.2 % weight loss was due to decomposition of PAMAM dendron. In the third stage, 30.2 % weight loss was due to pyrolysis and in fourth stage, about 26.42 % weight loss was observed leaving behind residual char. The weight loss from 481 to 560 K (second stage) confirms the presence of PAMAM dendron on the surface of SDB.

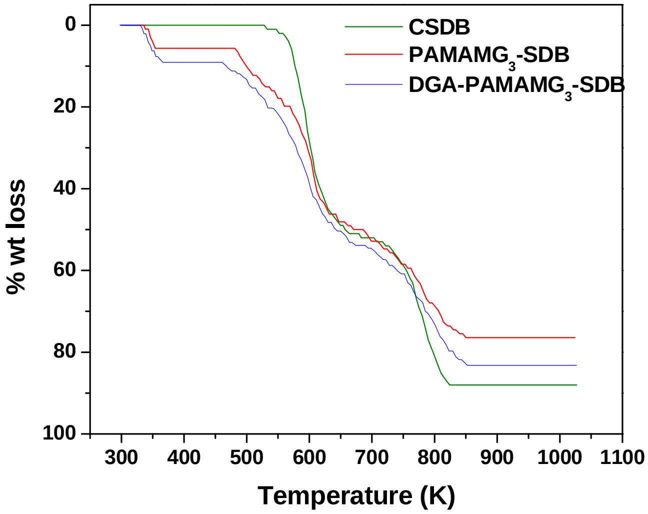

Fig.2.19 TG curve of CSDB, PAMAMG_3-SDB and DGA-PAMAMG_3-SDB

Similarly, TG curve of the chelating resin DGA-PAMAMG$_3$-SDB indicates weight loss in four stages; (i) 9 % at 330-366 K (ii) 11.2 % at 466-534 K (iii) 33.5 % at 543-674 K and (iv) 29.3 % at 689-852 K. Hence, the chelating resins (PAMAMG$_3$-SDB and DGA-PAMAMG$_3$-SDB) are observed to be stable up to 466 K.

2.9.4 Potentiometric titration

The number of primary and tertiary amino groups in the PAMAM dendron was determined by potentiometric titration. Experimental data reveal that the number of terminal and tertiary amine groups slightly deviate from the theoretical values (Table 2.6) indicating defects in the dendron structure. Similarly, the number of DGA groups also slightly deviates from the theoretical value. The pKa values of primary, tertiary and DGA functional groups determined from potentiometric titration are found to be 9.3-9.8, 6.2-6.5 and 4.1-4.4 respectively.

Table 2.6 Theoretical and experimentally determined number of primary (1°), tertiary (3°) amines and DGA functional groups in the PAMAM-SDB and DGA-PAMAM-SDB chelating resins.

Amine and DGA terminated PAMAM dendron-SDB resin					
Dendron generation	**1**	**2**	**3**	**4**	**5**
Theoretical number of amino groups	1°- 3, 3°- 2	1°- 6, 3°- 5	1°-12, 3°-11	1°-24, 3°-23	1°- 48, 3°- 47
Number of amino groups by Potentiometric titration	1°- 3, 3°- 2	1°- 6, 3°- 5	1°-10±1, 3°-9±1	1°-20±2, 3°-19±2	1°- 42±2, 3°-39±3
Theoretical number of DGA groups	3	6	12	24	48
Number of DGA groups by Potentiometric titration	3	5	10±1	20±1	41±3

2.10 Synthesis of xanthate functionalized PAMAM dendrimer

2.10.1 Ester terminated PAMAM Dendrimer

The procedure for synthesis of ester terminated ($G_{0.5}$) PAMAM dendrimer is given section 2.7.1.

2.10.2 Hydroxyl terminated PAMAM dendrimer

A mixture of TRIS (tri-hydroxymethylaminoethane) and anhydrous potassium carbonate was added to the solution of PAMAM$G_{0.5}$COOMe in anhydrous dimethyl sulfoxide under argon atmosphere. The solution was heated in an oil bath maintained at 313 K for 96 h. The reaction mixture was filtered to remove solid reagent and excess solvent in filtrate was removed by vacuum distillation. The resulting thick oil was dissolved in a minimum quantity of distilled water and precipitated with propanone [121]. The precipitation was repeated three to four times to get the pure product. The resulting hygroscopic hydroxy terminated dendrimer was dried in a vacuum oven.

2.10.3 Xanthate functionalization

Aqueous solution of hydroxyl terminated PAMAM dendrimer was mixed with aqueous NaOH and then carbon disulfide was added to the mixture. After overnight stirring, the solvent was removed from the reaction mixture by vacuum drying leaving XFPD as a yellow hygroscopic viscous liquid. The overall synthetic scheme is given in Fig.2.20.

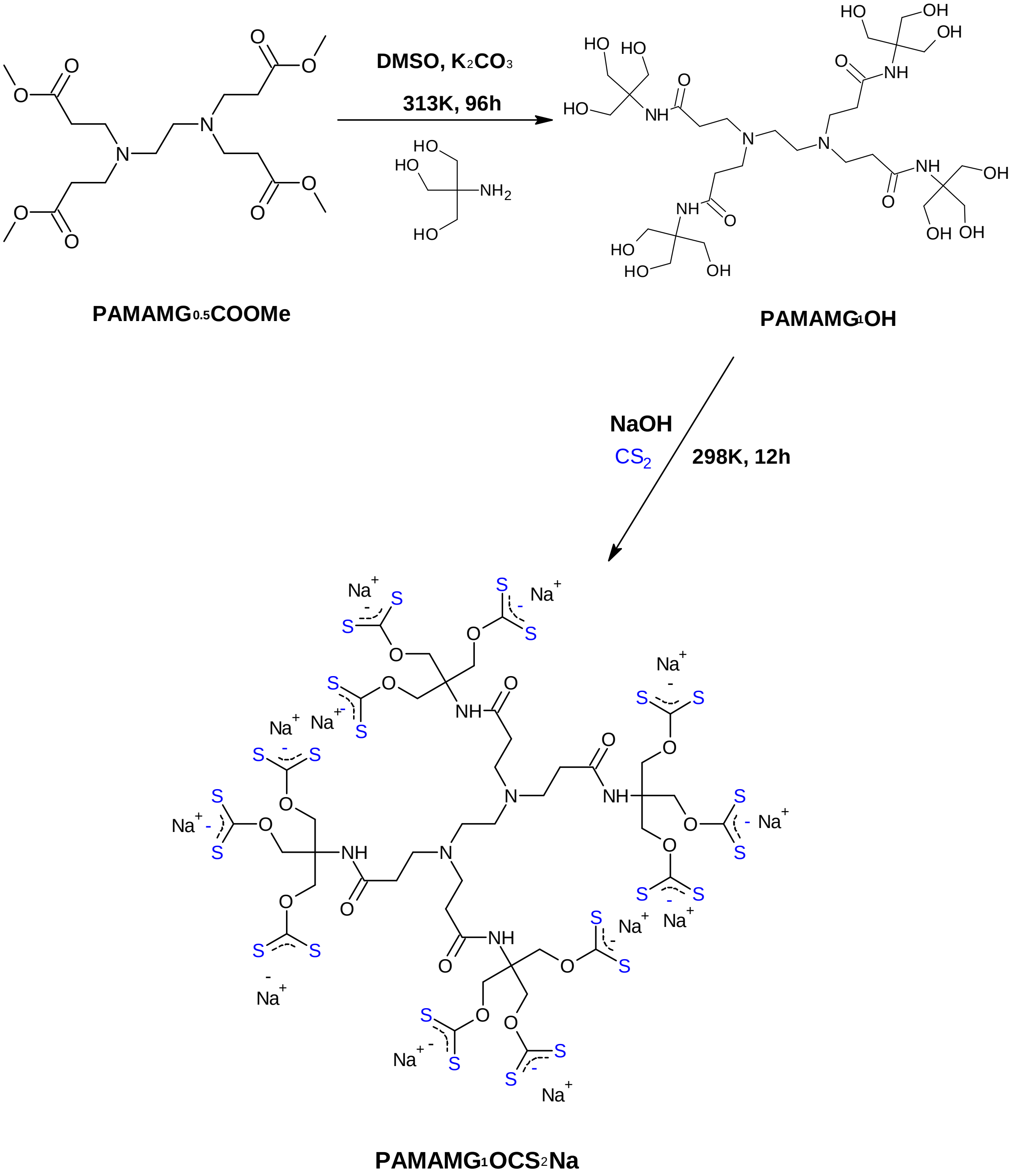

Fig.2.20 Synthesis of xanthate functionalized PAMAM dendrimer

2.11 Characterization

2.11.1 UV absorption spectra

UV spectra of PAMAMG_1OH and XFPD are shown in Fig.2.21. In the spectra of XFPD, the first band in the range 200-212 nm is attributed to n →σ* transition and the second band in the range 218-231 nm as a shoulder attributed to π →π* transition. In case of PAMAMG_1OH dendrimer, a broad band corresponding to both n →σ* and π →π* transitions in the range of 200-231 nm is observed. In XFPD, an additional absorption band in the range of 295-355 nm is observed due to combination of π →π* and n →π* transitions of xanthate functional group [122]. Thus, UV spectrum confirms the presence of xanthate group in the chelating ligand.

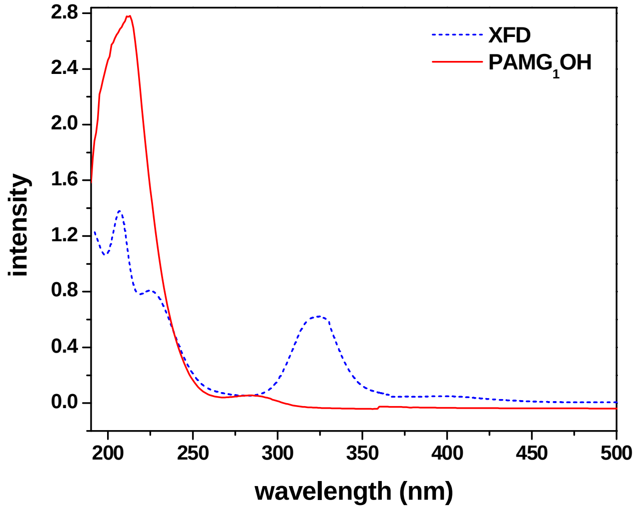

Fig.2.21 UV-Visible spectra of PAMG_1OH & XFPD

2.11.2 FTIR spectra

FTIR spectra of PAMAMG_1OH and XFPD are shown in Fig. 2.19. In the spectrum of PAMAMG_1OH (Fig.2.22 (a)), the appearance of a peak at 3372 cm^{-1} is due to the stretching of –OH and –NH and the peaks at 2932 and 2853 cm^{-1} are due to -CH stretching. The C=O stretching and N–H bending vibrations of an amide group is defined by peaks at 1643 cm^{-1} and 1565 cm^{-1} respectively. The observed peak at 1461 cm^{-1} is attributed to C–N stretching and the strong peak at 1039 cm^{-1} is due to C–O stretching of primary alcoholic group. In the spectrum of XFPD (Fig.2.22 (b)), unlike in PAMAMG$_1$OH dendrimer, the strong peak at 1039 cm^{-1} has disappeared and new peaks appear in the region of 1230–830 cm^{-1} which are related to vibrations of xanthate group. The peaks at 1137 cm^{-1} and 998 cm^{-1} are attributed to asymmetric and symmetric stretching vibrations of –CS$_2^-$ group. The peak at 883 cm^{-1} is assigned for deformation vibration of –CSS$^-$ [123, 124]. Thus, the presence of xanthate functional group at the surface of PAMAMG$_1$OH dendrimer is confirmed.

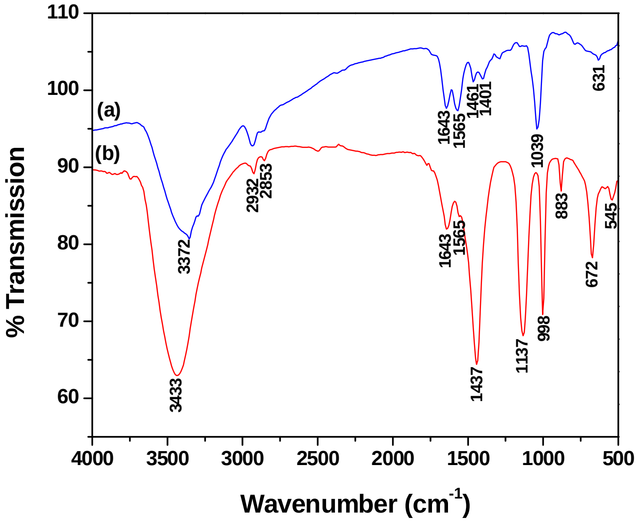

Fig.2.22 FTIR Spectra of (a) PAMAMG$_1$OH, (b) XFPD

2.11.3 ^{1}H & ^{13}C NMR spectra

^{1}H & ^{13}C NMR spectra of PAMAMG$_1$OH are shown in Fig.2.23. The resonance from methyl ester at 3.67 ppm (Fig.2.11) is no longer visible, confirming complete conversion of ester groups. Furthermore, a new singlet at 3.41 ppm, resulting from resonance of methylene protons adjacent to the terminal hydroxyl groups, is clearly evident. ^{13}C NMR spectrum also shows a single carbonyl peak at 176.12 ppm (amides).

^{1}H NMR (D_2O): 3.41 (24H, s, CH_2OH), 2.72 (8H, t, NCH_2), 2.62 (4H, bt, CH_2N), 2.29 (8H, t, CH_2CO); ^{13}CNMR (D_2O): 164.96;

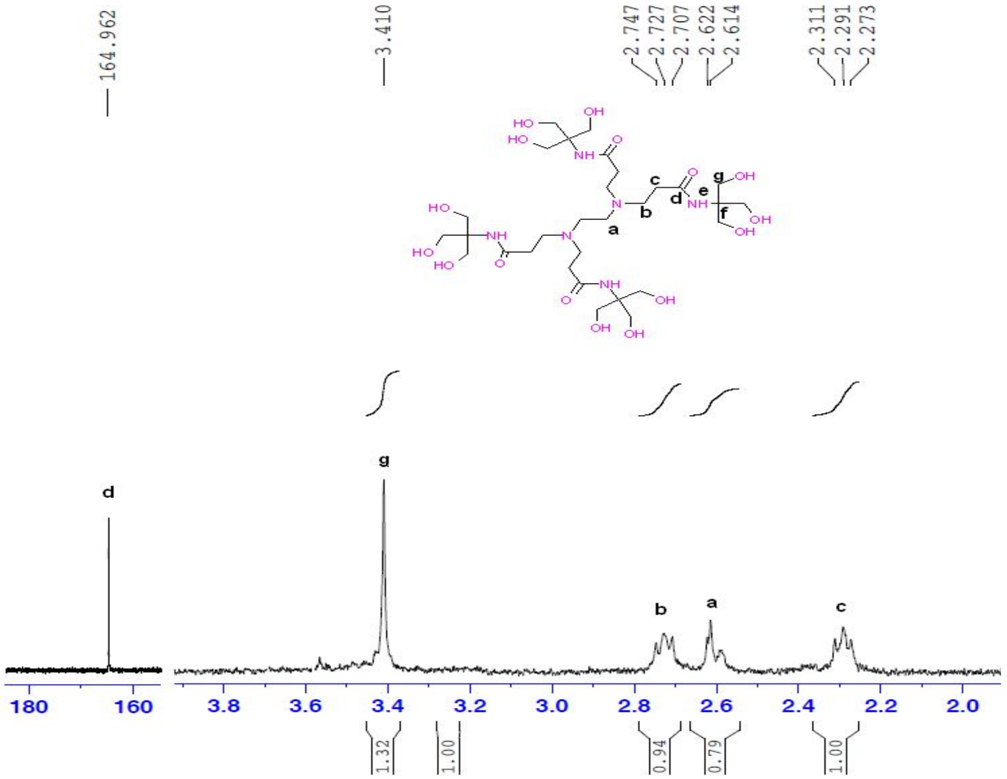

Fig.2.23 ^{1}H & ^{13}C spectra of PAMAMG$_1$OH

2.11.4 MALDI-Mass spectrum

Fig.2.24 shows the MALDI-MS spectrum of PAMAMG$_1$OH dendrimer. The peaks at 799.8 (M+K$^+$) and 380.5 (M/2)$^+$ are due to molecular ion and half fragmentation of the molecule respectively confirming the compound formation.

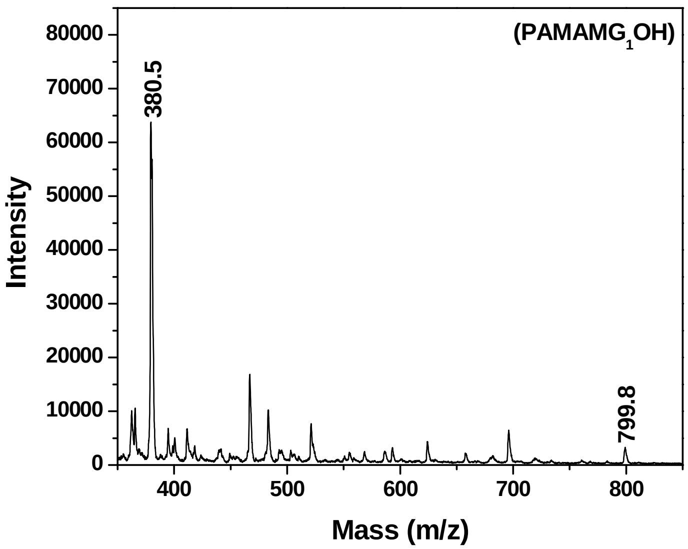

Fig.2.24 Mass spectrum of PAMAMG_1OH

2.11.5 Determination of extent of xanthate functionalization in XFPD ligand

A stock solution of 0.1M XFPD was prepared and 2 ml of this solution was acidified with excess of 0.01M HCl. This acid neutralizes the unreacted NaOH and then hydrolyzes the ligand into neutral carbon disulphide and alcohol. The excess acid was back titrated against standardized 0.01M sodium hydroxide using methyl red as indicator. Another 2 ml of the stock solution was titrated with 0.1M HCl using phenolphthalein as indicator to determine the amount of unreacted sodium hydroxide in the solution. Using these two titration results, the volume of acid consumed for the production of neutral carbon disulphide and alcohol was calculated from which the extent of xanthate functionalization on PAMAMG_1OH dendrimer was determined to be 92- 95 %. The molar mass of XFPD was determined by SEC -1862 (g/mole) which is closer to the theoretical molar mass-1938 (g/mole).

Chapter-3

REMOVAL OF ACTINIDES FROM AQUEOUS SOLUTION BY ULTRAFILTRATION (UF) AND DENDRIMER ASSISTED ULTRAFILTRATION (DAUF)

3.1 Introduction

Removal of radionuclides from aqueous waste by membrane separation process is being adopted in nuclear industries. Pressure driven membrane processes including Reverse Osmosis (RO), Nano-filtration (NF), Microfiltration (MF), Ultrafiltration (UF), Polymer Assisted Ultrafiltration (PAUF) etc., offer advantages such as high decontamination factor, large volume reduction and low energy consumption [16,125]. RO membranes are very effective in retaining dissolved inorganic and organic solutes with molar mass below 1000 Da. NF membranes, on the other hand, are very effective in removing hardness (e.g., multivalent cations) and organic solutes with molar mass between 1000–3000 Da. Both RO and NF membranes require high pressure (600-1000 kPa) for operation. In case of UF and MF membranes, relatively low pressure (100–700 kPa) is required for operation. But they are not very effective in removing dissolved organic and inorganic solutes with molar mass below 3000 Da [126]. However, removal was achieved in UF by increasing size of species through sorption/precipitation/complexation.

The size enhancement by using water soluble metal binding polymers coupled with UF (PAUF) for selective concentration and recovery of metal ions from wastewater has been reported [36-51]. Diallo et al [127] have developed a dendrimer-enhanced ultrafiltration (DEUF) process for recovery of metal ions from aqueous solution. Binding of metal ions to the polymer/dendrimer macromolecular ligands allow effective removal of metal ions through ultrafiltration. Dendrimers have much lower intrinsic viscosities than linear polymers with similar molar mass because of their globular shape [121].

They also have a very low tendency to fouling (plugging the pores) in membranes [128]. Hence, DEUF could be operated at lower pressures.

In the present study, removal of U(VI) and Th(IV) from aqueous solution by UF and dendrimer assisted ultrafiltration (DAUF) is described. Experiments were carried out using regenerated cellulose acetate ultrafiltration membrane and poly(amido)amine (PAMAM) dendrimer chelating agent. Effect of U(VI) and Th(IV) speciation on adsorption/mass deposition at membrane surface and binding with PAMAM dendrimer are discussed. The speciation of U(VI) and Th(IV) ions in the presence of PAMAM dendrimer were investigated by potentiometric and fluorescence studies. Effect of pH, ionic strength, PAMAM dendrimer generation and its concentration on removal of U(VI) and Th(IV) metal ions are discussed. Studies on selective and collective removal of U(VI) and Th(IV) metal ions from SNLW by UF and DAUF are presented in this chapter.

3.2 Experiments

3.2.1 Ultrafiltration

The feed solutions of U(VI) and Th(IV) metal ions (5 mg L^{-1} concentration in 10 mL) were prepared and pH was adjusted from 3 to 9 by adding either 0.1M HNO_3 or 0.1M NaOH. Before ultrafiltration, the solutions were analyzed for corresponding metal ions to find out any precipitation or adsorption on polypropylene centrifuge tube during pH equilibration. Solutions were transferred into Millipore Amicon Ultra-15 centrifugal filter device and centrifuged for 50 minutes at 6000 rpm. After ultrafiltration through regenerated cellulose acetate membrane, the concentrations of metal ion in retentate and permeate were determined by spectrophotometry using Arsenazo(III) complexing agent [115].

The percentage removal (% R) was calculated using equation 3.1.

$$\%\mathbf{R} = (\frac{\mathbf{C_f - C_p}}{\mathbf{C_f}}) \times 100 \tag{3.1}$$

where C_f is the concentration of metal ion in feed and C_p is the concentration of metal ion in permeate.

The percentage of metal ions in the retentate (R_r), permeate (R_p) and percentage total recovery (R_t) were calculated using equations 3.2 to 3.4.

$$\%\mathbf{R_r} = (\frac{\mathbf{W_r \times C_p}}{\mathbf{W_0 \times C_0}}) \times 100 \tag{3.2}$$

$$\%\mathbf{R_p} = (\frac{\mathbf{W_f \times C_f}}{\mathbf{W_0 \times C_0}}) \times 100 \tag{3.3}$$

$$\%\mathbf{R_t} = \%\mathbf{R_r} + \%\mathbf{R_p} \tag{3.4}$$

where, W_r = total weight of retentate before assay, W_o = weight of feed solution, W_f = weight of permeate, C_r = concentration of metal ion in the retentate, C_o = concentration of metal ion in the feed solution, C_f = concentration of metal ion in the permeate.

Membrane was equilibrated with 0.01M nitric acid and the percentage mass of metal ion adsorbed/deposited on the membrane was calculated by analyzing equilibrated acidic solution. Membrane was regenerated by equilibrating with 0.01M NaOH followed by rinsing with Millipore water at the end of each experiment.

3.2.2 PAMAM assisted ultrafiltration

A feed solution containing 5 mg L^{-1} of U/Th metal ion and 2 mg L^{-1} of $PAMAMG_4$ was prepared in 10 mL. The pH of resultant solution was adjusted by adding either 0.1 M HNO_3 or 0.1 M NaOH and then equilibrated for one hour using an orbital shaker at 200 rpm. The equilibrated solution was transferred into Millipore Amicon

Ultra-15 centrifugal filter device and centrifuged for 50 minutes at 6000 rpm for separation of metal-laden PAMAM from aqueous solution. The concentration of U(VI) and Th(IV) in the retentate and permeate was determined. The percentage removal, retentate and permeate were calculated using equation 3.1-3.3 respectively. The percentage mass deposition on the membrane was calculated by measuring concentration of metal ions in acidic solution equilibrated with membrane surface.

DAUF experiments were carried out with increasing concentration of PAMAMG$_4$ dendrimer in the range of 0.5 mg L^{-1} to 5 mg L^{-1} at pH 6 to optimize the concentration of PAMAMG$_4$ required for preventing the mass deposition on the membrane surface. Similarly, effect of PAMAM dendrimer generation on retention of U(VI) and Th(IV) in the retentate was studied.

The effect of ionic strength on removal of U(VI) and Th(IV) in both UF and DAUF were investigated with electrolytes such as $Ca(NO_3)_2$ and NaCl in the concentration range of 0.5 - 2.5 mM.

3.3 Results and Discussion

3.3.1 Removal of U(VI) and Th(IV) by Ultrafiltration

Ultrafiltration of U(VI) and Th(IV) solutions over the pH range 3-9 reveal that these metal ions are retained by membrane at pH > 4 due to adsorption/mass deposition on the membrane surface. The formation of characteristic species due to hydrolysis of UO_2^{2+} and Th^{4+} ions over the pH range 3-9 leads to adsorption/mass deposition on membrane surface.

Uranium exists as uranyl ion (UO_2^{2+}) under acidic conditions (pH < 3), whilst a range of U(VI) complexes are formed with increasing basicity. Carbonate and hydroxide are two important ligands of uranyl ion complex formation in aqueous solution. Uranium species such as $UO_2(OH)^+$, $(UO_2)_2(OH)_2^{2+}$, $(UO_2)_3(OH)_5^+$, $UO_2(OH)_2$, $UO_2(CO_3)(OH)_3^-$,

$UO_2(CO_3)_2^{2-}$ and $UO_2(CO_3)_3^{4-}$ (Fig. 3.1(a)) are formed in the aqueous solution at pH > 3 [129,130]. Th(IV) mostly exist as Th^{4+} at pH $\leq$ 2, the species such as $Th(OH)^{3+}$, $Th(OH)_2^{2+}$, $Th(OH)_4$ are formed in aqueous solution at pH > 2 (Fig.3.1(b)) [131,132]. The relative abundance of above species is a strong function of pH and concentration of U(VI) and Th(IV) in the solution.

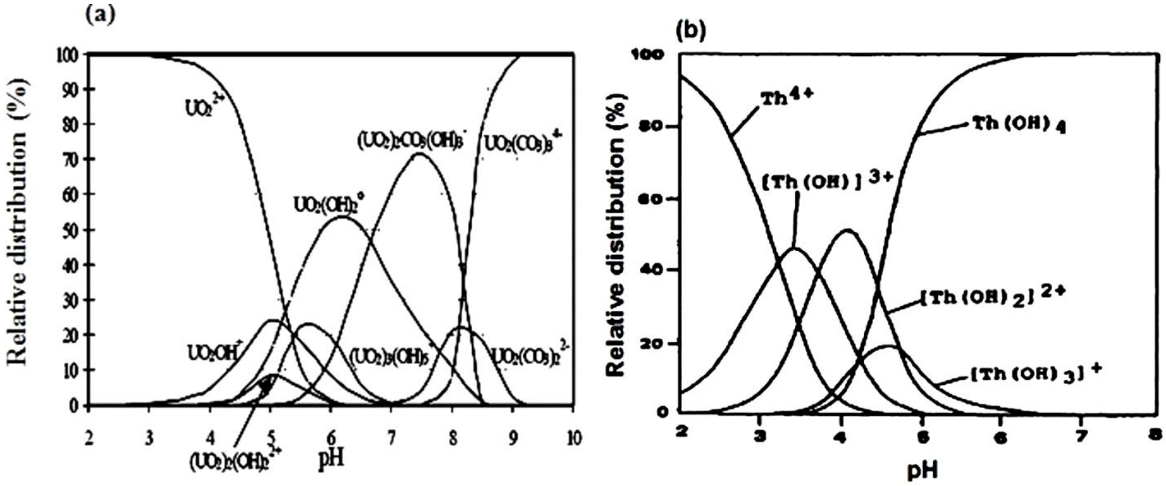

Fig.3.1 Speciation diagram of (a) U(VI) and (b) Th(IV) ions as a function of pH in aqueous solution at atmospheric condition [130,131]

The maximum removal of uranium at pH 5-7 is due to adsorption/mass deposition of uranium species such as $(UO_2)_2(OH)_2^{2+}$, $(UO_2)_3(OH)_5^{+}$ and $UO_2(OH)_2$ on the membrane surface. Giblin et al. [133] confirmed that adsorption of hydrolyzed species occurs more easily than UO_2^{2+} ion. This is due to weak attraction of hydrolyzed uranium species with surrounding water molecules, allowing them to interact with the membrane surface. It was observed that 70–90 % of uranium adsorbed on the membrane (Fig.3.2 (a)) and the percentage removal of uranium was found to be 80-97 % (Fig.3.2 (b)) at pH 5-7. The pH is an important parameter that influences both the speciation of metal ions and charge on the membrane surface. At pH > 7, the percentage of uranium deposited on the membrane surface decreased due to the repulsion between the anionic uranium species

($UO_2(CO_3)^{2-}$, $UO_2(CO_3)(OH)_3^-$ and $UO_2(CO_3)^{4-}$) and negatively charged membrane surface [23]. Hence, uranium gets concentrated in the retentate and the removal of uranium was observed to be more than 80 %. At pH < 5, the percentage uranium removal decreased due to weak interaction of hydrated UO_2^{2+} species with membrane.

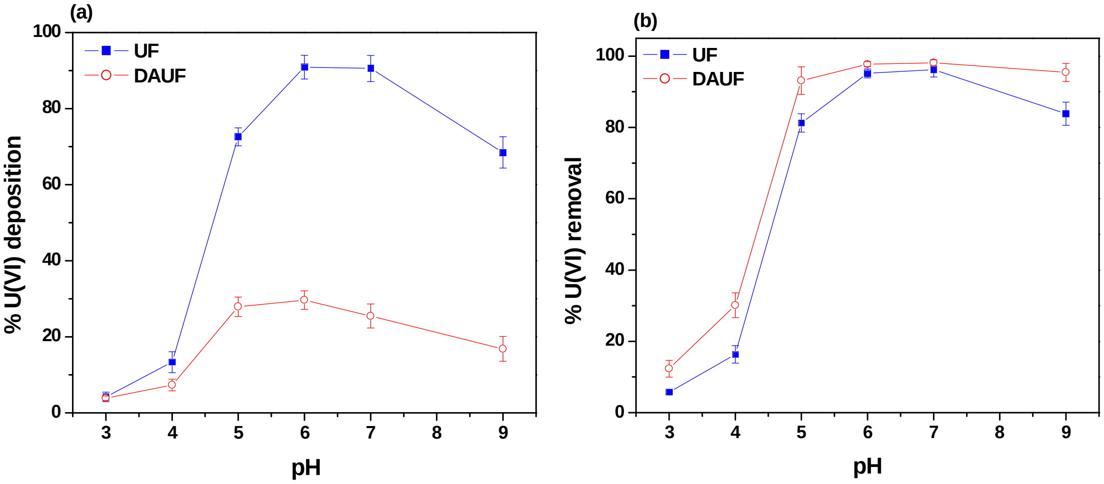

Fig.3.2 Effect of pH on (a) U(VI) deposition and (b) uranium removal

The effect of pH on removal of thorium by ultra filtration is shown in Fig.3.3 (b). At pH 3, the percentage removal of thorium was observed to be < 20 % due to the existence of stable hydrated Th^{4+} ions which passes through the membrane. When pH is increased above 3, the percentage removal of thorium increases and attains maximum at about pH 6 (~97 %). Further increase in pH, does not have any significant effect on removal of thorium (Fig 3.3 (b)). The increase in thorium removal at pH > 3 is due to adsorption/deposition of $[Th_x(OH)_y]^{(4x-y)+}$ species on the surface of regenerated cellulose acetate membrane.

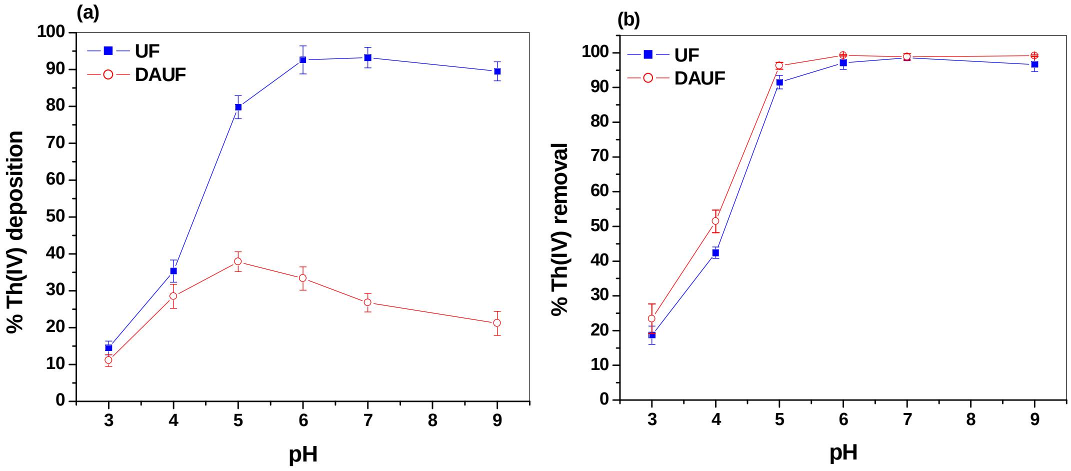

Fig.3.3 Effect of pH on (a) Th(IV) deposition and (b) thorium removal

3.3.2 PAMAM dendrimer assisted UF removal of U(VI) and Th(IV)

The role of PAMAM dendrimer chelating agent on removal of U(VI) and Th(IV) in ultrafiltration technique was studied. It was observed that both the metal ions get concentrated in the retentate by binding with PAMAM dendrimer and mass deposition on the membrane surface was significantly reduced. The PAMAM dendrimer present in aqueous solution effectively forms complexes with U(VI) and Th(IV) and hence concentrates these metal ions in the retentate.

3.3.3 Effect of pH on binding of U(VI) and Th(IV) with PAMAM dendrimer

PAMAM dendrimer assisted ultrafiltration removal of U(VI) and Th(IV) over the pH range 3-9 are shown in Fig.3.2 (b) and 3.3 (b) respectively. At pH < 4, the removal of U(VI) and Th(IV) was observed to be less than 20 % and 30 % respectively. The pH of aqueous solution plays an important role in both metal ion speciation and charges on chelating agent. The charge on chelating agent depends on pKa of the functional group. The pKa of tertiary and primary amine group of PAMAM dendrimer are in the range of 6.3-6.9 and 9.3-9.8 respectively. Hence, at pH < 4, all amine groups of PAMAM dendrimer are completely protonated and only amide groups are available for coordination. The hydrated UO_2^{2+} and Th^{4+} ions are the predominant species in aqueous solution at lower pH (pH < 4). Though the large number of amide functional groups is available, strong electrostatic force of attraction is needed to overcome hydration sphere for coordination with metal ions. Hence, the availability of limited number of complexing sites as well as weak electrostatic force of attraction leads to poor binding of UO_2^{2+} and Th^{4+} cations with PAMAM dendrimer at pH < 4. When pH is increased above 4, deprotonation of tertiary and primary amine functional groups lead to increase in electron density. Moreover, the actinides undergo hydrolysis at pH > 3 and the hydrolyzed species are less hydrated than UO_2^{2+} and Th^{4+} ions. At pH > 4, the hydrolyzed species are effectively binding with PAMAM dendrimer leading to increase in percentage removal of U(VI) and Th(IV) metal ions. In aqueous solution, actinides form strong complexes with hard donor ligands such as CO_3^{2-}, F^-, SO_4^{2-}, PO_4^{3-}, $-COO^-$ etc. In case of soft donor ligands, hydrolysis of actinides occurs predominantly in aqueous solution [134]. Hydrolysis of UO_2^{2+} and Th^{4+} cations in the presence of PAMAM dendrimer was confirmed from fluorescence and potentiometric studies.

3.3.3.1 Fluorescence study

It is reported that speciation strongly affects lifetime as well as emission spectrum of excited uranium [135]. The fluorescence emission spectrum of uranium solution over the pH range of 2-8 is shown in Fig.3.4. The emission spectrum of U(VI) was measured between 475 and 545 nm with an excitation wavelength of 304 nm. The spectrum displays well-resolved peaks at 493, 514 and 539 nm at pH 2. When pH is raised from 2 to 3.8, there is peak broadening with poor band resolution due to the formation of dimer $(UO_2)_2(OH)_2^{2+}$ species [136]. This reveals that hydrolysis of uranyl ions starts at pH > 3. At pH 4.4, the emission is mostly due to trimer $(UO_2)_3(OH)_5^+$ species and the emission intensity increases with further increase in pH upto pH 6 without much change in shape of the emission spectrum. The increase in emission intensity is due to the formation of more and more $(UO_2)_3(OH)^{5+}$ species in the solution. In the range of pH 6-8, the fluorescence emission intensity further increases due to the formation of $UO_2(CO_3)$ species. Thus, fluorescence emission spectra reveal the formation of various uranium species as a function of solution pH.

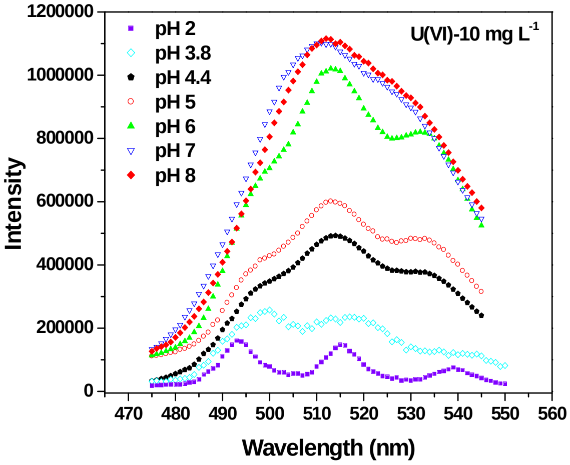

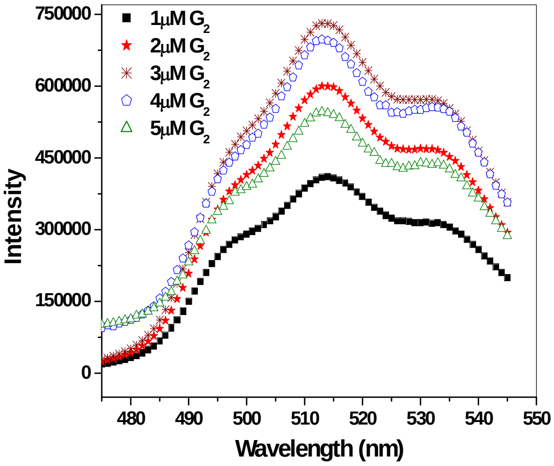

Fig.3.4 Fluorescence emission spectra of U(VI) solution as a function of pH

Fig.3.5 Fluorescence emission spectra of U(VI) as a function of PAMAMG_2

The variation in fluorescence emission intensity of uranium as a function of PAMAM dendrimer concentration (1 to 5 µM) is shown in Fig.3.5. It is observed that the emission intensity increases initially upto 3 µM PAMAM dendrimer concentration and then decreases with further increase in PAMAM concentration. The gradual addition of PAMAM increases pH of the uranium solution due to the protonation of amine groups in PAMAM. As discussed earlier, with increase in pH the emission intensity increases due to formation of various hydrolyzed uranium species. Hence, the emission intensity increases with increase in PAMAM concentration upto 3 µM. Further increase in concentration of PAMAM decreases the emission intensity due to binding of hydrolyzed uranium species with PAMAM. The emission spectrum of U(VI) with 3 µM PAMAM (Fig.3.5) closely resemble the emission spectrum of uranium solution at pH 4.4 (Fig.3.4). At pH 4.4, the emission is predominantly from $(UO_2)_3(OH)_5^+$, with small contribution from $(UO_2)_2(OH)_2^{2+}$. The binding of these hydrolyzed uranium species with PAMAM dendrimer at pH > 4.4 causes quenching of fluorescence and hence, the emission intensity decreases with further increase in PAMAM dendrimer (i.e above 3 µM).

3.3.3.2 Potentiometric titration

Potentiometric titration of $PAMAMG_3$ with UO_2^{2+} and Th^{4+} ions are shown in Fig.3.6. The equal molar concentration of $PAMAMG_3$ and metal ion in 20 mL was titrated against potassium hydroxide under argon atmosphere. The potentiometric curve of $PAMAMG_3$ with UO_2^{2+} shows similar behavior of $PAMAMG_3$ upto pH 4. When pH is raised further (> 4), the curve deviates and continued upto the end of titration. This reveals that at pH < 4, uranium mostly exists as uranyl ion (UO_2^{2+}). The hydrolysis of UO_2^{2+} ions lead to the formation of $UO_2)_3(OH)_5^+$, $(UO_2)_2(OH)_2^{2+}$ and $UO_2(OH)_2$ species showing deviation in potentiometric curve at pH > 4. In case of thorium, hydrolysis starts at pH 3 and the formation of hydrolyzed species such as $Th(OH)^{3+}$, $Th(OH)_2^{2+}$, $Th(OH)^{3+}$ and $Th(OH)_4$ lead to deviation in potentiometric curve at pH > 3. Thus, potentiometric titration confirms the hydrolysis of UO_2^{2+} and Th^{4+} cations even in the presence of PAMAM dendrimer.

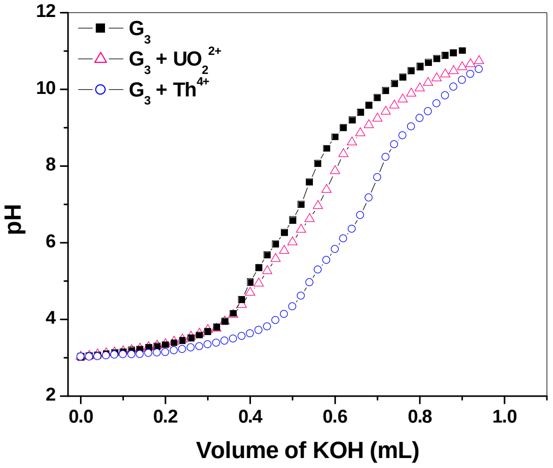

Fig.3.6 Potentiometric titration of $PAMAMG_3$ with UO_2^{2+} and Th^{4+} ions

3.3.4 Effect of dendrimer concentration and generation

DAUF experiments carried out with various concentration of PAMAM dendrimer showed that binding of both uranium and thorium increases with increasing concentration of PAMAMG$_4$ dendrimer and reaches more than 95 % at about 2.5-3 mg L^{-1} of PAMAMG$_4$ dendrimer for an initial concentration of 5 mg L^{-1} of U(VI) and Th(IV) (Fig. 3.7). Hence, the quantity of PAMAMG$_4$ dendrimer required for retaining 1g of U(VI)/Th(IV) in the retentate at pH 6 is calculated to be about 0.6 g. The mole ratio of U(VI)/Th(IV) to PAMAMG$_4$ dendrimer is determined to be about 59 and hence, all subsequent experiments were carried out with a constant mole ratio of 59.

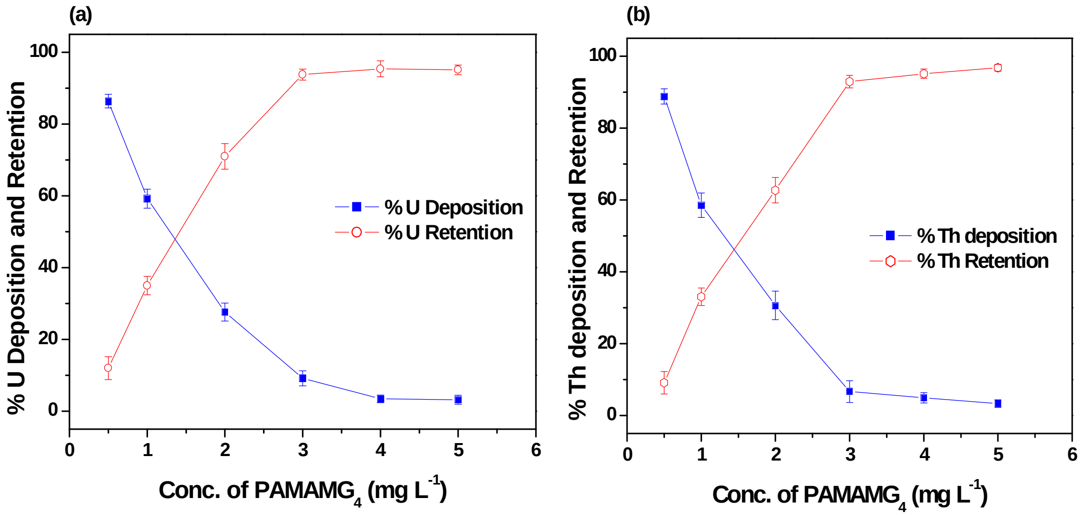

Fig.3.7 Effect of PAMAMG$_4$ concentration on retention and mass deposition of (a) U(VI) and (b) Th(IV)

The number of functional groups and size of PAMAM dendrimer increases as a function of dendrimer generation (Table 2.1). As expected, the concentration of PAMAM dendrimer required for effective binding of U(VI) and Th(IV) metal ions decreases with increase in PAMAM dendrimer generation. It is estimated that about 1.1, 0.6 and 0.45 g of PAMAMG$_3$, PAMAMG$_4$ and PAMAMG$_5$ dendrimers are required for the retention of 1g of U(VI) and Th(IV) in the retentate at pH 6.

3.3.5 Effect of ionic strength on metal ion removal

The effect of $Ca(NO_3)_2$ on removal of U(VI) and Th(IV) is shown in Fig.3.8. In both UF and DAUF, the gradual decrease in percentage removal of U(VI) and Th(IV) were observed with increase in concentration of $Ca(NO_3)_2$. The decrease in percentage removal of U and Th is due to increase in calcium ion which could compete for the co-ordination with PAMAM dendrimer and adsorption on membrane surface.

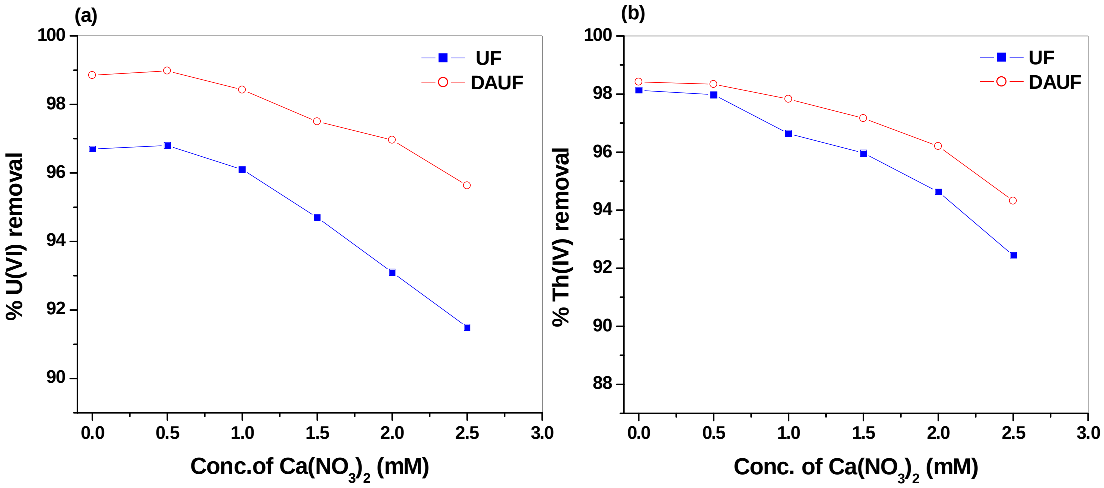

Fig.3.8 Effect of $Ca(NO_3)_2$ concentration on removal of (a) U(VI) and (b) Th(IV)

The effect of chloride ion on percentage removal of uranium and thorium is shown in Fig.3.9. In UF, the initial increase in percentage removal of uranium (upto 1 mM NaCl) is due to the formation of species such as UO_2Cl^+ and $UO_2(OH)Cl$ [137,138] followed by their adsorption on the membrane surface. With further increase in concentration of NaCl, the percentage removal of U(VI) is decreased due to increase in ionic strength which reduces the interaction of uranium species with the membrane. In DAUF, the percentage removal of uranium gradually decreases with increase in chloride ion concentration. It is due to the formation of uranium chloride complex as well as increase in ionic strength which suppresses the binding of uranium with PAMAM dendrimer. Similarly in the case of thorium, the percentage removal gradually decreased with increase in concentration of NaCl in both UF and DAUF.

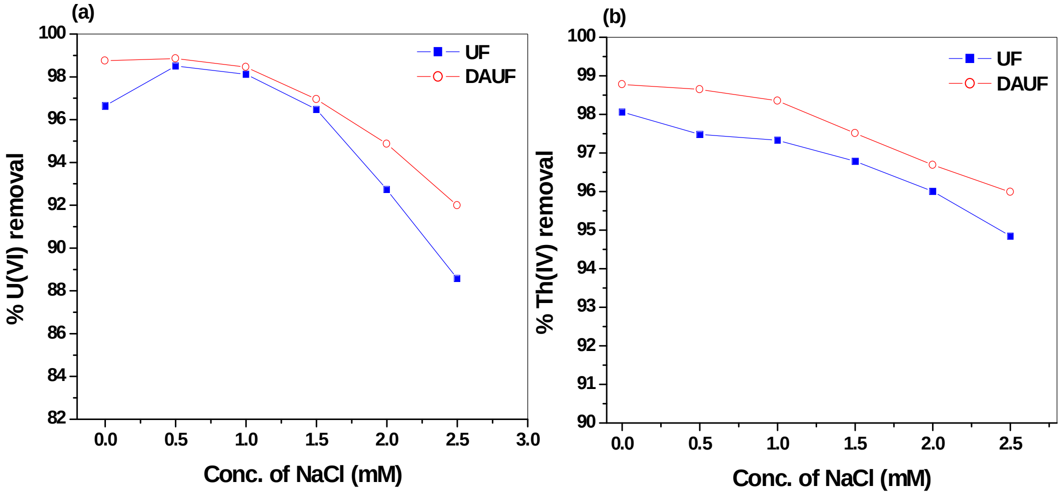

Fig.3.9 Effect of NaCl concentration on removal of (a) U(VI) and (b) Th(IV)

3.3.6 Removal of Eu(III) and Co(II) metal ions by UF and DAUF

Radioactive waste generated in nuclear industry along with actinides will also contain lanthanides, fission product and activated transition metal ions. Hence, UF and DAUF studies were extended for removal of Eu(III) (representative of lanthanides and surrogate of americium) and Co(II) ions (representative of divalent transition metal ions) from aqueous solution. The removal of Eu(III) and Co(II) metal ions over the pH range 3-11 by UF and DAUF technique are shown in Fig.3.10 (a & b). In the absence of PAMAM dendrimer, the removal of these metal ions by UF is maximum at pH > 7. At pH > 7, Eu(III) and Co(II) cations undergo hydrolysis resulting in formation of hydrolyzed species such as $Eu(OH)^{2+}$, $Eu(OH)_2^{+}$, $Eu(OH)_3$ and $Eu(OH)_4^{-}$ [139] and $Co(OH)^{+}$, $Co(OH)_2$ and CoOOH species [140]. The adsorption/ mass deposition of those hydrolyzed species on the membrane surface lead to increase in their removal. The addition of PAMAM dendrimer in aqueous solution effectively binds with hydrolyzed species of Eu(III) and Co(II) metal ions at pH >7 and gets concentrated in the retentate.

The deviation in potentiometric curve for Eu(III) and Co(II) (Fig.3.11) confirms the hydrolysis of Eu(III) and Co(II) metal ions in the presence of PAMAM dendrimer.

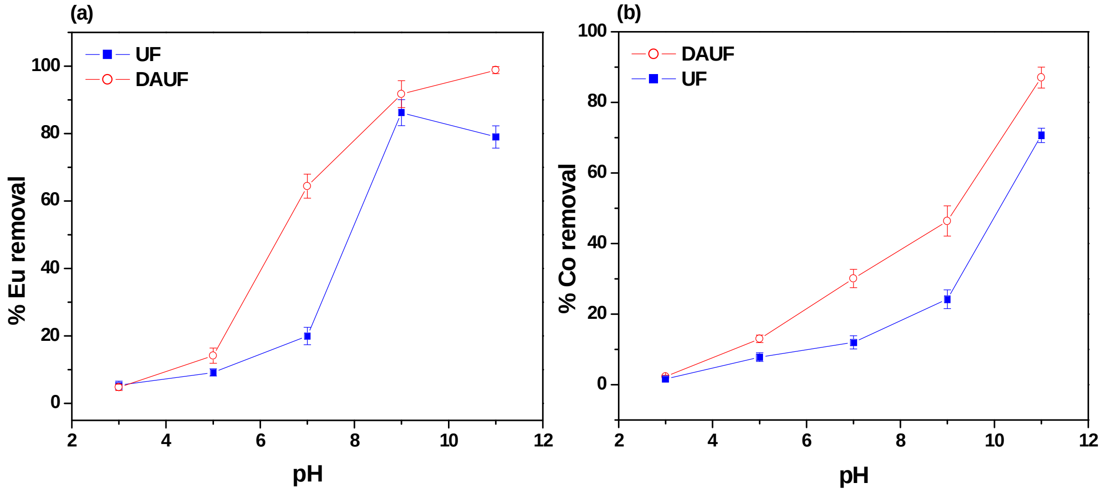

Fig.3.10 Effect of pH on removal of (a) Eu(III) and (b) Co(II) by UF and DAUF

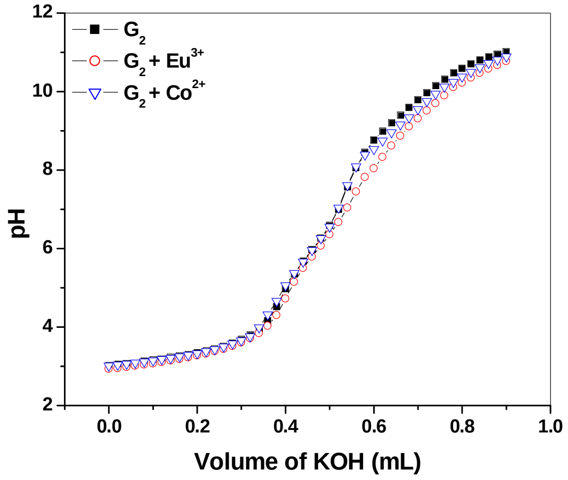

Fig.3.11 Potentiometric tirration curve of PAMAMG$_3$ with Eu^{3+} and Co^{2+} metal ions

3.3.7 Selective and collective removal of U(VI) and Th(IV) metal ions

For successful remediation of wastewater, the chelating agent should possess the ability to bind selectively with metal ions. Separation of target ions allows for proper waste disposal or recycling. Studies on UF and DAUF of U(VI), Th(IV), Eu(III) and Co(II) as a function of pH depict that metal ions speciation plays an important role on removal of these metal ions. The presence of PAMAM dendrimer in aqueous solution does not prevent hydrolysis of metal ions. Instead, it effectively binds with hydrolyzed species of metal ions. The above removal studies also reveal that both U(VI) and Th(IV) metal ions are effectively removed at pH 5-7. In case of Eu(III) and Co(II) metal ions, the removal is maximum at pH > 7. Hence, the selective removal of U(VI) and Th(IV) from SNLW at pH 5.5 were investigated. In both UF and DAUF, the removal of U(VI) and Th(IV) are greater than 90 % whereas for other metal ions it is less than 40 % (Table 3.1).

Table 3.1 Percentage removal of metal ions from SNLW in UF and DAUF at pH 5.5 and 12.5

Metal ions	**% Removal in UF**		**% Removal in DAUF**	
	pH 5.5	**pH 12.5**	**pH 5.5**	**pH 12.5**
Ba	18.57	32.85	18.57	64.29
Ce	35.60	96.96	34.85	93.94
Co	21.66	86.66	26.66	86.66
Gd	35.25	97.43	23.08	94.87
La	23.52	97.06	17.65	94.12
Mn	32.52	92	22.86	84.45
Nd	33.59	96.88	26.56	93.75
Ni	13.09	54.76	19.05	76.19
Sm	39.58	97.22	26.38	94.44
Sr	26.51	31.06	25.76	51.52
Th	**98.07**	**97.59**	**96.15**	**96.15**
U	**93.20**	**98.06**	**90.29**	**95.15**
Zn	28.37	94.59	29.73	89.19
Cs	7.85	12.14	4.28	14.29

Hence, selective removal of U(VI) and Th(IV) from SNLW could be achieved by carrying out UF and DAUF at pH 5.5. Experiments repeated with SNLW at pH 12.5, shows that except alkali and alkaline earth metal ions (Ba, Sr and Cs) the percentage removal of all other metal ions was found to be > 80 % (Table 3.1). Hence, DAUF technique can be used for decontamination of radioactive waste.

3.4 Conclusion

- Removal of U(VI) and Th(IV) ions from aqueous solution by ultrafiltration (UF) and dendrimer assisted ultrafiltration (DAUF) were investigated.
- In UF process, removal of U(VI) and Th(IV) metal ions are observed to be based on adsorption/mass deposition on membrane. Though both U(VI) and Th(IV) ions could be removed in UF by adsorption/mass deposition on the membrane surface, membrane fouling (plugging of membrane pores) occurs on repeated use.
- The pH of the solution plays an important role in removal of both U(VI) and Th(IV) ions. The maximum adsorption of uranium on membrane occurs at pH 5-7 and thorium at pH > 5.
- PAMAM dendrimer effectively binds with U(VI) and Th(IV) in aqueous solution thereby preventing the mass deposition of U(VI) and Th(IV) species on membrane surface. Binding is very effective for both metal ions at pH > 4 and get concentrated in the retentate. The concentration of PAMAM dendrimer required for preventing the mass deposition of metal ions decreases with increase in dendrimer generation.
- PAMAM dendrimer effectively forms complex with hydrolyzed U(VI) and Th(IV) species in aqueous solution. The hydrolysis of U(VI) and Th(IV) ions in presence of PAMAM dendrimer was confirmed from fluorimetric and potentiometric studies.
- Studies on effect of ionic strength revealed that removal of Th(IV) and U(VI) metal ions decreases with increasing concentration of electrolytes (NaCl and $Ca(NO_3)_2$) in both UF and DAUF. However, removal of Th(IV) and U(VI) in DAUF is more effective than UF in the presence of electrolytes.

- Selective and collective separation of Th(IV) and U(VI) was achieved by carrying out UF and DAUF at pH 5.5 and 12.5. The binding of metal ion with PAMAM is very less at acidic pH (pH < 3). Hence, the loaded metal ions can be recovered and regeneration of the PAMAM chelating agent can also be achieved by reducing the pH of aqueous solution.

Chapter-4

ADSORPTION OF U(VI) AND Th(IV) ON PAMAM DENDRON GRAFTED STYRENE DIVINYLBENZENE (PAMAM-SDB) CHELATING RESIN

4.1 Introduction

PAMAM dendrimer contains a large number of nitrogen and oxygen atoms as amino and amide groups on branches and terminal surface showing strong chelating action towards metal ions. Though, dendrimer assisted ultrafiltration (DAUF) using PAMAM chelating agent is effective in removal of metal ions from aqueous solution, the following factors restrict its ease and cost effective operation; (i) synthesis and purification of symmetrical higher generation PAMAM dendrimer and (ii) use of pressure driven ultrafiltration system. Separation methods based on solid phase adsorption are being developed considerably in the last few decades due to their simplicity, rapidity, easy operation and cost effectiveness. PAMAM chelating agent can be functionalized on the surface of solid support by adopting solid-phase synthesis [141]. PAMAM dendron grown on the surface of solid silica particles was used for removal of various metal ions, organic dyes and surfactants from water [142, 143]. If the terminal groups are designed to be binding moieties for target material, then it is apparent that a dendrimer functionalized bead, compared to a macroscopic bead of ion exchange resin (which will have a much smaller surface area than an equivalent amount of dendrimer), can potentially bind with large amount of target materials.

The present study deals with adsorption of uranium and thorium on indigenously developed PAMAM dendron grafted styrene divinyl benzene chelating resin (PAMAM-SDB). Adsorption of uranium and thorium on the surface of this chelating resin was studied by batch experiments. Parameters affecting the adsorption phenomenon such as pH, equilibrating time, metal ion concentration, adsorbent dose, dendron generation and temperature were investigated. Desorption of U(VI) and Th(IV) from the resin surface was studied as a function of pH. Adsorption kinetics was studied using pseudo-first-order, pseudo-second-order, Elovich and intraparticle diffusion models. The adsorption isotherms were analysed by using Langmuir and Freundlich isotherms. The thermodynamic parameters (ΔG^o, ΔH^o and ΔS^o) were evaluated from temperature dependent data. Selectivity of PAMAM-SDB chelating resin towards U(VI) and Th(IV) in SNLW was studied at specific pH condition.

4.2. Experimental

4.2.1. Adsorption studies-Batch experiments

Adsorption experiments were carried out in 50 ml polypropylene centrifuge tube under ambient condition. About 0.01 g of the chelating resin was equilibrated with 10 ml each of 100 mg L^{-1} U(VI) and 20 mg L^{-1} of Th(IV) solutions separately. The pH of the equilibration solutions was adjusted from 2 to10 by using either 0.1M HNO_3 or 0.1M NaOH. After 2 h equilibration at 250 rpm in an orbital shaker, 2 mL of the aliquot was taken and then centrifuged for 5 minutes at 12000 rpm. The concentration of U(VI) and Th(IV) in the supernatant was determined by a spectrophotometer using Arsenazo III complexing agent [115]. The percentage adsorption (% Ads) of U(VI) and Th(IV) were obtained from equation 4.1

$$\% Ads = \frac{C_o - C_e}{C_o} \times 100 \qquad (\%) \tag{4.1}$$

Where C_o and C_e are the initial and equilibrium metal ion concentration (mg L^{-1}).

Blank experiments were conducted without adsorbent to ensure that there was no adsorption of metal ions on the walls of the centrifuge tubes.

4.2.1.1 Adsorption kinetics

Kinetics of sorption describing the solute uptake rate (which in turn governs the residence time of sorption reaction) is one of the important characteristics defining efficiency of sorption. Hence, adsorption of U(VI) and Th(IV) on PAMAMG$_3$-SDB was investigated as a function of contact time between 1 to 180 minutes. For studying kinectics of adsorption, 0.0458 g of PAMAMG$_3$-SDB chelating resin was dispersed in 40 mL of Millipore water and then equilibrated at 250 rpm by adding 40 mL of uranium solution containing 6 mg of U(VI). At various time intervals, 2 mL of aliquot was withdrawn and the concentration of U(VI) in the supernatant was determined. These experiments were repeated with 0.02 g of PAMAMG$_3$-SDB chelating resin and 0.85 mg of Th(IV).

The amount of U(VI) and Th(IV) adsorbed on PAMAMG$_3$-SDB chelating resin at time 't' and at equilibrium were calculated from the following equation 4.2 & 4.3

$$q_t = (C_0 - C_t) \times \frac{V}{m} \qquad (\text{mg g}^{-1}) \tag{4.2}$$

$$q_e = (C_0 - C_e) \times \frac{V}{m} \qquad (\text{mg g}^{-1}) \tag{4.3}$$

Where C_t is the metal ion concentration (mg L^{-1}) at time t, V is the volume of the solution in L and m is the mass (g) of the PAMAMG$_3$-SDB.

Four kinetic models were tested to fit the experimental data of U(VI) and Th(IV) adsorption on PAMAMG$_3$-SDB: pseudo-first-order, pseudo-second-order, Elovich and intraparticle diffusion model. Linear mathematical expressions of these models are given in equation 4.4 – 4.7 respectively [144, 145].

$$\ln(q_e - q_t) = \ln q_e - k_1 t \tag{4.4}$$

$$\frac{t}{q_t} = \frac{1}{k_2 q_e^2} + \frac{t}{q_e} \tag{4.5}$$

$$q_t = \frac{1}{\beta}\ln(\alpha\beta) + \frac{1}{\beta}\ln t \tag{4.6}$$

$$q_t = k_i t^{0.5} + c \tag{4.7}$$

Where k_1 (min^{-1}), k_2 ($g\ mg^{-1}\ min^{-1}$) and k_i ($mg\ g^{-1}\ min^{-1/2}$) are the rate constants of the pseudo-first-order, pseudo-second-order and intraparticle diffusion model respectively. α is the initial adsorption rate ($mg\ g^{-1}\ min^{-1}$), β is the desorption constant ($g\ mg^{-1}$) and c ($mg\ g^{-1}$) is a constant related to adsorption capacity.

4.2.1.2 Adsorption isotherm

Adsorption isotherms were investigated by equilibrating 0.01g of PAMAMG$_3$-SDB chelating resin with various concentrations of both U(VI) and Th(IV) metal ions separately. The experimental adsorption data was analyzed with Langmuir and Freundlich models. The following equations (4.8 & 4.9) are linear forms of Langmuir and Freundlich isotherm models respectively:

$$\frac{C_e}{q_e} = \frac{1}{q_0 b} + \frac{C_e}{q_0} \tag{4.8}$$

$$\ln q_e = \ln K_F + \frac{1}{n}\ln C_e \tag{4.9}$$

Where q_0 ($mg\ g^{-1}$) is Langmuir saturated monolayer adsorption capacity and b ($L\ mg^{-1}$) is Langmuir constant which is related to free energy of adsorption. K_F ($mg^{1-n}\ L^n\ g^{-1}$) and 1/n are Freundlich constants related to adsorption capacity and the adsorption intensity.

4.2.1.3 Adsorption thermodynamics

To study the effect of temperature on U(VI) and Th(IV) adsorption and determining thermodynamic parameters, experiments were carried out at various temperatures between 298 K and 348 K. The thermodynamic parameters (ΔH^o, ΔS^o and ΔG^o) for U(VI) and Th(IV) adsorption on PAMAMG$_3$-SDB can be obtained from the temperature dependent data. Standard enthalpy change, ΔH^o (kJ mole^{-1}) and standard entropy change, ΔS^o (kJ mole^{-1} K^{-1}) were calculated from the linear plot of ln K_d Vs 1/T using Van't Hoff equation 4.10.

$$\ln K_d = \frac{\Delta S^0}{R} - \frac{\Delta H^0}{RT} \tag{4.10}$$

Where, K_d is the distribution coefficient calculated by $K_d = \frac{C_o - C_e}{C_e} \times \frac{V}{m}$ (mL g^{-1}), V is the volume of the solution (mL), R (J K^{-1} mole^{-1}) is universal gas constant and T- temperature in kelvin (K).

Standard free energy change, ΔG^o, (kJ mole^{-1}) is calculated from equation 4.11

$$\Delta G^o = \Delta H^o - T\Delta S^o \tag{4.11}$$

The effect of adsorbent dose on percentage removal of U(VI) and Th(IV) was studied by varying the amount of the chelating resin between 0.0025 and 0.02 g with constant metal ion concentration (U(VI) - 150 mg L^{-1} and Th(IV)-30 mg L^{-1}).

The presence of electrolyte in aqueous medium can vary the adsorption environment by altering the electrostatic interactions between the adsorbent surface and metal ions. Hence, the effect of ionic strength on adsorption was studied with electrolytes such as NaCl, $Ca(NO_3)_2$ and $NaNO_3$ in the concentration range of 0.01–0.1 mol L^{-1}.

4.2.2. Desorption studies

Desorption of metal ions from the chelating resin was studied as a function of reducing pH. About 0.01g of the adsorbent was equilibrated separately with 10 ml of 100 mg L^{-1} U(VI) and 30 mg L^{-1} of Th(IV) solution. After 1 h equilibration, the amount of metal ions adsorbed was estimated. Desorption studies were carried out by adjusting the pH of the above equilibrated solution between 1 and 5. The increase in concentration of U(VI) and Th(IV) in the supernatant was determined and the percentage desorption was calculated from equation 4.12.

$$\%Desorption = \frac{\text{Amount of metal ion released in supernatant (mg L}^{-1}\text{)}}{\text{Amount of metal ion adsorbed (mg L}^{-1}\text{)}} \times 100 \qquad (4.12)$$

4.3. Results and Discussion

4.3.1. Effect of pH on U(VI) and Th (IV) adsorption

Adsorption of U(VI) and Th(IV) on PAMAMG$_3$-SDB as a function of equilibrium pH is shown in Fig.4.1. Adsorption of U(VI) and Th(IV) at pH $\leq$ 4 is observed to be less than 30% due to complete protonation of all primary and tertiary amino groups in PAMAM dendron and only amide groups are available for coordination. At lower pH, hydrated UO_2^{2+} and Th^{4+} species are predominantly exist and their adsorption on chelating resin poor due to the availability of limited number of complexing sites as well as weak electrostatic force of attraction with amide functional group. At pH > 4, the adsorption of U(VI) and Th(IV) were increased due to deprotonation of amino groups leading to increase in adsorption sites and formation of various hydrolyzed species by the hydrolysis of UO_2^{2+} and Th^{4+} ions [130,131] which effectively bind with amine and amide functional groups.

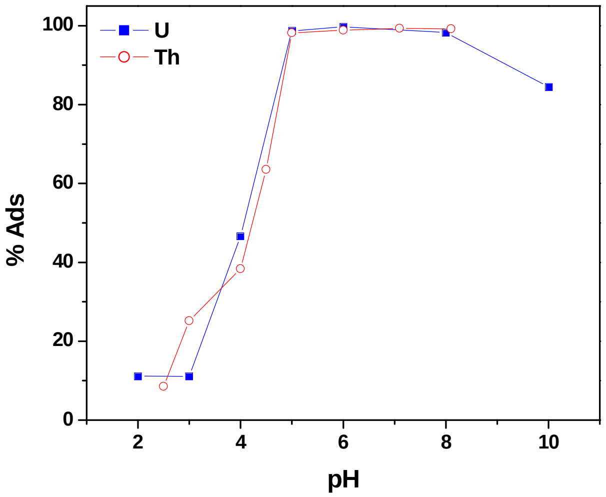

Fig.4.1 Effect of pH on adsorption of U(VI) and Th(IV) onto PAMAMG$_3$-SDB

At higher pH (pH > 7), uranium is present in the anionic form by complexation with carbonate and hydroxyl anions which has less interaction with dendron functional group of chelating resin leading to decrease in adsorption. Studies on effect of pH on adsorption of U(VI) and Th(IV) revealed that strong adsorption of these metal ions occur at pH between 5-7. Hence, all the subsequent experiments were carried out at pH 5-5.5.

4.3.2. Effect of contact time on adsorption

The time profile of U(VI) and Th(IV) adsorption on PAMAMG$_3$-SDB in terms of adsorption capacity is shown in Fig.4.2. It was observed that adsorption of U(VI) and Th(IV) were rapid for the first 5 minutes and then gradually attains equilibrium within 60 minutes suggesting a strong chemisorption or surface complexation of U(VI) and Th(IV) with PAMAMG$_3$-SDB. The rapid adsorption rate suggests high affinity and efficiency of adsorption. From this study, though 60 minutes is enough to achieve equilibrium, the subsequent adsorption experiments were carried out with 120 minutes as equilibration time.

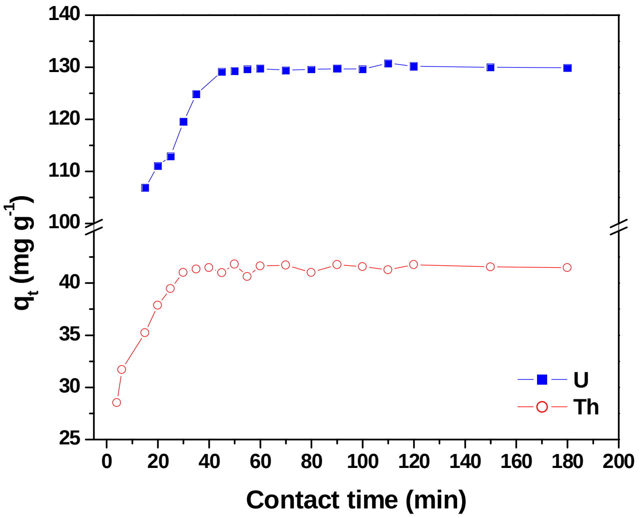

Fig.4.2 Effect of contact time on adsorption of U(VI) and Th(IV) onto PAMAMG$_3$-SDB

4.3.3. Effect of initial metal ion concentration

The measured adsorption capacity of PAMAMG$_3$-SDB for U(VI) and Th(IV) as a function of initial metal ions concentration is shown in Fig.4.3. The amount of U(VI) and Th(IV) adsorbed on the chelating resin increases with increase in metal ion concentration due to the increase in interaction between adsorbate and the adsorbent. Uranium adsorption capacity increases with increase in initial concentration upto 150 mg L^{-1} and beyond which it remains constant. This could be attributed to the saturation of adsorption sites on PAMAMG$_3$-SDB. Similarly for thorium, the adsorption capacity increases with increase in initial metal ion concentration. It is known that thorium forms various $[Th_x(OH)_y]^{(4x-y)+}$ hydroxide species and the relative abundance of Th(IV) species is a strong function of pH and concentration of metal ion [131]. Hence, adsorption study for thorium was carried out at pH 5 and upto a concentration of 40 mg L^{-1} to avoid the precipitation of thorium as $Th(OH)_4$. Experimentally determined adsorption capacity of PAMAMG$_3$-SDB for U(VI) and Th(IV) are 130.25 mg g^{-1} and 36.2 mg g^{-1} for initial concentration of 150 mg L^{-1} and 40 mg L^{-1} respectively.

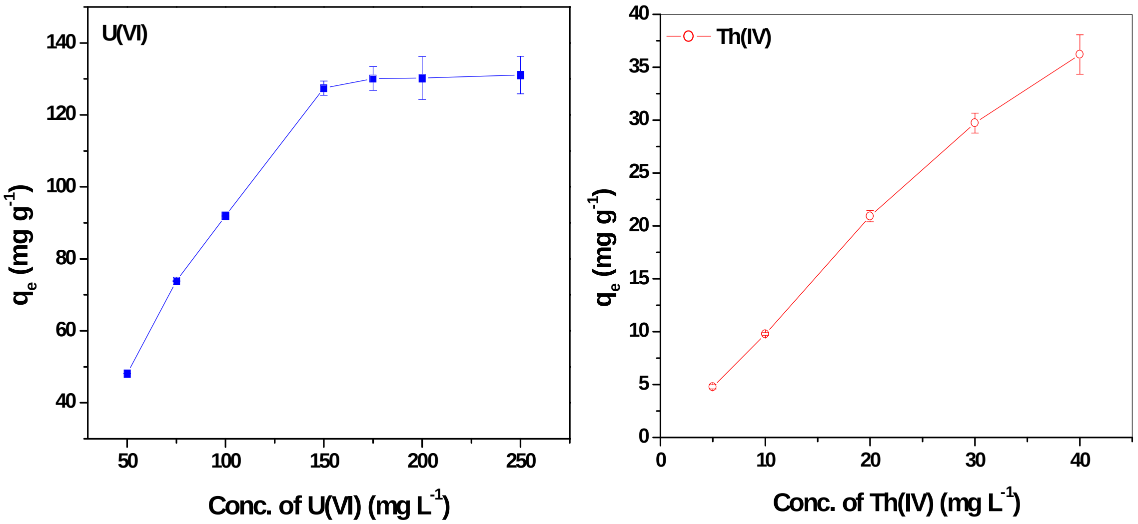

Fig.4.3 Effect of initial concentration of U(VI) and Th(IV) on PAMAMG_3-SDB adsorption capacity

4.3.4 Adsorption Kinetics

It is known that the sorption process could be controlled with mechanisms like mass transfer, diffusion control, chemical reaction and particle diffusion. To investigate the mechanism of adsorption, four kinetic models were tested to fit experimental data of U(VI) and Th(IV) adsorption on PAMAMG_3-SDB: pseudo-first-order, pseudo-second-order, Elovich and intraparticle diffusion model.

Pseudo-first and pseudo-second order models are macroscopic kinetic models commonly used for describing adsorption process. This suggests that adsorption can be considered as either first or second order chemical reaction where the adsorption process is the rate determining step. Intraparticle diffusion model is used to describe the adsorption process where the intraparticle diffusion resistance is rate determining step [52]. Elovich model is used to describe the kinetics of heterogeneous chemisorptions [146].

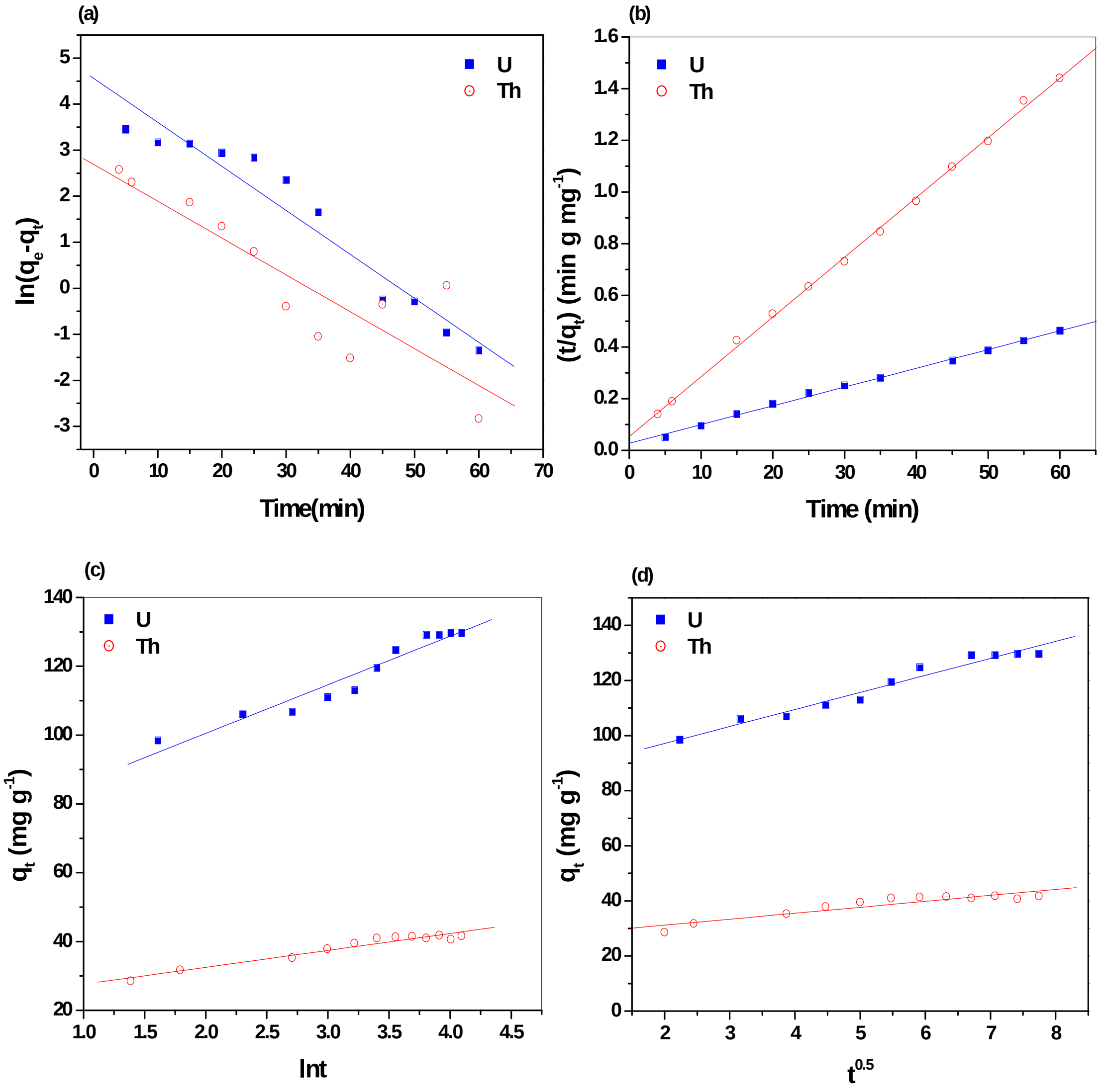

Fig.4.4 Kinetic models for U(VI) and Th(IV) adsorption on PAMAMG$_3$-SDB (a) pseudo-first-order, (b) pseudo-second-order, (c) Elovich and (d) intra-particle kinetic models.

Table 4.1 Kinetic parameters for U(VI) and Th(IV) adsorption on PAMAMG$_3$-SDB

Kinetic model	parameters	U	Th
Pseudo-first-order	k_1 (min^{-1})	0.095	0.080
	q_e (mg g^{-1})	95.94	14.76
	R^2	0.969	0.878
	SD	0.480	0.856
Pseudo-second-order	k_2 (g mg^{-1} min^{-1})	0.002	0.009
	q_e (mg g^{-1})	137.7	43.25
	R^2	0.998	0.999
	SD	0.007	0.016
Elovich	α (mg g^{-1} min)	2357	6.108
	b (g mg^{-1})	0.071	0.203
	R^2	0.968	0.972
	SD	3.004	1.083
Intraparticle diffusion	k_i (mg g^{-1} min$^{1/2}$)	6.180	2.163
	c (mg g^{-1})	84.76	26.86
	R^2	0.982	0.925
	SD	2.292	1.750

Kinetic parameters for above four models of U(VI) and Th(IV) adsorption on PAMAMG$_3$-SDB were calculated from corresponding linear plots such as 'ln(q_e-q_t)' Vs 't', '(t/q_t)' Vs 't', 'q_t' Vs 'lnt' and 'q_t' Vs. '$t^{0.5}$' (Fig. 4.4(a-d)) and the values are listed in Table 4.1. The calculated adsorption capacity of PAMAMG$_3$-SDB for U(VI) and Th(IV) (137.7 mg g^{-1} for U(VI) and 43.25 mg g^{-1} for Th(IV)) at equilibrium time (q_e) from pseudo-second order model is closer to the experimentally determined adsorption capacity (q_0) (130.25 mg g^{-1} for U(VI) and 36.2 mg g^{-1} for Th(IV)). This ensures the applicability of pseudo-second order kinetic model for the adsorption process. Also, the strongest correlation (R^2) and very low SD values (Table 4.1) support the description of pseudo-second order kinetic model. These finding eventually confirmed that the nature of adsorption was concentration dependent and hence, chemical sorption is the rate-controlling step.

4.3.5 Adsorption isotherm

Adsorption isotherms are mathematical models that describe the distribution of adsorbate species among liquid and adsorbents, based on a set of assumptions that are mainly related to the heterogeneity/homogeneity of adsorbents, the type of coverage, and possibility of interaction between the adsorbate species. The Langmuir model assumes that adsorbate molecules do not interact among them self and adsorption is localized in a monolayer. The Freundlich isotherm model is an empirical model describing the sorption of solutes from a liquid to a solid surface and assumes that involvement of various adsorption sites with several adsorption energies [147].

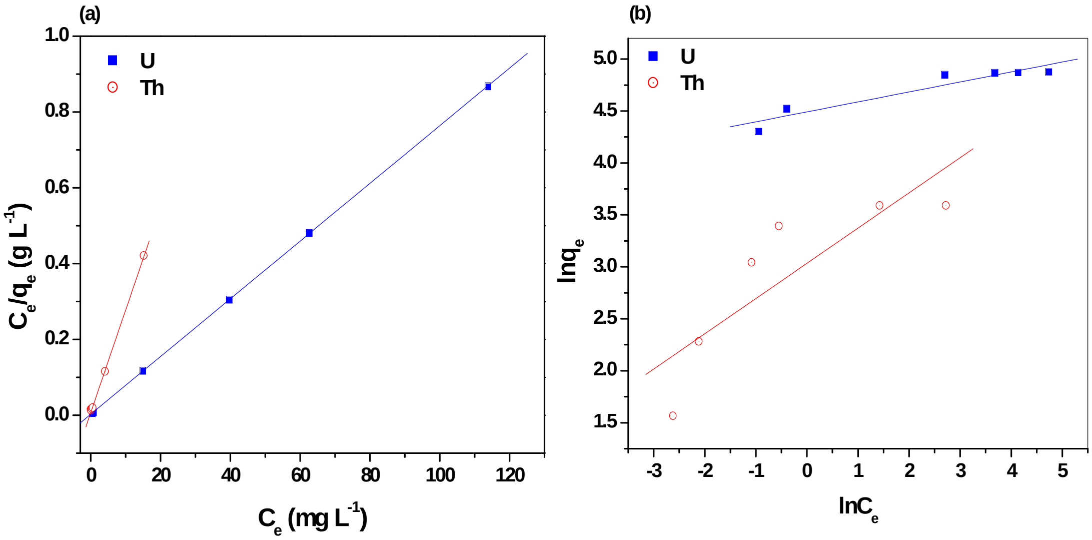

Fig.4.5 (a) Langmuir and (b) Freundlich adsorption isotherm for U(VI) and Th(IV) adsorption on PAMAMG_3-SDB

In order to understand the adsorption capacity of the adsorbent, the equilibrium data was evaluated based on Langmuir and Freundlich models. Linear forms of both models are graphically represented in Fig.4.5 (a & b). The isotherm parameters of each model were calculated by linear regression analysis and the values are given in Table 4.2.

From the values of R^2 and SD, it is concluded that Langmuir isotherm fits with experimental data better than Freundlich model. The results have shown that the calculated adsorption capacities (q_o, 131.58 mg g^{-1} for U(VI) and q_o, 37.01 mg g^{-1} for Th(IV)) from Langmuir isotherm model exhibit good agreement with the experimental values (q_e,130.25 mg g^{-1} for U(VI) and q_e, 36.2 mg g^{-1} for Th(IV)). Hence, the applicability of Langmuir model suggests the monolayer adsorption of U(VI) and Th(IV) on the homogeneous surface of PAMAMG_3-SDB.

Table 4.2 Adsorption isotherm parameters for U(VI) and Th(IV) on PAMAMG_3-SDB

Isotherm	**Langmuir**				**Freundlich**			
Parameters	q_o (mg g^{-1})	b (L mg^{-1})	R^2	SD	K_F (mg g^{-1})	n	R^2	SD
U	131.5	2.105	0.999	0.0014	89.26	10.41	0.949	0.086
Th	37.01	3.636	0.999	0.0040	20.79	2.948	0.854	0.477

The applicability of Langmuir adsorption isotherm was further analyzed by dimensionless equilibrium parameter called separation factor, R_L [148] and is given by following equation (4.13)

$$R_L = \frac{1}{1+bC_0} \tag{4.13}$$

where, b is the Langmuir constant (L mg^{-1}) and C_0 is the initial concentration of metal ion in mg L^{-1}.

R_L is defined as the ratio of unused adsorbent capacity to the maximum adsorbent capacity. The value of R_L indicates the nature of isotherm like unfavorable ($R_L > 1$), linear ($R_L = 1$), favorable ($0 < R_L < 1$) or irreversible ($R_L = 0$). It was observed that the calculated R_L values within 0 – 1 (Fig. 4.6) indicates favorable adsorption of U(VI) and Th(IV) on PAMAMG_3-SDB and the applicability of Langmuir isotherm.

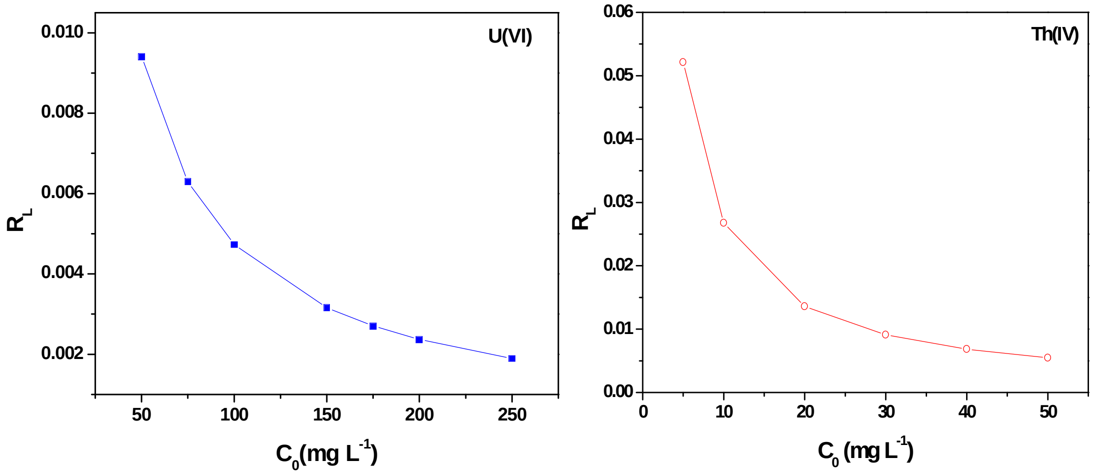

Fig.4.6 Langmuir separation factor (R_L) as a function of initial metal ion concentration

4.3.6. Effect of PAMAMG$_3$-SDB dosage

The percentage removal of U(VI) and Th(IV) with increasing amount of PAMAMG$_3$-SDB chelating resin is shown in Fig.4.7. Experimental results reveal that the removal efficiency increases with increasing adsorbent dosage due to increase in adsorption sites and/or surface area. About 99 % removal of U(VI) was achieved with 0.0105 g of adsorbent for initial U(VI) of 150 mg L^{-1} at pH 5.5. In case of Th(IV), about 90 % removal was achieved with 0.0105 g of adsorbent for initial Th(IV) concentration of 30 mg L^{-1} at pH 5.

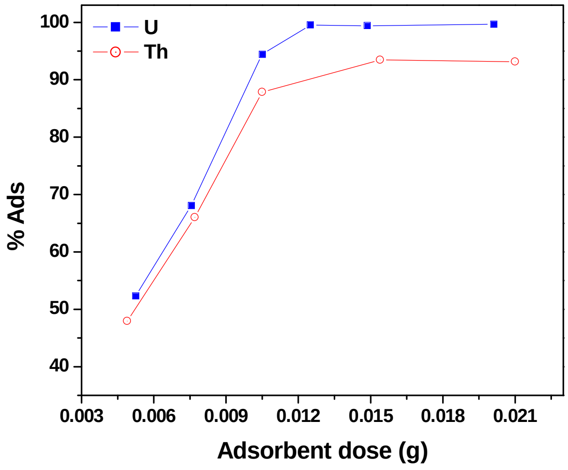

Fig.4.7 Effect of PAMAMG$_3$-SDB dosage on adsorption of U(VI) and Th(IV)

4.3.7. Adsorption thermodynamics

Studies on effect of temperature on uranium adsorption showed that uranium adsorption increases with increasing temperature (Fig.4.8). A positive value of ΔH^o (Table 4.3) indicates uranium adsorption is endothermic in nature. To get adsorbed on the adsorption sites of PAMAMG$_3$-SDB, the hydration shell surrounding uranium ions has to be broken. Thus, dehydration process requires energy input. Energy will be released when these dehydrated uranium ions get adsorbed on the surface of the PAMAMG$_3$-SDB. If the energy inputs in the former process exceed the energy released in the later process, then the adsorption becomes endothermic [149]. The negative value of free energy of adsorption (ΔG^o) confirms the feasibility and spontaneous nature of adsorption process. The negative value of ΔG^o increases with increase in temperature. This indicates that effective adsorption occurs at higher temperature. Uranium ions are readily dehydrated at higher temperature and hence their adsorption is more favorable. The positive value of ΔS^o suggests an increase in randomness at the solid/liquid interface during adsorption process. Randomness arises due to the destruction of hydrated uranium ions prior to the adsorption on the surface of the adsorbent.

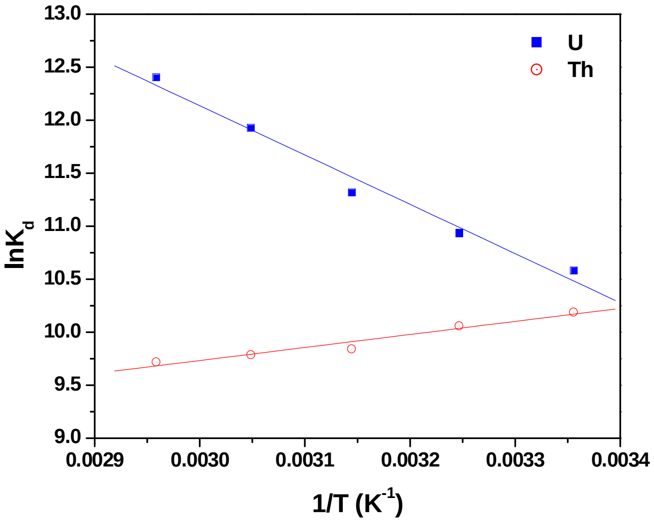

Fig.4.8 Effect of temperature on U(IV) and Th(IV) adsorption onto PAMAMG$_3$-SDB

In case of thorium, the increase in K_d with decrease in temperature (Fig.4.8) indicates that adsorption is more effective at lower temperature. The negative value of ΔH^o (Table 4.3) shows that the adsorption process is exothermic. The negative ΔG^o value indicates that the adsorption is thermodynamically favorable and spontaneous. One possible interpretation of exothermicity of enthalpy of adsorption is that Th(IV) ions are weakly hydrated at pH 5 and hence hydration energy is low. The exothermicity associated with the adsorption of Th(IV) ions exceed the dehydration energy of Th(IV) ions and hence, the adsorption process is exothermic [150]. The positive value of ΔS^o reflects an increased randomness at adsorbate-adsorbent interface during the adsorption process due to destruction of hydrated thorium prior to adsorption on the surface of PAMAMG_3-SDB.

Table 4.3 Thermodynamic parameters of U and Th adsorption on PAMAMG_3-SDB

Thermo-dynamic Parameters	**ΔH^o (kJ mol^{-1})**	**ΔS^o (kJ mol^{-1} K^{-1})**	**ΔG^o (kJ mol^{-1})**				
			298 K	**308 K**	**318 K**	**328 K**	**338 K**
U	38.65	0.216	-25.97	-27.14	-30.31	-32.48	-34.65
Th	-10.50	0.049	-25.21	-25.70	-26.19	-26.69	-27.18

4.3.8 Effect of dendron generation

Adsorption capacity of PAMAMG_3-SDB for U(VI) and Th(IV) as a function of PAMAM dendron generation are shown in Fig. 4.9. In both cases, adsorption capacities increased exponentially with increasing dendron generation due to exponential increase in number of amide, tertiary and primary amino groups in the chelating resin. The number of amine, amide and primary amino groups as a function of PAMAM dendron generation (G_1-$_5$) is given in Table 2.6 (chapter 2). Adsorption capacity of PAMAMG_5 dendron–SDB for U(VI) and Th(IV) metal ions is found to be 493 and 253.7 mg g^{-1} at pH 5.5 and 5 respectively.

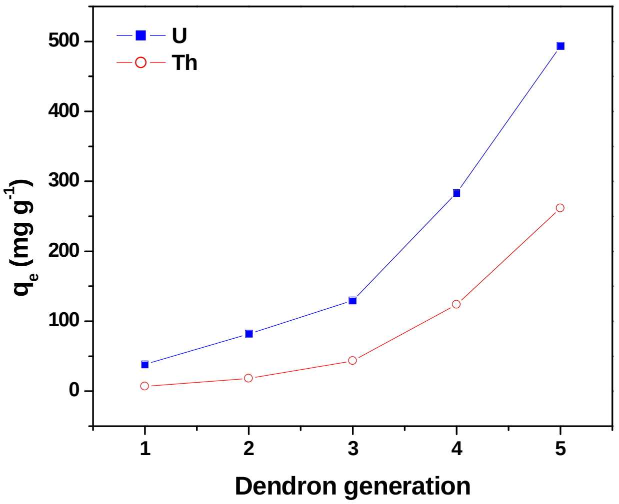

Fig.4.9 Effect of PAMAM dendron generation on uranium adsorption capacity

4.3.9. Effect of ionic strength

The effect of ionic strength on adsorption studied with electrolytes such as NaCl, $Ca(NO_3)_2$ and $NaNO_3$ is shown in Fig. 4.10. The results show that presence of $NaNO_3$ has no significant effect on adsorption of both U(VI) and Th(IV) metal ions at this concentration range. Adsorption of U(VI) and Th(IV) were observed to be increased with increase in sodium chloride concentration upto 0.05 mol L^{-1} and then decreased. The initial increase in adsorption may be attributed to the formation of neutral polar species ($UO_2(OH)Cl$, $Th(OH)_3Cl$ and $Th(OH)_2Cl_2$) [137, 138] which enhances the adsorption process. At higher NaCl concentration, the increase in ionic strength reduces the interaction of uranium and thorium species with adsorbent surface attributing to decrease in adsorption. In case of $Ca(NO_3)_2$, a gradual decrease in adsorption was observed with increase in concentration of calcium ions due to reduction in U(VI) and Th(IV) interaction with adsorbent surface.

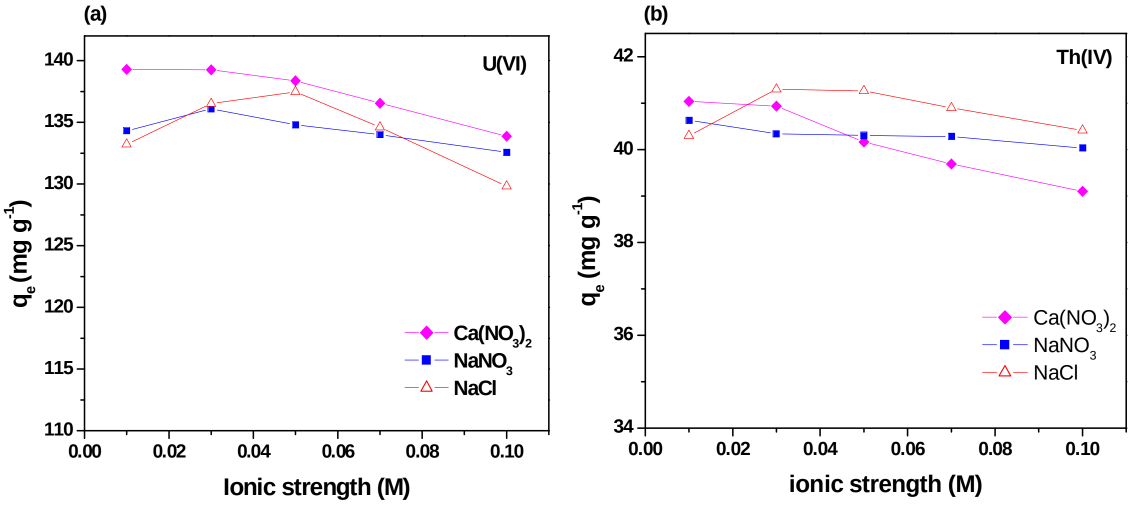

Fig.4.10 Effect of ionic strength on (a) U(VI) and (b) Th(IV) adsorption

4.3.10 Desorption of U(VI) and Th(IV) from resin

Regeneration and reusing of adsorbent significantly reduces the overall cost of removal process in industrial scale. Experimental results on adsorption of U(VI) and Th(IV) as a function of pH reveal that the adsorption is very low at acidic pH (Fig.4.1) and hence, the desorption of metal ions from the chelating resin could be achieved by lowering the pH. Desorption studies carried out at pH range between 5 and 1 show that the percentage desorption increases with decrease in pH (Fig.4.11) and a maximum desorption of ~99% was achieved at pH 1.

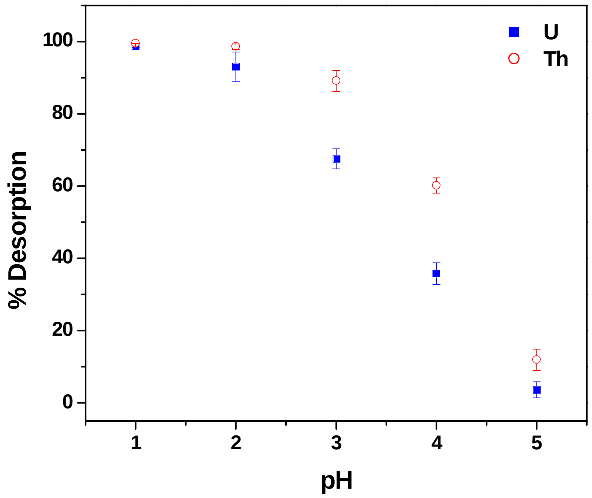

Fig.4.11 Desorption of U(VI) and Th(IV) from adsorbent as a function of pH

4.3.11. Recovery of U(VI) and Th(IV) from SNLW

The main objective of developing this chelating resin is to recover actinides from nuclear aqueous waste. Adsorption of actinides on PAMAM dendron-SDB chelating resin was studied from SNLW. Equilibration of PAMAMG$_3$-SDB with SNLW at pH 5.5 clearly indicates a higher degree of affinity of chelating resin towards U(VI) and Th(IV) over other diverse ions (Table 4.4), thereby proving its application in selective removal of actinides from aqueous nuclear waste. Decontamination of SNLW at pH 12.5 shows that except cesium and strontium, actinides and lanthanides are effectively removed.

Table 4.4 Percentage removal of metal ions from simulated nuclear waste

Metal ions	% Removal at pH 5.5	% Removal at pH 12.5
Ba	21.43	71
Ce	37.88	99.39
Co	20	98
Gd	19.23	99.49
La	17.65	99.41
Mn	44	98.4
Nd	26.56	99.38
Ni	21.43	82.62
Sm	22.22	99.44
Sr	18.18	60.61
Th	99.62	99.62
U	89.32	99.61
Zn	16.22	98.92
Cs	4.29	18.57

4.4. Conclusion

- A new PAMAM dendron-functionalized styrene divinylbenzene chelating resin, first of its kind, was synthesized. Adsorption of U(VI) and Th(IV) on PAMAMG$_3$-SDB chelating resin was studied in a series of batch experiments.
- Adsorption capacity of PAMAMG$_3$-SDB chelating resin was observed to be dependent on contact time, pH, initial concentration of metal ion and temperature. Kinetic study shows that the adsorption process is fast and reaches equilibrium within 60 minutes. The kinetic data fits well with pseudo-second-order model. Langmuir adsorption isotherm is found to be more suitable for explaining adsorption process. The kinetic and isotherm data confirm chemisorption of U(VI) and Th(IV) on PAMAMG$_3$-SDB.
- The chelating resin shows high adsorption capacity even at high ionic strength. Adsorption capacity of PAMAMG$_5$-SDB chelating resin for U(VI) and Th(IV) was estimated to be 493 and 253.7 mg g^{-1} at pH 5.5 and 5 respectively.
- The adsorbed U(VI) and Th(IV) metal ions can be easily desorbed from resin by reducing the pH of the solution and maximum of ~ 99 % desorption was observed at pH 1. The influence of pH on adsorption suggests that adsorption of metal ions on PAMAMG$_3$-SDB chelating resin is dominated by surface complexation.
- The effect of temperature on adsorption of U(VI) and Th(IV) metal ions were investigated and thermodynamic parameters (ΔH°, ΔS°, ΔG°) were evaluated. It is observed that, adsorption of uranium on PAMAMG$_3$-SDB is endothermic whereas adsorption of thorium is exothermic.
- Studies with simulated nuclear waste reveal that PAMAM dendron-SDB chelating resin is effective in selective removal of U(VI) and Th(IV) in presence of various fission and activated corrosion products.

- The study demonstrates that growth of PAMAM dendron on surface of SDB is a successful strategy for efficient and easy removal/ pre-concentration of actinides from aqueous waste.

Chapter-5

STUDIES ON REMOVAL OF U(VI) AND Th(IV) FROM AQUEOUS AND NITRIC ACID MEDIUM USING DIGLYCOLAMIC ACID FUNCTIONALIZED PAMAM-SDB CHELATING RESIN (DGA-PAMAM-SDB)

5.1 Introduction

Radioactive wastes generated during various stages of nuclear fuel cycle generally contain actinides and various fission products in aqueous and nitric acid medium. Though, indigenously developed PAMAM dendron-SDB resin is effective in removal of uranium and thorium from aqueous solution, it becomes less effective in acidic medium. Quantitative recovery of actinides in trace level from highly acidic medium is the most challenging task.

In strong acidic medium, various chelating resins containing phosphate and amide chelating groups were employed for recovery of actinides [66-79]. Amide based resins posses advantages such as innocuous degradation products, high radiolytic stability and complete incinerability [77-79]. A number of amide based resins have been extensively studied for the separation of radionuclides from acidic waste solution. Among them, tridentate diglycolamides (DGA) [151] and diglycolamic acid [152, 153] are reported to exhibit high distribution coefficient for actinides and lanthanides in high acidic condition.

In the present work, terminal primary amine groups in PAMAM dendron-SDB were modified with DGA functional groups and abbreviated as DGA-PAMAM-SDB chelating resin. Synthesis and characterization of this resin is described in section 2.2 of chapter-2. Adsorption of U(VI) and Th(IV) metal ions onto DGA functionalized third generation PAMAMG$_3$-SDB chelating resin (DGA-PAMAMG$_3$-SDB) was studied in batch experiments. The influence of pH, nitric acid concentration, initial metal ion concentration, adsorbent dosage, ionic strength and dendrimer generation on adsorption was investigated. Kinetics of adsorption was analyzed from contact time dependence data. Adsorption isotherm was analysed by using Langmuir and Freundlich equations. Effect of temperature on uptake of U(VI) and Th(IV) by DGA-PAMAMG$_3$-SDB chelating resin was studied and thermodynamic parameters (ΔH°, ΔS° and ΔG°) were determined. Selective removal of U(VI) and Th(IV) from SNLW using DGA-PAMAMG$_3$–SDB chelating resin was studied. The reusability of the resin was tested by conducting desorption experiments.

5.2 Experimental

5.2.1 Adsorption studies-Batch experiments

About 0.01 g of DGA-PAMAMG$_3$-SDB chelating resin was equilibrated separately with 10 mL of 250 mg L^{-1} U(VI) and 100 mg L^{-1} of Th (IV) solutions. The pH of equilibrium solutions were adjusted between 2 and 9 by using either 0.1M HNO$_3$ or 0.1M NaOH. After 2 h equilibration at 250 rpm using an orbital shaker, 2 mL of aliquot was taken and centrifuged for 5 minutes at 12000 rpm. The concentration of U/Th metal ions in the supernatant was estimated by spectrophotometry using Arsenazo III complexing agent [115]. The percentage adsorption (% Ads) of U(VI) and Th(IV) were calculated using equation 4.1. Effect of nitric acid concentration on adsorption of U(VI) and Th(IV) on DGA-PAMAMG$_3$-SDB was investigated by varying concentration of nitric acid from 0.5 M to 6 M.

Adsorption of U(VI) and Th(IV) on DGA-PAMAMG$_3$-SDB was investigated as a function of contact time for a period of 1-180 minutes. For studying kinetics of adsorption, 0.022 g of DGA-PAMAMG$_3$-SDB resin was dispersed in 50 mL of Millipore water and then equilibrated with 50 ml of U(VI) solution containing 6 mg of uranium. At various time intervals, 2 mL of aliquot was withdrawn and the concentration of U(VI) in supernatant was determined. Similarly, experiments were repeated with 0.041 g of DGA-PAMAMG$_3$-SDB resin and 10.3 mg of Th(IV). The amount of U(VI) and Th(IV) adsorbed on DGA-PAMAMG3-SDB chelating resin with time ‘t’ and at ‘equilibrium’ were calculated by using equations 4.2 & 4.3.

Adsorption isotherms were investigated by equilibrating 0.01g of DGA-PAMAMG_3-SDB chelating resin separately with various concentrations of U(VI) and Th(IV) between 100 mg L^{-1} and 600 mg L^{-1}. Adsorption capacity of DGA-PAMAM-SDB as function of dendron generation were determined by equilibrating with various initial concentration of U(VI) and Th(IV) metal ions.

The effect of adsorbent dose on percentage removal of U(VI) and Th(IV) was studied by varying the amount of chelating resin between 0.0025 g and 0.02 g in 10 mL with constant metal ion [U(VI)-250 mg L^{-1} and Th(IV)-100 mg L^{-1}] concentration. Effect of ionic strength on adsorption was studied with various concentration of NaCl, $Ca(NO_3)_2$ and $NaNO_3$ between 0.01 and 0.1 mol L^{-1}.

To study the effect of temperature on U(VI) and Th(IV) adsorption, the above experiments were carried out at various temperatures between 298 K and 348 K. The thermodynamic parameters (ΔH^o, ΔS^o and ΔG^o) for U(VI) and Th(IV) adsorption on DGA-PAMAMG_3-SDB were determined from the temperature dependent data.

5.2.2 Desorption studies

About 0.01g of adsorbent was equilibrated separately with 10 ml of 250 mg L^{-1} U(VI) and 150 mg L^{-1} of Th(IV) solution. After 1 h equilibration, the supernatant was analyzed for metal ion concentration and the amount adsorbed was estimated. Desorption experiments were carried out by varying the acid concentration in the above equilibrated solution between 10^{-5} M and 1 M. The concentration of metal ion in the supernatant was determined and the percentage desorption was calculated using equation 4.12.

5.3 Results and Discussion

5.3.1. Effect of pH on U(VI) and Th (IV) adsorption

The solution pH is one of the dominant parameters controlling adsorption. Fig.5.1 shows the percentage adsorption of both U(VI) and Th(IV) on DGA-PAMAMG$_3$-SDB as a function of equilibrium pH between 2 and 9. Adsorption of U(VI) at pH ≤ 3 is observed to be less than 20% due to complete protonation of tertiary amino groups of PAMAM chelating resin as well as weak interaction between amide and unionized DGA groups with solvated uranyl ions. At pH > 3, the ionization of DGA groups and deprotonation of tertiary amine groups increase the electron donating ability of the resin. Hence, the percentage removal of uranium increased from ~ 10 % (pH 2) to ~ 94 % (pH 6). Similarly, the percentage adsorption of thorium increases with increase in pH and attains maximum at about pH 6. Further increase in solution pH (pH > 6), the percentage removal of both U(VI) and Th(IV) was decreased due to the weak interaction of metal ion species with the surface functional groups of the resin. At pH > 6, complete ionization of diglycolamic acid groups (pK$_a$- 4.2) result in negative charges on the resin surface and the neutral $Th(OH)_4$ has weak interaction with this negatively charged resin. In case of uranium, the anionic species such as $UO_2(CO_3)(OH)_3^{-}$, $UO_2(CO_3)_2^{2-}$ and $UO_2(CO_3)_3^{4-}$ at pH (> 6) are getting repelled from negatively charged surface of the chelating resin. Hence, adsorption of both U(VI) and Th(IV) metal ions on the chelating resin decreases at pH > 6. At pH 2-4, Th(IV) shows high percentage of adsorption due to strong complexation with DGA functional groups whereas U(VI) shows significant adsorption only at pH > 4 (Fig. 5.1). Hence, separation of U and Th from each other at lower acidic region (pH 3-4) is feasible by using DGA-PAMAMG$_3$-SDB.

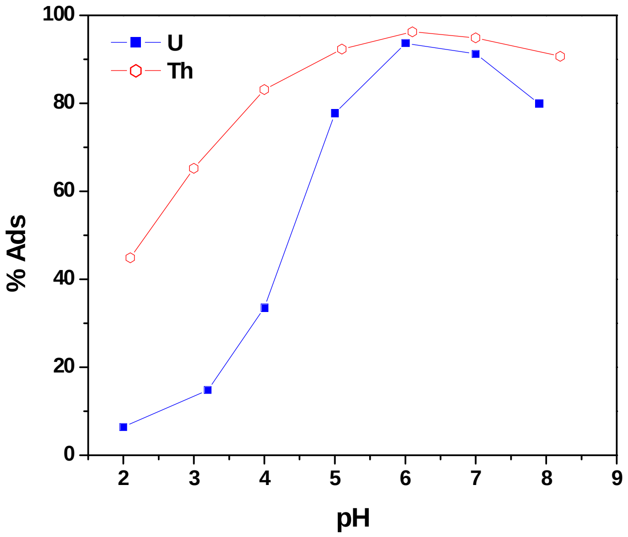

Fig.5.1 Effect of pH on adsorption of U(VI) and Th(IV) onto DGA-PAMAMG_3-SDB

5.3.2 Effect of nitric acid concentration on adsorption

The percentage adsorption of U(VI) and Th(IV) determined as a function of nitric acid concentration is shown in Fig.5.2. It shows that percentage adsorption increases gradually with increase in nitric acid concentration and reaches maximum at 3-4 M. Further increase in HNO_3 concentration does not alter the percentage of adsorption. At acidic condition (pH < 2), DGA group remains in unionized form and all tertiary amine groups are completely protonated. At acidic medium DGA act as neutral chelating group and can bind effectively with neutral metal nitrate species. The increase in percentage adsorption with increase in nitric acid concentration can be explained based on law of mass action (equilibrium reaction 5.1) [77].

$$M^{n+} + nNO_3^- + \text{DGA-PAMAM-SDB} \leftrightarrow M(NO_3)_n.\text{DGA-PAMAM-SDB} \qquad (5.1)$$

Formation of $M(NO_3)_n$ species increases with increase in nitric acid concentration thereby increases the percentage of adsorption. This study suggests that DGA modified PAMAM-SDB resin is applicable for the removal of U and Th from nitric acid medium.

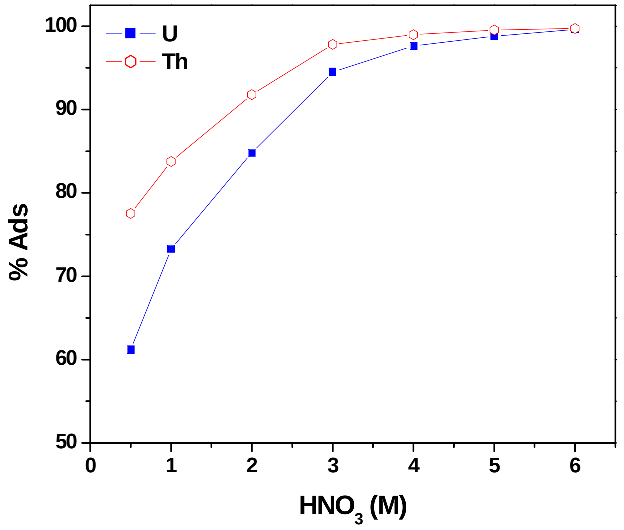

Fig.5.2 Effect of HNO_3 concentration on adsorption of U(VI) and Th(IV) onto DGA-PAMAMG_3-SDB

5.3.3 Effect of contact time

The time profile of U(VI) and Th(IV) adsorption on DGA-PAMAMG3-SDB in terms of adsorption capacities (q_t) are shown in Fig.5.3. The study reveals that adsorption of U(VI) and Th(IV) is rapid in the beginning and then gradually attain equilibrium within 60 minutes. Initially, rapid adsorption occurs due to the surface complexation of U(VI) and Th(IV) on DGA-PAMAMG_3-SDB chelating resin. Subsequently, the adsorption process is slowed down due to saturation of complexation site at the surface. Further adsorption could be possible due to the diffusion of the metal ions onto the resin. From the contact time study, though 60 minutes is enough to achieve equilibrium (Fig. 5.3), the subsequent adsorption experiments were carried out with 120 minutes to ensure attaining of equilibrium.

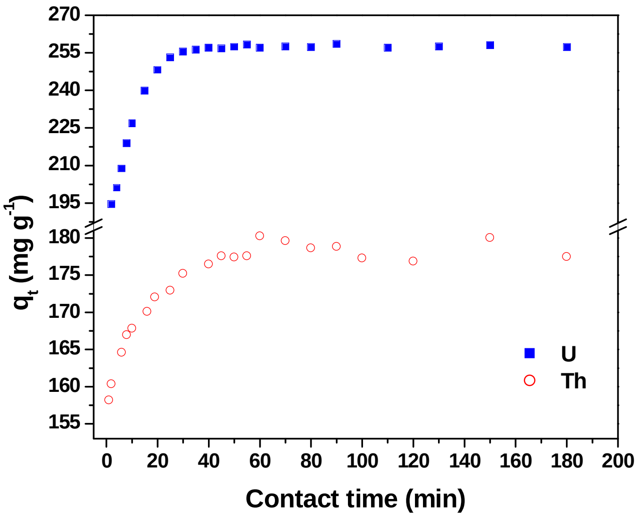

Fig.5.3 Effect of contact time on adsorption of U and Th onto DGA-PAMAMG$_3$-SDB

5.3.4 Effect of initial metal ion concentration

The adsorption capacity of DGA-PAMAMG$_3$-SDB for U(VI) and Th(IV) determined as a function of initial metal ion concentrations is shown in Fig. 5.4. It reveals that the amount of U(VI) and Th(IV) adsorbed on the chelating resin increase with increase in metal ion concentration. The increase in mass driving force from bulk solution to the adsorbent surface enhances the interaction between adsorbate and the adsorbent. Adsorption capacity of DGA-PAMAMG$_3$-SDB for uranium increases with increase in uranium concentration upto 350 mg L^{-1} after that almost remains constant (Fig.5.5). This can be attributed to the saturation of adsorption sites on DGA-PAMAMG$_3$-SDB. Similarly for thorium, the adsorption capacity increases with increase in Th(IV) concentration and saturates at about 300 mg L^{-1}. Adsorption capacity of DGA-PAMAMG$_3$-SDB for U(VI) and Th(IV) metal ions were determined to be 286 mg g^{-1} and 187 mg g^{-1} respectively.

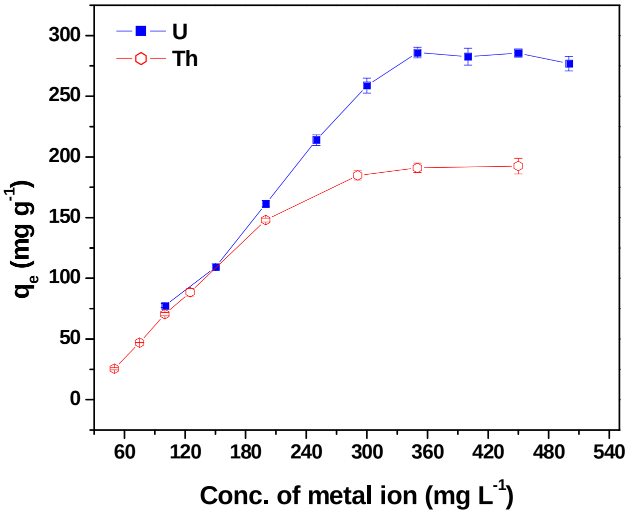

Fig.5.4 Effect of initial U(VI) and Th(IV) concentrations on adsorption capacity

5.3.5 Adsorption kinetics

To analyze the mechanism and rate of adsorption, four kinetic models such as pseudo-first order, pseudo-second order, Elovich and intraparticle diffusion model were tested to fit experimental data of U(VI) and Th(IV) adsorption as a function of contact time on DGA-PAMAMG$_3$-SDB. Linear mathematical expressions of these respective models are given in equations 4.4 to 4.7.

Kinetic parameters for all the above four models were calculated from corresponding linear plots 'ln(q_e-q_t)' Vs 't', 't/q_t' Vs 't', 'q_t' Vs 'lnt' and 'q_t' Vs. '$t^{0.5}$' respectively (Fig. 5.5 (a-d)) and the values are listed in Table 5.1. The calculated adsorption capacity of DGA-PAMAMG$_3$-SDB for U(VI) & Th(IV) (263.9 mg g^{-1} for U(VI) and 180.2 mg g^{-1} for Th(IV)) at equilibrium time (q_e) from pseudo-second-order model is closer to the experimental determined adsorption capacity (286 mg g^{-1} for U(VI) and 187 mg g^{-1} for Th(IV)). This ensures applicability of pseudo-second-order kinetic model for describing the adsorption process. The strongest correlation (R^2) and very low SD (Table 5.1) values also support the applicability of pseudo-second order kinetic model. Hence, the chemisorption may be the rate determining step in the adsorption process.

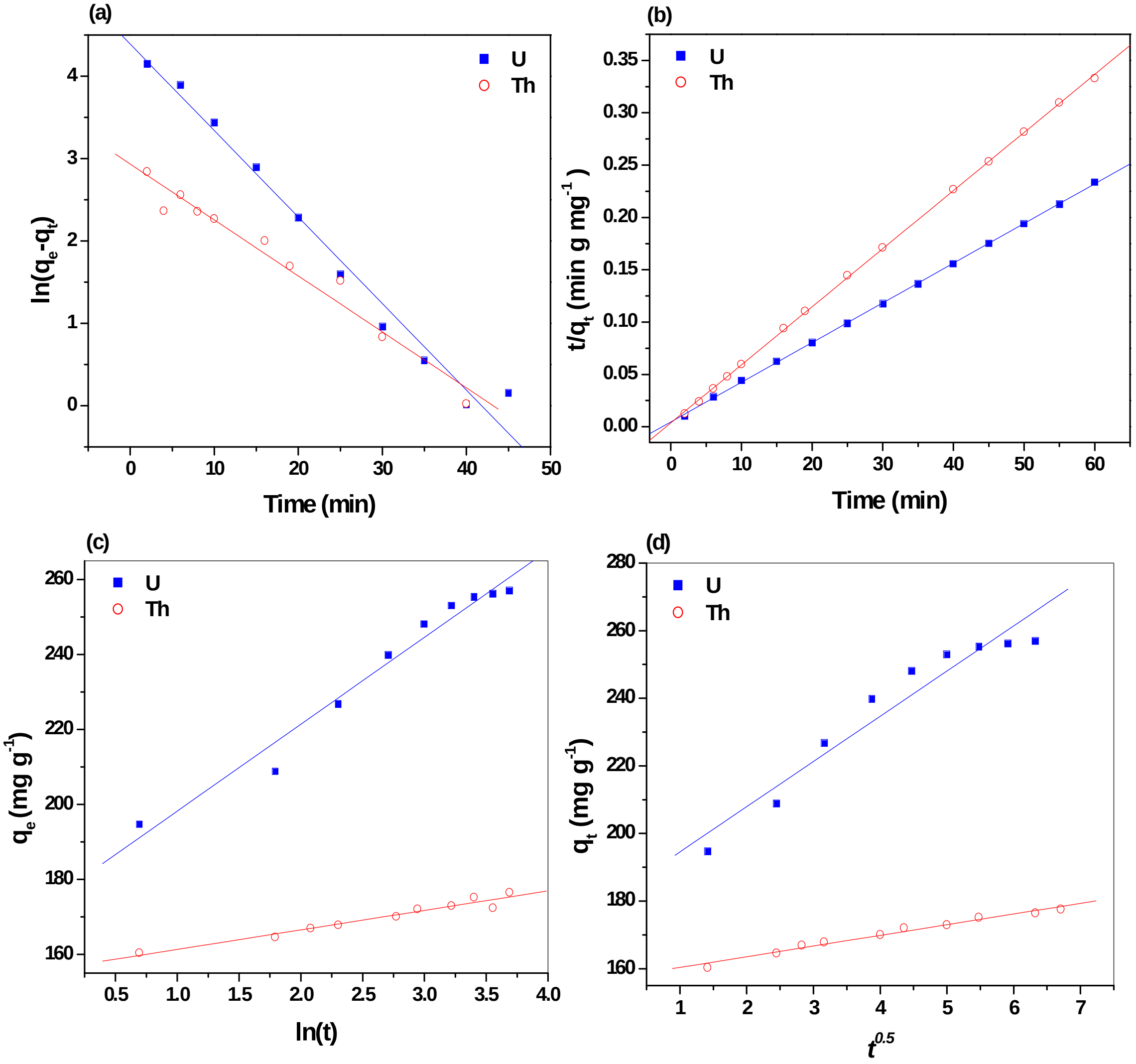

Fig.5.5 Kinetic models for U(VI) and Th(IV) adsorption on DGA-PAMAMG_3-SDB (a) pseudo-first-order, (b) pseudo-second-order, (c) Elovich and (d) intra-particle kinetic models

Table 5.1 Kinetic parameters for U(VI) and Th(IV) adsorption on DGA-PAMAMG$_3$-SDB

Kinetic model	Parameters	U	Th
Pseudo-first-order	k_1 (min^{-1})	0.105	0.068
	q_e (mg g^{-1})	80.55	18.81
	R^2	0.989	0.982
	SD	0.235	0.173
Pseudo-second-order	k_2 (g mg^{-1} min^{-1})	0.003	0.008
	q_e (mg g^{-1})	263.9	180.2
	R^2	0.999	0.999
	SD	0.001	0.002
Elovich	α (mg g^{-1} min)	4.4×10^4	5.5×10^{13}
	b (g mg^{-1})	0.043	0.192
	R^2	0.985	0.977
	SD	4.163	1.121
Intraparticle diffusion	k_i (mg g^{-1} min$^{1/2}$)	13.37	3.150
	c (mg g^{-1})	181.2	157.2
	R^2	0.965	0.989
	SD	6.381	0.850

5.3.6 Adsorption isotherm

In order to understand the adsorption behavior of U(VI) & Th(IV) on DGA-PAMAMG$_3$-SDB resin, the equilibrium data was evaluated based on Langmuir and Freundlich models. Linear form of both Langmuir and Freundlich isotherm models (equation 4.8 & 4.9) are graphically represented in Fig.5.6. The isotherm parameters of each model were calculated by linear regression analysis and the values are given in Table 5.2. From the values of R^2 and SD, it is clear that experimental data fits well with Langmuir isotherm than Freundlich isotherm. The results also show that the calculated adsorption capacity of DGA-PAMAMG$_3$-SDB for uranium (275.5 mg g^{-1}) and thorium (198 mg g^{-1}) from Langmuir isotherm model exhibits good agreement with the experimentally determined adsorption capacity (286 mg g^{-1} for U and 187 mg g^{-1} for Th). Applicability of Langmuir model suggests the monolayer adsorption of U(VI) and Th(IV) on the homogeneous surface of DGA-PAMAMG_3-SDB.

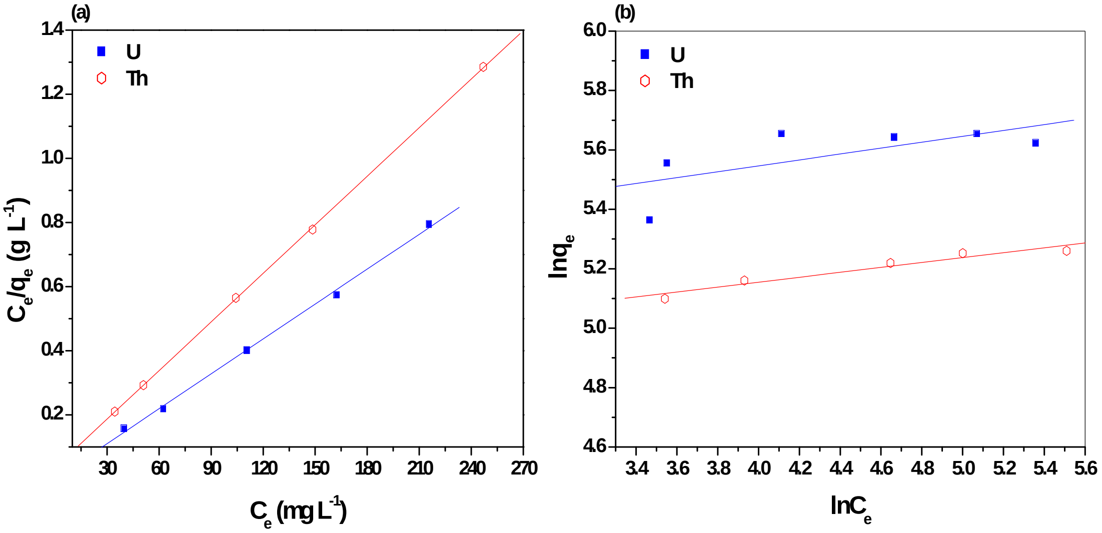

Fig.5.6 (a) Langmuir and (b) Freundlich adsorption isotherm for U(VI) and Th(IV) adsorption on DGA-PAMAMG_3-SDB

Langmuir separation factor (R_L) for various concentrations of U(VI) and Th(IV) were calculated by using equation 4.13. The value of R_L lie between 0 and 1 (Fig. 5.7) indicating favorable adsorption of U(VI) and Th(IV) on DGA-PAMAMG_3-SDB.

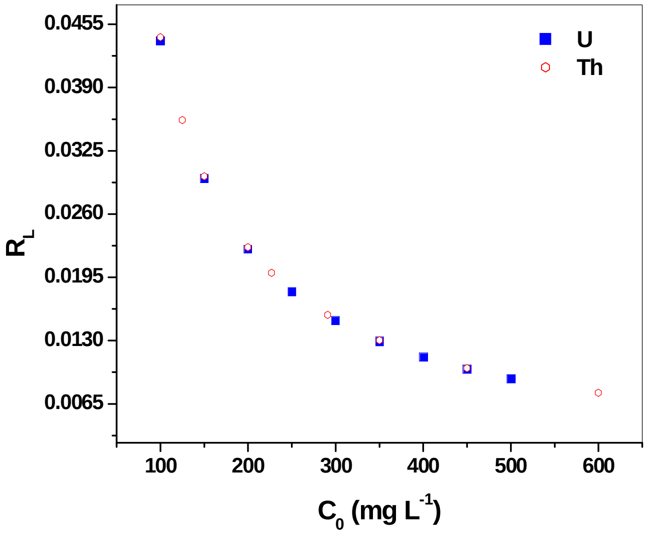

Fig.5.7 Langmuir separation factor (R_L) as a function of metal ion concentration (C_0)

Table 5.2 Isotherm parameters of U(VI) and Th(IV) adsorption on DGA-PAMAMG$_3$-SDB

Isotherms	**Langmuir**				**Freundlich**			
Parameters	q_o (mg g^{-1})	b (L mg^{-1})	R^2	SD	K_F (mg g^{-1})	n	R^2	SD
U	275.5	2.388	0.998	0.014	172.22	10.05	0.691	0.092
Th	198.0	0.144	0.999	0.005	124.58	12.12	0.967	0.019

5.3.7 Effect of DGA-PAMAMG$_3$-SDB dosage

The percentage removal of U(VI) and Th(IV) with increasing amount of DGA-PAMAMG$_3$-SDB chelating resin is shown in Fig.5.8. Experimental results show that the removal efficiency increases with increasing adsorbent dosage due to increase in adsorption sites. More than 90 % removal was achieved for U(VI) and Th(IV) metal ions using about 0.01 g of chelating resin.

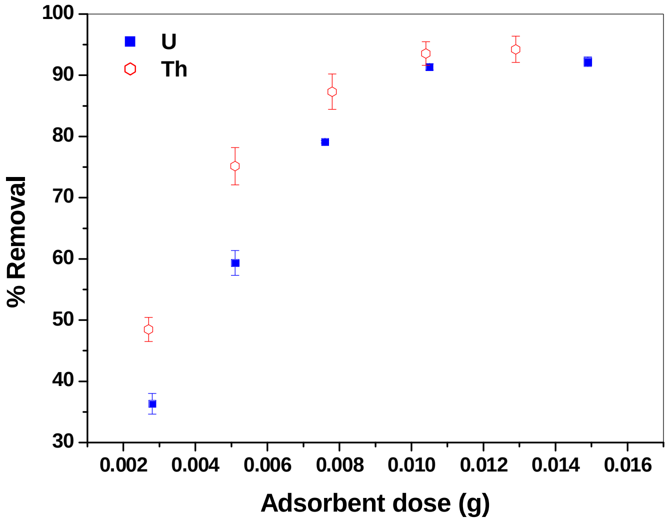

Fig.5.8 Effect of DGA-PAMAMG$_3$-SDB dosage on U(VI) and Th(IV) adsorption

5.3.8 Adsorption thermodynamics

Thermodynamic parameters (ΔH^o and ΔS^o) were calculated from the linear plot of $\ln K_d$ Vs 1/T (Fig.5.9) using Van't Hoff equation (equation 4.11) and ΔG^o was calculated from equation 4.12. All the thermodynamic parameters are given in Table 5.3.

Studies of effect of temperature on thorium adsorption show that adsorption increases with increasing temperature (Fig.5.9). The positive value of ΔH^o (Table 5.3) indicates endothermic nature of adsorption. At pH 3.5, Th(IV) exists as Th^{4+} and partially hydrolyzed thorium species ($Th(OH)^{3+}$ & $Th(OH)_2^{2+}$) and these Th(IV) species are solvated by water molecules. Adsorption of thorium involves breaking of hydration shell (endothermic) and adsorption of dehydrated thorium species on the surface of DGA-PAMAMG$_3$-SDB (exothermic). The energy required for the former process exceeds the energy released in the later process and hence, the overall adsorption process becomes endothermic [149]. The negative value of free energy of adsorption (ΔG^o) confirms the feasibility and spontaneous nature of adsorption process. The value of ΔG^o becomes more negative with increase in temperature indicating that more efficient adsorption occurs at higher temperature. At higher temperature, thorium ions are readily dehydrated and hence their adsorption becomes more favorable. The positive value of ΔS^o suggests an increase in randomness at solid/liquid interface during adsorption process. Randomness arises due to the destruction of hydration shell of thorium species prior to adsorption on the surface of the adsorbent.

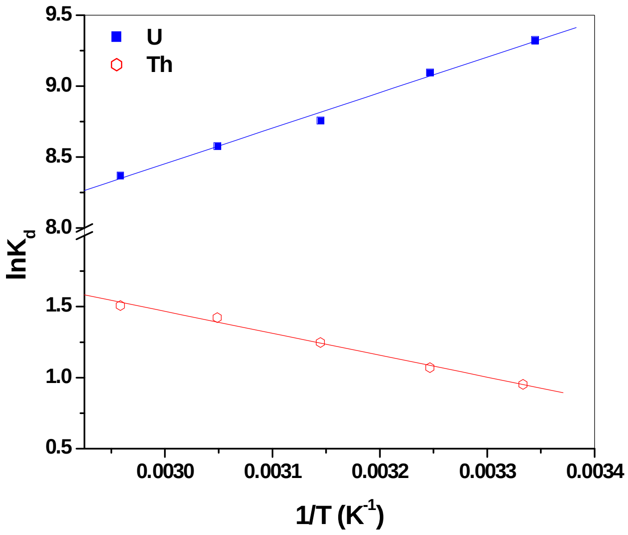

Fig.5.9 Effect of temperature on adsorption of U(VI) and Th(IV) onto DGA-PAMAMG$_3$-SDB

In case of uranium, the increase in adsorption with decrease in temperature (Fig.5.9) indicates more efficient adsorption at lower temperature. The negative ΔG^o value indicates that adsorption is thermodynamically favorable and spontaneous. The negative value of ΔH^o (Table 5.3) shows exothermic nature of adsorption process. The energy released during adsorption process due to strong electrostatic force of attraction between DGA-PAMAMG$_3$-SDB and U(VI) ions exceeds the dehydration energy of U(VI) ions. Hence, the overall reaction is exothermic. The positive values of ΔS^o reflects an increased randomness at the adsorbate-adsorbent interface during the adsorption process. The randomness arises from the destruction of the hydration shell of uranium species prior to adsorption on the surface of DGA-PAMAMG$_3$-SDB.

Table 5.3 Thermodynamic parameters of U(VI) and Th(IV) adsorption on DGA-PAMAMG$_3$-SDB

Thermo dynamic Parameters	**ΔH^o (kJ mol^{-1})**	**ΔS^o (kJ mol^{-1} K^{-1})**	**ΔG^o (kJ mol^{-1})**				
			299K	**308 K**	**318K**	**328K**	**338K**
U	-20.84	0.008	-23.16	-23.23	-23.31	-23.38	-23.46
Th	12.84	0.051	-28.06	-28.46	-28.97	-29.47	-29.98

5.3.9 Effect of dendron generation

Fig. 5.10 illustrates the adsorption capacity of DGA-PAMAM-SDB for U(VI) and Th(IV) metal ions as a function of dendron generation. Adsorption capacity increases exponentially with increasing dendron generation due to the exponential increase in number of chelating groups (Table 2.6). Adsorption capacity of DGA-PAMAMG$_5$–SDB for U(VI) and Th(IV) are found to be 682 and 544.2 mg g^{-1} at pH 5.5 and 3.5 respectively.

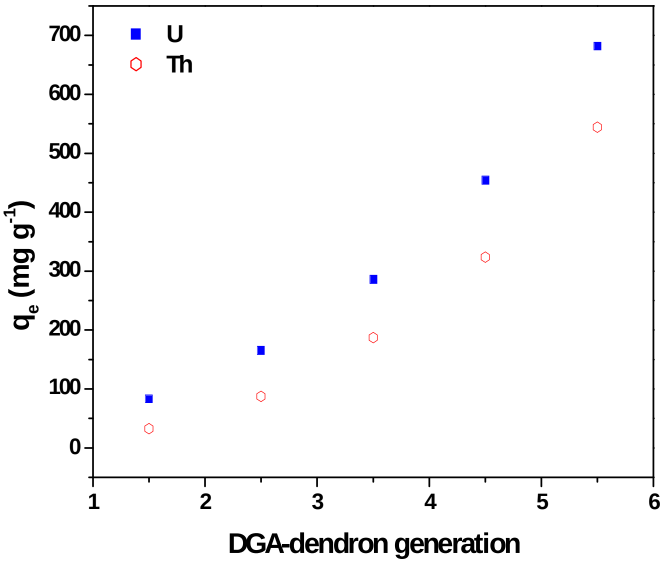

Fig.5.10 Effect of DGA-PAMAM dendron generation on adsorption capacity

5.3.10 Effect of ionic strength

Effect of ionic strength on adsorption studied with various concentration of NaCl, $Ca(NO_3)_2$ and $NaNO_3$ between 0.01 and 0.1mol L^{-1} are shown in Fig. 5.11. The results show that adsorption capacity of uranium increases gradually with increase in $NaNO_3$ and $Ca(NO_3)_2$ concentration upto 0.1 mol L^{-1} due to the increase in electrostatic force of attraction between U(VI) ion species and DGA-PAMAMG_3-SDB chelating resin. At pH 5.5, the surface charge on DGA-PAMAMG_3-SDB resin is negative due to ionization of DGA functional groups. The increase in concentration of $NaNO_3$ and $Ca(NO_3)_2$, reduces the negative charge on the surface of chelating resin favoring the adsorption of neutral uranium species ($UO_2(OH)_2$ and UO_2CO_3). This effect is more pronounced for divalent Ca^{2+} ion than monovalent Na^+ ion. In case of NaCl, the adsorption capacity increases with increase in concentration of NaCl upto 0.03 mol L^{-1} and then decreased. The initial increase in adsorption may be attributed due to the formation and adsorption of UO_2Cl^+ and $UO_2(OH)Cl$ species on the surface of resin. The soluble uranium UO_2Cl_2 species formed at higher NaCl concentration weakly interacts with resin surface attributing to decrease in adsorption. In case of thorium at pH 3.5, a gradual decrease in adsorption was observed with increase in ionic strength (Fig. 5.11). The increase in ionic strength reduces the interaction of thorium metal ion on resin surface attributing to decrease in adsorption capacities.

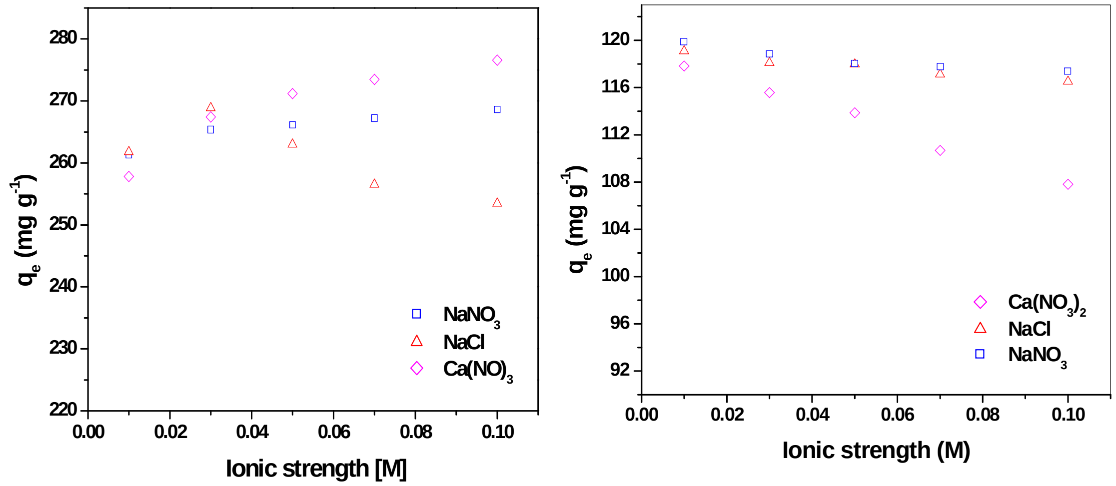

Fig.5.11 Effect of ionic strength on U(VI) and Th(IV) adsorption onto DGA-PAMAMG3-SDB

5.3.11 Desorption of U(VI) and Th(IV) from resin

Studies on desorption of U(VI) and Th(IV) from resin show that percentage desorption increases with increase in acid concentration (Fig.4.11) and maximum of ~99 and 76 % desorption can be achieved for U(VI) and Th(IV) with 0.1 M and 0.3 M HCl respectively.

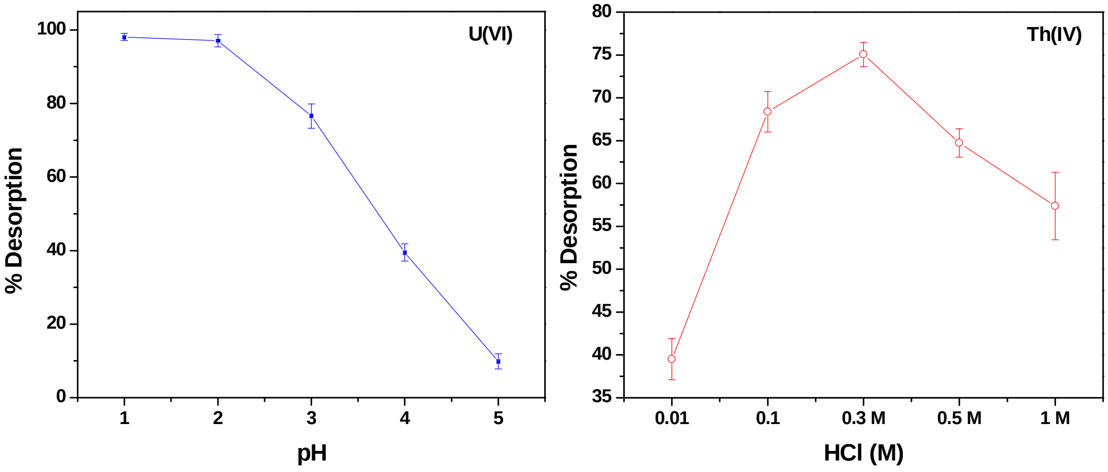

Fig.5.12 Desorption of U(VI) and Th(IV) from DGA-PAMAMG3-SDB adsorbent

5.3.12 Removal of metal ions from SNLW

Studies on selective removal of U(VI) and Th(IV) from SNLW at pH 5.5 reflects the affinity of DGA-PAMAMG_3-SDB chelating resin towards U(VI) and Th(IV) as well as lanthanides. Decontamination of SNLW at pH 12.5 reveals that except cesium, the percentage removal of all other metal ions is > 85 % (Table 5.4).

Table 5.4 Removal of U(VI) and Th(IV) from SNLW at pH 5.5 and 12.5.

Metal ions	% Removal at pH 5.5	% Removal at pH 12.5
Ba	28.57	88.00
Ce	77.27	99.39
Co	30.00	98.66
Gd	84.62	99.48
La	55.88	99.41
Mn	40.00	98.40
Nd	75.00	99.37
Ni	35.71	92.85
Sm	63.33	99.44
Sr	34.84	85.61
Th	**96.15**	**99.62**
U	**96.12**	**99.61**
Zn	40.54	98.92
Cs	8.571	26.57

5.4 Conclusion

- A new DGA-PAMAM-SDB chelating resin, first of its kind, was synthesized by modifying the terminal primary amine group of PAMAM-SDB with DGA functional group. Adsorption of U(VI) and Th(IV) on DGA-PAMAMG$_3$-SDB chelating resin in aqueous and nitric acid medium were investigated by batch experiments.
- Adsorption capacity of DGA-PAMAMG$_3$-SDB chelating resin was observed to be dependent on contact time, pH, initial metal ion concentration and temperature. Kinetic study showed that equilibrium has reached within 60 minutes and kinetic data fits well with pseudo-second-order model. Langmuir adsorption isotherm was found to be more suitable for explaining adsorption process.
- This chelating resin shows high adsorption efficiency even at high ionic strength. The maximum adsorption capacities of DGA-PAMAMG$_5$-SDB chelating resin for U(VI) and Th(IV) was estimated to be 682 and 544.2 mg g^{-1} at pH 5.5 and 3.5 respectively.
- The adsorbed U(VI) and Th(IV) metal ions can be desorbed from resin by equilibrating with acidic solution and maximum of ~99 and 76 % desorption can be achieved for U(VI) and Th(IV) with 0.1 M and 0.3 M HCl respectively.
- The effect of temperature on adsorption of U(VI) and Th(IV) was also investigated. The positive value of ΔH^o and negative value of ΔG^o shows endothermic and spontaneous nature of thorium adsorption on DGA-PAMAMG$_3$-SDB. In case of uranium, the negative values of ΔH^o and ΔG^o reveals that adsorption is exothermic and spontaneous.

- Studies with SNLW reveal that DGA-PAMAM-SDB chelating resin is effective in selective removal of U(VI), Th(IV) and lanthanides (La, Ce, Gd, Nd and Sm etc.,) in presence of various fission and activated corrosion products.

Chapter-6

DECONTAMINATION OF RADIOACTIVE WASTE BY PRECIPITATION USING XANTHATE FUNCTIONALIZED PAMAM DENDRIMER (XFPD) CHELATING AGENT

6.1 Introduction

Decontamination of radioactive waste (i.e. removal of all radionuclides from waste) will significantly reduce the volume of waste which is important criteria in management of radioactive waste. Precipitation is one of the best suited method for decontamination of liquid wastes generated in nuclear industries. A wide range of precipitants and mixture of precipitants are being employed to improve overall decontamination. Hydroxides, carbonates, peroxides, sulphides, sulphates, phosphates and copper/nickel ferrocyanides are useful precipitants for removal of radionuclides [5, 95]. These precipitants are effective in removal of radionuclides at $pH \geq 8$. Studies carried out with SNLW by using indigenously developed PAMAM, PAMAMG$_3$-SDB and DGA-PAMAM-SSB reveal that decontamination process is effective at $pH \geq 12$. The above processes require addition of large quantity of alkali and control of solution pH. It is reported that chelating agents such as xanthate (R-OCS$_2^-$) and dithiocarbamate (R-NHCS$_2^-$) form complexes with various metal ions at $pH > 3$ [124, 154]. Xanthate complexes of copper, nickel, cobalt, iron, platinum, palladium, chromium, zinc, arsenic, mercury, antimony, bismuth and lead have been reported [155-165]. Owing to low solubility product and high stability constant of metal-xanthate complex, the xanthate chelating agent has been used for removal of heavy metal ions from wastewater [166]. In comparison with other precipitation processes, xanthate treatment offers the following advantages; i) high percentage of metal removal, ii) less sensitivity to pH variation, iii) less sensitivity to coexisting complexing agent, iv) improved sludge dewatering property and v) capability for selective removal of metals [154].

Molecules with single and multiple xanthate groups have been widely used for effective removal of heavy metal ions. Molecules with multiple xanthate groups exhibit excellent binding capacity and better settling behaviour [124, 167]. Hence, it is desirable to increase the number of xanthate functional group in a molecule to enhance binding and precipitating abilities. In recent years, xanthate functional groups have been introduced in macromolecules to increase its capacity and removal efficiency [168, 169]. Dendrimer macromolecules are choice of our interest and definite number of desired functional groups can be introduced at the periphery by exploiting the reactivity of terminal groups.

In the present work, xanthate functional groups were introduced in first generation hydroxyl terminated PAMAM dendrimer. This xanthate functionalized PAMAM dendrimer (XFPD)-PAMAMG1OCS$_2$ was used for the removal of metal ions such as copper, cobalt (representative of radioactive divalent transition metal ions) and europium (representative of lanthanide ions & surrogate of americium) from aqueous solution by precipitation. The effect of pH and ionic strength on removal of the above metal ions was studied. The settling time of precipitate as a function of time and loading capacity of XFPD as a function of metal ion concentration were investigated. Toxicity Characteristics Leaching Procedure (TCLP) and Semi-Dynamic Leaching Test (SDLT) were conducted to investigate the metal leachability and stability of metal-XFPD complex. The indigenously developed XFPD chelating ligand was deployed for the treatment of Radioactive Liquid Waste (RLW) and results are discussed in this chapter.

6.2 Experimental

6.2.1 Removal of Cu^{2+}, Co^{2+} and Eu^{3+} metal ions from aqueous solution

Stock solutions of Cu^{2+}, Co^{2+}, Eu^{3+} metal ions (1 g/L) and XFPD (2.7860 mM) chelating agent were prepared. Precipitation studies were carried out individually with various concentrations (25, 50, 100, 250 and 500 mg/L) of Cu^{2+}, Co^{2+} and Eu^{3+} metal ions by adding 0.5 mL of 2.7860 mM XFPD ligand. The resultant precipitate was filtered through whatmann 542 ashless filter paper and washed with distilled water for three times. The precipitate was dried at 343 K in a vacuum oven. The metal-XFPD precipitate was characterized by FT-IR, XPS and SEM-EDS spectroscopy. The concentration of cobalt in filtrate was determined by measuring absorbance at 520 nm using Nitroso-R salt. The concentration of europium and copper metal ions was determined using ICP-OES. Effect of pH on removal of Cu^{2+}, Co^{2+} and Eu^{3+} metal ions were studied by varying the pH between 3.0 and 9.0. The pH of feed solution was adjusted by adding either 0.1 M HNO_3 or 0.1 M NaOH.

The percentage removal of Cu^{2+}, Co^{2+} and Eu^{3+} metal ions at various pH were calculated by using the following equation 6.1.

$$\%R = (\frac{C_f - C_{fi}}{C_f}) \times 100 \tag{6.1}$$

Where, C_f is the concentration of metal ion in feed and C_{fi} is the concentration of metal ion in filterate.

Metal ion removal efficiency depends on effective complexation and its settling. Suspended particles of metal-XFPD complexes could be removed from aqueous solution by centrifugation or filtration or sedimentation process. Among these, sedimentation process is generally used for solid–liquid separation which involves settling of suspended particles. Therefore, the settling behaviour of XFPD complex of Cu, Co and Eu was studied by measuring residual turbidity of the solution as a function of time.

The influence of electrolytes such as $Ca(NO_3)_2$ and $NaNO_3$ on quantitative removal of metal ions was investigated. Experiments were carried out by varying the concentrations of electrolyte from 0.01M to 0.5 M with constant metal ion to XFPD mole ratio.

6.2.2 Extent of binding of metal ions

The extent of binding (EOB), number of moles of metal ion complexed per mole of XFPD, of Cu^{2+}, Co^{2+} and Eu^{3+} metal ions as a function of their concentration was studied. About 9 ml of metal ion ($Co^{2+}/Cu^{2+}/Eu^{3+}$) solution was mixed with 1 ml of 2.786 mM XFPD solution in 50 ml centrifuge tube. The resultant precipitate was centrifuged, washed with water, dissolved in concentrated HNO_3 and made upto 25 ml in a standard flask. This solution and the filtrate were analyzed to estimate loaded metal ion on XFPD ligand. The EOB was calculated by using the following equation 6.2

$$EOB = \frac{[C_M]}{[C_{XFPD}]} \qquad (6.2)$$

Where, $[C_M]$ is the concentration of metal ion ($Co^{2+}/Cu^{2+}/Eu^{3+}$) complexed with XFPD (mol L^{-1}) and $[C_{XFPD}]$ is the concentration of XFPD in solution (mol L^{-1}).

6.2.3 Leaching test of Co-XFPD precipitate

The metal-XFPD precipitate was subjected to toxicity characteristics leaching procedure (TCLP). TCLP (USEPA, 1986) test is meant for classifing materials as hazardous or nonhazardous [166]. A mixture of solid precipitate and 0.1 M acetic acid at a liquid-to-solid ratio of 20:1 was equilibrated at 30 rpm in an orbital shaker at room temperature for 18 h. The leachate was filtered through a whatmann filter paper and the filtrate was analyzed for metal ion concentration.

In addition to TCLP test, a series of semi-dynamic leaching test (SDLT) using acetic acid and sodium hydroxide solutions as leachant were conducted to examine the metal ion leachability and stability characteristics of the metal-XFPD complex in simulated landfill environment [166]. Samples were collected at seven days interval for 30 days and concentration of metal ions in leachate was determined. In SDLT, equilibration of the precipitate was continued for 30 days with three sets of leachants such as acetic acid (pH 2.5 & 6.0) and NaOH solution (pH 11.0). During the test, the liquid-to-solid ratio was maintained as 100:1.

6.2.4 Removal of metal ions from liquid wastes

Studies on removal of metal ions from simulated nuclear waste (SNLW) and radioactive liquid waste (RLW) were carried out using XFPD ligand. The preparation procedure and composition of SNLW & RLW are given in Table 2.1 of chapter 2. The performance of XFPD ligand in SNLW was evaluated by adding required amount of XFPD ligand into 20 ml of SNW taken in a 50 ml centrifuge tube. The percentage removal was calculated by determining concentration of metal ions in the filtrate using ICP-OES and AAS. Similarly, experiment with RLW was carried out by adding required quantity of XFPD into 10 ml of RLW taken in a 20 ml glass tube. The resultant suspended particles were allowed to settle for an hour and the residual activity in the supernatant was measured using HPGe detector. The percentage decontamination (% D) of each metal ion was calculated by using the following equation 6.3.

$$\%D = \frac{A_i - A_f}{A_i} \times 100 \qquad (6.3)$$

Where, A_i and A_f are activities (dps) of metal ions in feed solution and supernatant respectively.

6.3 Results and Discussion

6.3.1 Complexation of Cu^{2+}, Co^{2+} and Eu^{3+} metal ions with XFPD

A dark-brown precipitate was obtained by the addition of XFPD ligand to Co^{2+} and Cu^{2+} solution. FTIR spectrum of Cu-XFPD complex are shown in Fig. 6.1 (a & b). The appearance of vibrational peaks in the region of 1250-850 cm^{-1} depicts the presence of xanthate group. The peaks appear at 1049 cm^{-1} and 1197 cm^{-1} are attributed to asymmetric and symmetric vibration of $-CS_2^-$ group. In addition,

$\Delta\upsilon[\upsilon(CS_2)_{asym}-\ \upsilon(CS_2)_{sym}]$ value can also illustrate the coordination fashion of the complex [123, 170]. The $\Delta\upsilon$ value $[\upsilon(CS_2)_{asym}-\ \upsilon(CS_2)_{sym}]$ is 148 cm^{-1}, almost similar to the corresponding sodium xanthate value ($\Delta\upsilon$ = 139 cm^{-1}), which in turn suggests that XFPD ligand adopts a unidentate coordination mode in this complex (Fig.6.2(a)). In case of Co-XFPD complex, asymmetric and symmetric stretching vibrations of $-CS_2^-$ group gives peaks at 1203, 998 cm^{-1} and $\Delta\upsilon$ value $[\upsilon(CS2)_{asym}-\ \upsilon(CS2)_{sym}]$ is 205 cm^{-1}, much larger than the corresponding sodium xanthate values ($\Delta\upsilon$ = 139 cm^{-1}). Therefore, it is expected that coordination of xanthate groups with Co^{2+} metal ion could be in tetradentate fashion (Fig.6.2 (d)).

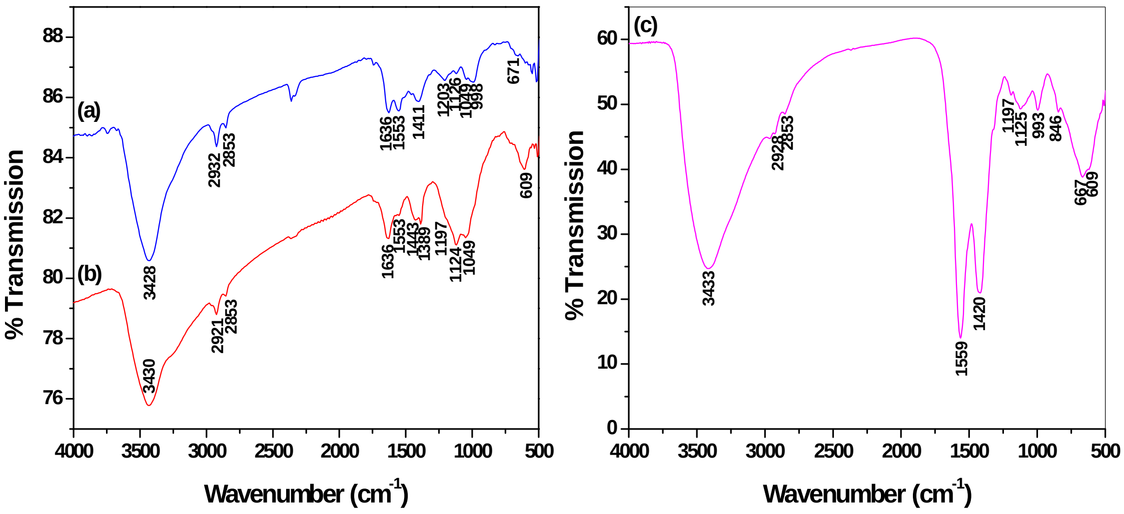

Fig.6.1 FTIR Spectra of (a) Cu-XFPD, (b) Co-XFPD and (c) Eu-XFPD complexes

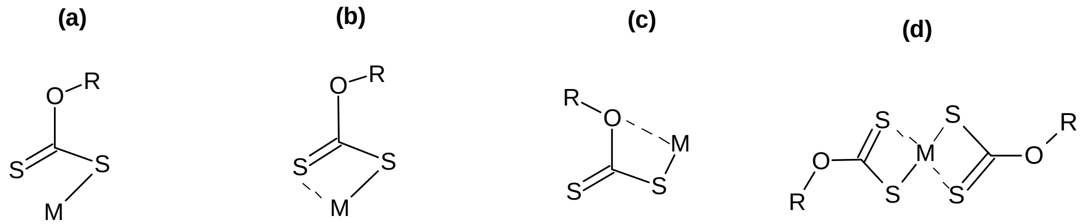

Fig.6.2 Coordination pattern of xanthate ligand (a) unidentate (b) anisobidentate (c) co-ordination with two hetero atom (d) anisotetradentate

SEM images of Cu-XFPD, Co-XFPD and Eu-XFPD complexes are shown in Fig.6.3. The morphology of the particles is observed to be irregular size in the range of 20-60 µm.

The elemental analysis of Cu-XFPD complex by EDS analysis indicates the presence of copper and sulfur (Fig.6.3) with weight and atom percentages as Cu-23.2%, S-22.4% and Cu-6.7%, S-12.8% respectively. From the above percentages, the calculated mole ratio of S to Cu is about 2:1. This mole ratio depicts coordination between one copper ion and two sulfur atoms. The mechanism of complexation could be explained as follows. The Cu^{2+} ion might be reduced to Cu^{+} ion by xanthate group with the formation of dixanthogen ($PAMAMG_1(OCS_2)_2$) and cuprous Cu-XFPD complex expressed below (equation 6.4).

$$\mathrm{PAMAMG_1OCS_2^- + Cu^{2+} \longrightarrow PAMAMG_1(OCS_2)_2 + PAMAMG_1OCS_2Cu} \tag{6.4}$$

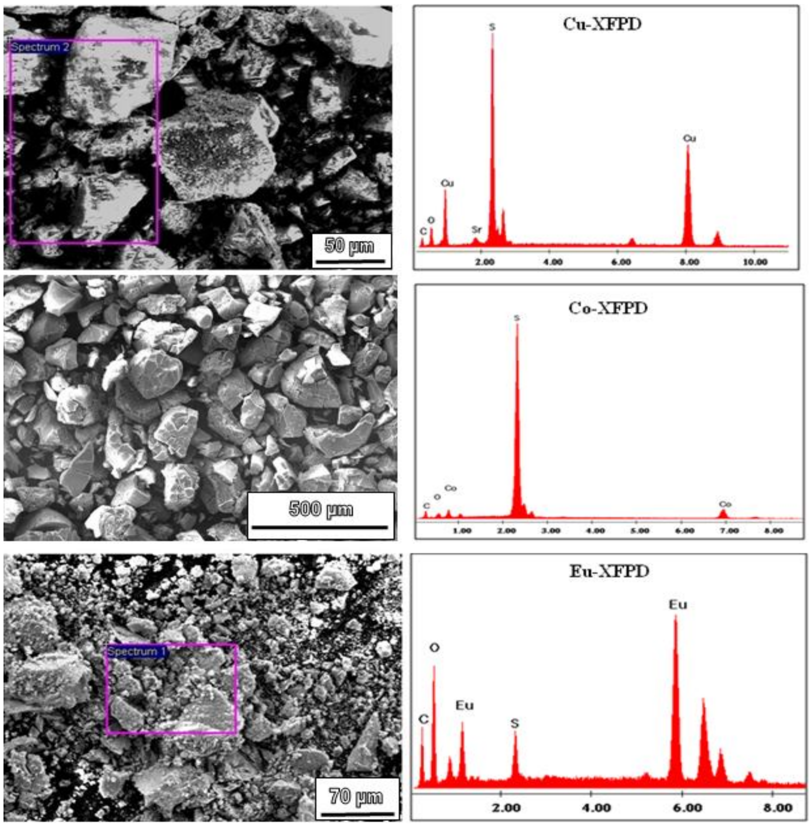

Fig.6.3 SEM-EDS spectra of Cu-XFPD, Co-XFPD and Eu-XFPD complexes

The mechanism has been supported by XPS analysis. The XPS spectrum of Cu2p from Cu-XFPD complex is shown in Fig.6.4 (a). Two major peaks at binding energies of 932 and 953 eV are the characteristics of cuprous xanthate signal [166] and the absence of cupric xanthate (absence of satellite structure at binding energies of 944 and 963 eV in the (Fig.6.4 a) suggests that xanthogenate unit (R-O-CS_2^-) coordinated with Cu^+ ion and thus cuprous form of xanthate complex (Cu-XFPD) is precipitated. Similar result was reported by Q. Chang et al [156]. Hence XPS analysis, reveal the presence of cuprous species in the Cu-XFPD complex.

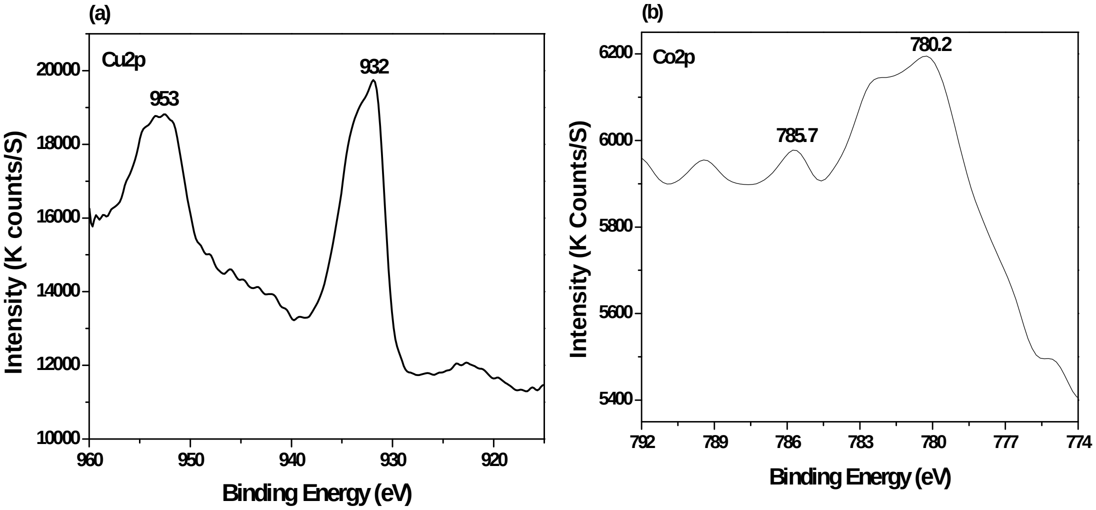

Fig.6.4 XPS spectra of Cu2p & Co2p from Cu-XFPD and Co-XFPD complexes

XPS spectrum of Co2p from Co-XFPD complex is also shown in Fig.6.4 (b). The appearance of statelite peak at 785.7 eV ($2p_{1/2}$) along with main peak at 780.2 eV ($2p_{3/2}$) suggests the presence of Co^{2+} ion [23]. The elemental analysis of Co-XFPD complex by EDS indicates the weight and atom percentage of cobalt and sulfur (Fig.6.3) as Co-18.48 %, S-38.54% and Co-7.27%, S-27.97% respectively. The calculated mole ratio of S to Cu is about 4:1, which depicts that four sulfur atoms are coordinated with one cobalt ion. Hence, one Co^{2+} ion is coordinated with four sulphur atoms (Fig.6.2).

In case of Eu^{3+}, a pale yellow precipitate of Eu-XFPD complex is formed and EDS spectrum shows the presence of europium and sulphur elements (Fig.6.3). The weight and atom percentage of europium and sulfur in Eu-XFPD complex are found to be Eu-56.84%, S-3.12% and Eu-10.91%, S-2.84% respectively. The low weight percentage of sulfur in Eu-XFPD complex is due to elimination of carbon disulphide (CS_2) from XFPD ligand during complex formation. According to Hard Saft Acid Base (HSAB) principle, the hard acid Eu^{3+} ion interacts strongly with hard base 'oxygen' as compared to soft base 'sulfur'. Hence, the coordination ability of europium with oxygen is stronger than that of sulfur atom [172]. Due to this oxophilic character of Eu^{3+} ion, some of the xanthate groups in XFPD ligand dissociate with the elimination of CS_2 group resulting existence of only few xanthate coordinations in Eu-XFPD complex. The presence of xanthate group in europium complex was confirmed from the appearance of vibrational peaks at 1197 cm^{-1} and 998 cm^{-1} corresponding to asymmetric and symmetric stretching vibrations of $–CS_2^-$ group (Fig. 6.1c). The $\Delta\upsilon$ [$\upsilon(CS_2)_{asym}– \upsilon(CS_2)_{sym}$] value (199 cm^{-1}) is much larger than the corresponding sodium xanthate value ($\Delta\upsilon$ = 139 cm^{-1}) and hence, it is expected that xanthate groups may coordinate with Eu^{3+} ions either in anisobidentate state or by coordination with two hetero atom fashions [123, 170] as shown in Fig.6.2. It is well known that Eu^{3+} exists in various chemical forms such as Eu^{3+}, $Eu(OH)^{2+}$ and $Eu(OH)_2^+$ in aqueous solution at pH 3-8 and hence various types of coordination might be possible in Eu-XFPD complex. In Fig. 6.1(c), the appearance of strong vibrational peaks at 3419 cm^{-1} and 1420 cm^{-1} are due to O–H stretching and bending vibrations suggesting the presence of hydrolyzed europium species such as $Eu(OH)^{2+}$ and $Eu(OH)_2^+$ in the complex.

The following types of possible complexation (equation 6.5-6.8) are predicted based on the above results.

$$\mathrm{PAMAMG_1(OCS_2^-)_3 + Eu^{3+} \longrightarrow PAMAMG_1(O_2EuCS_2) + 2CS_2} \qquad (6.5)$$

$$\mathrm{PAMAMG_1(OCS_2^-)_2 + Eu(OH)^{2+} \longrightarrow PAMAMG_1(O_2Eu(OH)) + 2CS_2} \qquad (6.6)$$

$$\mathrm{PAMAMG_1(OCS_2^-) + Eu(OH)_2^{+} \longrightarrow PAMAMG_1(OEu(OH)_2) + CS_2} \qquad (6.7)$$

$$\mathrm{PAMAMG_1(OCS_2^-) + Eu(OH)_2^{+} \longrightarrow PAMAMG_1(OCS_2Eu(OH)_2)} \qquad (6.8)$$

XPS study supports the above complexation mechanism. The influence of chemical environment on binding energy (BE) values for core level photoelectron peaks of O1s and Eu4d is shown in Fig.6.5. The shape of O1s signal is quite different for Eu-XFPD, when compared to other Eu(III) compounds reported by Mercier et al [173]. An intense peak appears at lower BE (531.1 eV) and a shoulder at high BE (531.6 eV) depicts various chemical environments of O1s in Eu-XFPD complex. The shoulder peak at high BE (531.6 eV) may be attributed to C-O of alcoholic group coordinated to Eu(III) and the peak at lower BE (531.1 eV) is attributed to C-O-C of xanthate group coordinated to the Eu(III). The same trend is found for the Eu4d peak (Fig.6.5). Again, various coordination of Eu(III) in Eu-XFPD complex have an influence on BE values of Eu4d. The peaks at 135.2 eV and 136.4 eV are attributed to BE of Eu(III) coordinated to the xanthate ((OCS$_2$–Eu(OH)) and alcoholic (C–O–Eu(OH)) groups respectively. Finally, simultaneous study of O1s and Eu4d core level photoelectron peaks allows to discriminate between various Eu(III) coordinations in the complex.

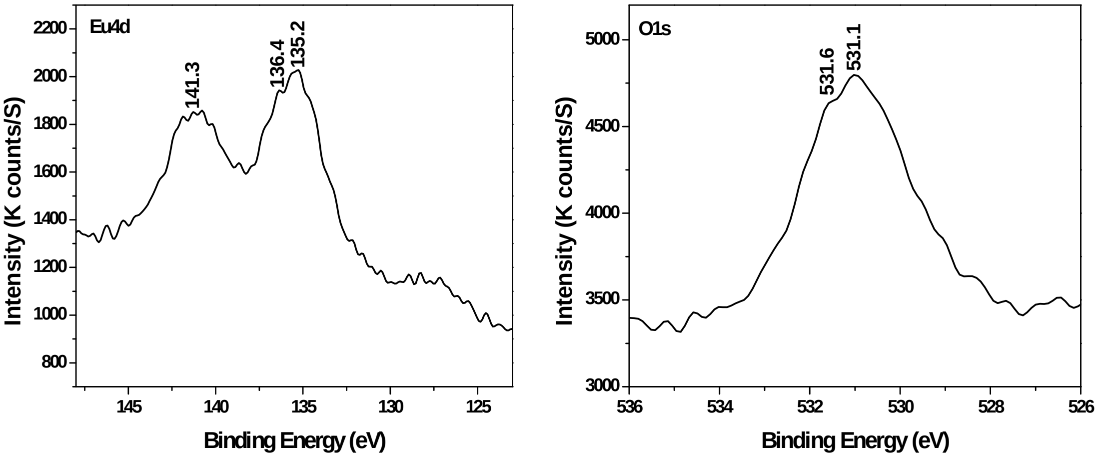

Fig.6.5. XPS spectra of O1s and Eu4d from Eu-XFPD complex

The coordination of europium with XFPD ligand is also confirmed by fluorimetric study. Fluorescence emission spectra of free Eu^{3+} and Eu-XFPD complex are shown in Fig.6.6. The emission spectra reveals well-known bands of europium luminescence corresponding to $^5D_0 \rightarrow {}^7F_0$ (580 nm), $^5D_0 \rightarrow {}^7F_1$ (593 nm) and $^5D_0 \rightarrow {}^7F_2$ (617 nm) transitions. Electric dipole transition ($^5D_0 \rightarrow {}^7F_2$) at 617 nm is observed to be stronger than magnetic dipole transition ($^5D_0 \rightarrow {}^7F_1$) at 593 nm, which indicates lower symmetry around Eu^{3+} ions. The so called "hypersensitive" $^5D_0 \rightarrow {}^7F_2$ transition is very sensitive to the surrounding microenvironment of Eu^{3+} ion and its intensity enhances due to complex formation with ligands [139]. Thus, the strong emission band at 617 nm ($^5D_0 \rightarrow {}^7F_2$) clearly indicates the coordination between Eu^{3+} and XFPD ligand.

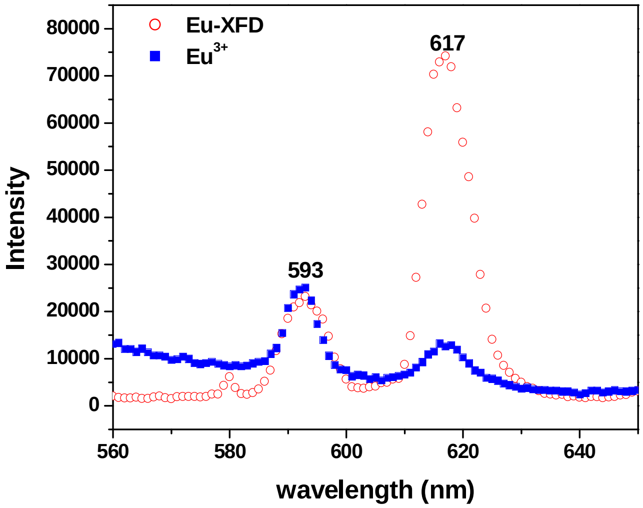

Fig.6.6 Fluorescence emission spectra of Eu^{3+} and Eu-XFPD complex

6.3.2 Effect of pH on complexation and metal ions removal efficiency

XFPD ligand could remove metal ions from aqueous solution quantitatively. The metal ion removal efficiency depends on formation of metal–XFPD complex followed by its settling. The pH of feed solution plays an important role on both formation of complex and settling of precipitate. The variation in percentage removal of Cu^{2+}, Co^{2+} and Eu^{3+} ions as a function of pH is shown in Fig.6.7. At pH < 3, the ligand undergoes decomposition by acid hydrolysis which suggests that pH of the feed solution must be maintained above 3. The percentage removal all the above metal ions increase with increasing pH between 3 and 5 beyond that it remains almost constant. At pH > 3, the xanthogenic acid groups of XFPD ligand ionize to negative xanthogenic acid radicals which enhance chelation between the XFPD and metal ions resulting increase in percentage removal of metal ions. At pH > 8, precipitation of Eu^{3+} ions as europium hydroxide ($Eu(OH)_3$) occur predominantly than Eu-XFPD complex formation. Hence effective removal of metal ions using XFPD ligand shall be carried out between pH 3 and 8.

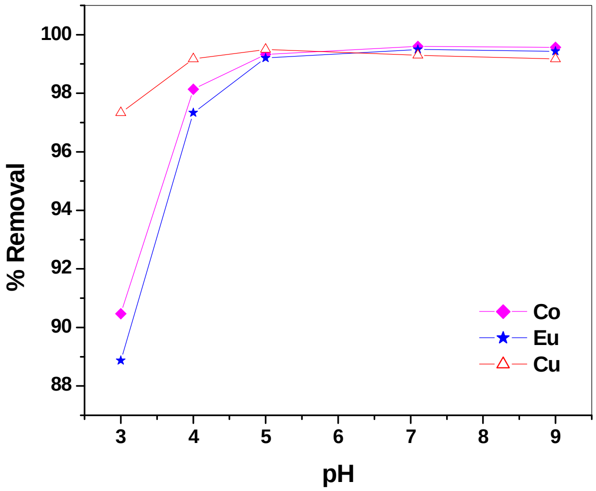

Fig.6.7 Effect of pH on removal of Cu, Co and Eu metal ions

6.3.3 Settling time of suspended particle

Studies on settling behaviour of metal-XFPD complexes as a function of time shows that Eu-XFPD complex possesses a favourable settling rate and the turbidity of the solution gets reduced by a factor of 14.6 within an hour (Fig. 6.8). In case of Co-XFPD and Cu-XFPD complexes, the settling time is highly pH dependent. At pH < 5, the precipitate has favourable settling speed whereas at pH > 6, the colloidal suspensions of Co-XFPD and Cu-XFPD complexes were not settling down by gravity for reasonable length of time. The suspended particles do not aggregate into larger particles due to similar charges associated with the complex [167]. It is also observed that these suspended particles settle down by the addition of coagulating agent like aluminium sulphate. The turbidity of Co-XFPD and Cu-XFPD colloidal solutions was reduced by a factor of 7.2 & 7.5 within one hour by addition of aluminium sulphate. Hence, about 2-3 h is sufficient for settling of metal complexes after the addition of XFPD ligand and coagulating agent.

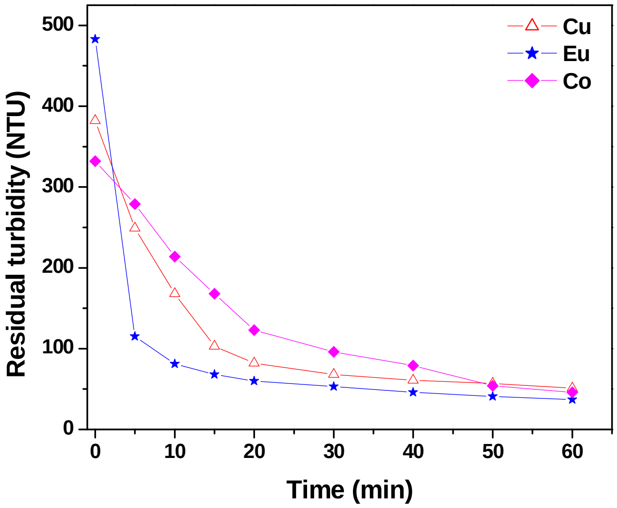

Fig.6.8 Residual turbidity of complexes as a function of time

6.3.4 Extent of binding of Eu^{3+} and Cu^{2+} metal ions

The extent of binding of Cu^{2+}, Co^{2+} and Eu^{3+} metal ions with XFPD ligand as a function of metal ion concentration is shown in Fig. 6.9. It is observed that loading of Cu^{2+}, Co^{2+} and Eu^{3+} ions increases with increasing concentration of metal ions and gets saturated at mole ratio of 12.3, 10 and 10.4 respectively. The higher loading capacity of XFPD ligand may be attributed to coordination of these metal ions with amine, amide and xanthate groups present in the XFPD ligand. From this EOB studies, a typical loading capacity for Cu^{2+}, Co^{2+} and Eu^{3+} metal ions were determined to be 0.355 g, 0.48 g and 0.94 g per gram of XFPD respectively. All subsequent experiments were carried out with the above mole ratios at pH 5.

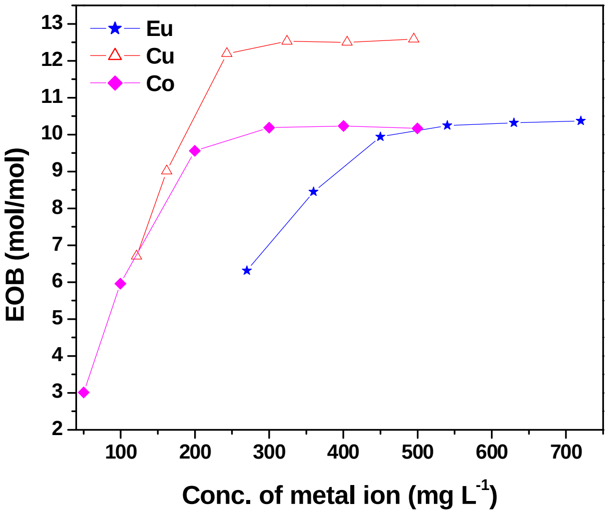

Fig.6.9 Extent of binding of Cu^{2+}, Co^{2+} and Eu^{3+} metal ions with XFPD ligand

6.3.5 Effect of ionic strength on metal ions removal

Studies on influence of electrolytes such as $Ca(NO_3)_2$ and $NaNO_3$ on quantitative removal of metal ions show that presence of sodium does not exhibit any significant effect on removal of Eu^{3+} ions whereas slightly enhances removal of Cu^{2+} and Co^{2+} ions (Fig. 6.10 a). In presence of divalent cations (Ca^{2+}), the percentage removal of Cu^{2+} and Co^{2+} ions were enhanced upto a concentration of 0.1 M and then levelled off (Fig.6.10 (b)). The enhancement in percentage removal of these metal ions is due to the coagulation of suspended particles caused by divalent calcium cation which improves solid-liquid separation. In case of Eu^{3+}, the percentage removal increased initially upto 0.1M and then decreased gradually. This decrease in percentage removal of Eu^{3+} could be explained by considering the competing interaction of Ca^{2+} ions with amine, amide and xanthate functional groups of XFPD ligand.

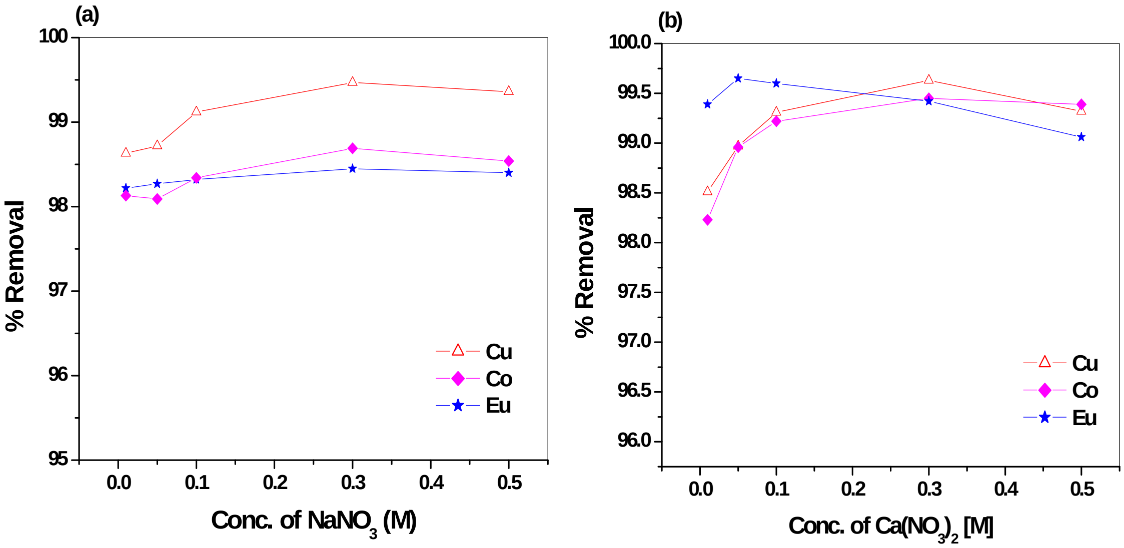

Fig.6.10 Effect of $NaNO_3$ and $Ca(NO_3)_2$ concentration on removal of Cu^{2+}, Co^{2+} and Eu^{3+} ions

6.3.6 TCLP and SDLT test

Experimental results on toxicity characteristics leaching procedure (TCLP) showed 13.31 %, 6.72 % and 23.4 % leaching of Cu^{2+}, Co^{2+} and Eu^{3+} metal ions respectively from their complexes within 18 h. Hence, these complexes could be classified as a leaching-toxic hazardous waste and it requires additional treatment before dump into sanitary landfills.

The percentage release of Cu^{2+}, Co^{2+} and Eu^{3+} from their respective complexes during SDLT test is given in table 6.1. The result shows that the release of metal ions at pH 3.0 is greater than at pH 7& 11. It is also observed that percentage of leaching in first seven days is rapid and later, the rate of leaching is low. The initial rapid release of metal ions during TCLP and SDLT (at pH 3) tests is due to leaching of metal ions coordinated to nitrogen and amide group of XFPD and the subsequent slow leaching may be due to slow decomposition of metal-xanthate coordination.

Table 6.1 SDLT test of Cu-XFPD, Co-XFPD and Eu-XFPD complexes

pH	pH 3				pH 6				pH 11			
Time	**7d**	**14d**	**21d**	**30d**	**7d**	**14d**	**21d**	**30d**	**7d**	**14d**	**21d**	**30d**
Cu-XFPD	29.1	31.2	31.9	32.4	2.1	2.4	2.9	3.8	0.9	1.3	2.8	3.5
Co-XFPD	26.2	31.9	33.8	35.0	5.2	6.3	8.5	10.1	2.1	4.0	5.9	7.9
Eu-XFPD	42.3	47.6	48.4	49.6	8.7	11.0	11.9	12.6	7.2	8.2	10.7	13.0

6.3.7 Removal of metal ions from liquid wastes

The percentage removal of various metal ions from SNLW by xanthate process is shown in Fig.6.11 (a). It is observed that except cesium, all other metal ions are effectively removed. The percentage removal of lanthanides (Ce, Gd, La, Nd, Sm) and actinides (Th & U) are observed to > 99 %. The percentage removal of Co, Ni and Zn are observed to be greater than 90 %. The precipitation of lanthanides and transition metal ions are mainly due to metal-xanthate complex formation whereas the precipitation of actinides is due to their hydroxide formation. Hydroxides of uranium and thorium were produced due to the increase in pH of the solution during the addition of XFPD. Though alkaline earth metal ions (Ba & Sr) does not form any precipitate with XFPD ligand, their percentage removal is observed to be about 50-70 %. The removal of Ba & Sr metal ions could be explained by considering their role as coagulating agent.

On the basis of above study, experiments were performed for decontamination of radionuclides from RLW using XFPD ligand. It is observed that XFPD ligand effectively removes all radionuclides except cesium. The percentage decontamination determined for various radionuclides (Fig. 6.11 b) is in the following order:

Zr ≈ Eu ≈ Co (>99.8) > Ce (98.84) > Sb (83.31) > Ru (79.44) > Mn (54.29) > Cs (24.02).

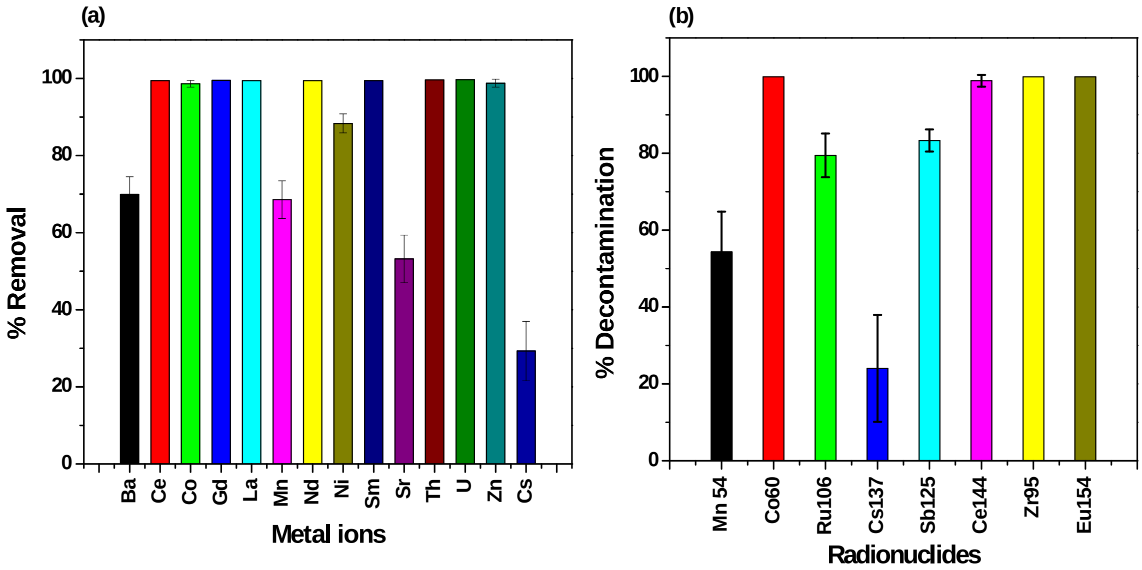

Fig.6.11 Removal of metal ions from (a) SNLW and (b) RLW

6.4. Conclusion

- A new xanthate functionalized PAMAM dendrimer (XFPD) chelating ligand, first of its kind, has been synthesized from first generation hydroxyl terminated poly(amido)amine dendrimer.
- Removal of Cu^{2+}, Co^{2+} and Eu^{3+} metal ions from aqueous solution as a function of pH was studied. XFPD forms water insoluble complexes with Cu^{2+}, Co^{2+} and Eu^{3+} metal ions. The pH of the solution plays an important role on both complexation and settling of suspended metal-xanthate complex.
- Removal of metal ions was observed to be effective in the pH range of 4-8 and quick settling of suspended metal-xanthate complexes from aqueous solution at pH > 6 was achieved by the addition of aluminium sulphate. Studies on settling behavior of precipitate reveal that 3 h was sufficient for effective solid-liquid separation. The solid–liquid separation was enhanced in the presence of alkali and alkaline earth metal ions by coagulation process.
- The loading capacities of Cu^{2+}, Co^{2+} and Eu^{3+} metal ions on XFPD were estimated to be 0.48 g, 0.355 g and 0.95 g respectively per gram of XFPD at pH 4.5. The high

loading capacity of XFPD ligand is due to the presence of large number of complexing groups.

- Experiments with SNLW showed that XFPD ligand forms water insoluble complexes with various metal ions. The indigenously developed XFPD chelating ligand was deployed for the treatment of RLW and percentage decontamination of radionuclides were observed to be in the following order; Zr ≈ Eu ≈ Co (> 99.8) > Ce (98.84) > Sb (83.31) > Ru (79.44) > Mn (54.29) > Cs (24.02). Decontamination studies reveal that, XFPD chelating ligand is very effective for the removal of various radionuclides (except ceasium) from RLW.
- The leaching of metal ions from the metal-complexes was observed and thus further studies need to be carried out for safe disposal of these complexes.

Chapter-7

SUMMARY AND FUTURE SCOPE

7.1 Summary

This chapter summarizes highlights of the results described in the thesis. Four compounds such as PAMAM dendrimer, Xanthate functionalized PAMAM dendrimer (XFPD) chelating agents, PAMAM-styrene divinyl benzene (solid supported PAMAM dendron) and DGA functionalized PAMAM-SDB chelating resin were synthesized. The potential application of the above dendrimer/dendron based chelating agents for the removal of actinides and other radionuclides from aqueous medium were explored.

Studies on ultrafiltration (UF) of uranium and thorium through regenerated cellulose acetate membrane reveal that removal of about 76-97 % of U(VI) and Th(IV) was achieved at pH 5-7. The removal of U(VI) and Th(IV) is mainly due to adsorption/mass deposition on the membrane surface. The water soluble PAMAM dendrimer chelating ligand had shown greater ability to bind with U(VI) and Th(IV) metal ions at pH > 5. These metal ions get concentrated in the retentate and adsorption/mass deposition on the membrane surface was significantly reduced. About 3 mg of G_3-NH_2 dendrimer is required for retaining 5 mg of U(VI) and Th(IV) in the retentate at pH 6. The required quantity of PAMAM chelating ligand was further drecresed with increase in dendrimer generation. It is estimated that about 1.1, 0.6 and 0.45 g of PAMAMG_3, PAMAMG_4 and PAMAMG_5 dendrimers are required to retain 1g of uranium and thorium in the retentate at pH 6. Formation of various metal ion species due to hydrolysis as a function of pH plays an important role on effective complexation and selective separation. The presence of PAMAM dendrimer chelating ligand does not prevent hydrolysis of metal ions whereas the hydrolyzed metal ion species are effectively binding with PAMAM dendrimer. The binding of uranium and thorium with PAMAM dendrimer is effective at pH > 5 and incase of Eu(III) and Co(II) effective binding occurs only at pH > 8. Hence, PAMAM dendrimer shall be employed for selective and collective removal of metal ions by adjusting the pH of the aqueous solution. Removal of U(VI) and Th(IV) from SNLW at pH 5.5 found to be greater than 90 % where as other metal ions are less than 40 %. At acidic pH (≤ 3), the binding of metal ions with PAMAM dendrimer was observed to be insignificant and hence PAMAM shall be regenerated.

Studies on adsorption of U(VI) and Th(IV) on indigenously developed PAMAMG$_3$-SDB chelating resin reveals that adsorption capacity of PAMAMG$_3$-SDB is dependent on contact time, pH and initial concentration of metal ions. The maximum adsorption of thorium on PAMAMG$_3$-SDB was observed at pH > 5 whereas in case of uranium it is between pH 5-8. Kinetic study shows that the adsorption process is fast and equilibrium is reached within 60 minutes. Adsorption follows pseudo-second order kinetics and Langmuir isotherm model suggesting chemical adsorption. Adsorption capacity of the chelating resin increases exponentially with increase in dendron generation. PAMAMG$_5$-SDB has adsorption capacity (q_e) of 493 and 261.5 mg g^{-1} for U(VI) and Th(IV) respectively. Study on effect of temperature on adsorption of U(VI) and Th(IV) metal ions reveals that adsorption of uranium on PAMAMG$_3$-SDB is endothermic whereas adsorption of thorium is exothermic. The nature of adsorption (endothermic or exothermic) also depends on the metal ion speciation. The chelating resin shows more than 98 % adsorption of U(VI) and Th(IV) even at high ionic strength. The adsorbed U(VI) and Th(IV) can be easily desorbed from resin by decreasing the pH of the solution and maximum of about 99 % desorption was observed at pH 1 which indicates the advantages of regeneration/reusability of the resin.

Diglycolic acid functionalized PAMAM dendron- styrene divinylbenzene (DGA-PAMAM-SDB) chelating resin is observed to be effective in removal of U(VI) and

Th(IV) metal ions from both aqueous and nitric acid medium. The adsorption capacity (q_e) depends on contact time, acidity of feed solution, concentration of metal ions and temperature. This chelating resin showed superior adsorption capacity compared with PAMAM dendron of same generation. The adsorption capacity of DGA-PAMAMG_5-SDB for U(VI) and Th(IV) are about 682 and 544 mg g^{-1} respectively. At pH 3-4, Th(IV) shows > 65 % of adsorption due to stronger complexation with DGA groups. On the other hand, U(VI) shows significant adsorption only above pH > 4. Hence, the separation of U and Th from each other at lower acidic region (pH 3-4) is feasible by using DGA-PAMAMG_3-SDB. Study on effect of temperature on adsorption of U(VI) and Th(IV) metal ions reveals that adsorption of uranium on PAMAMG_3-SDB is exothermic whereas adsorption of thorium is endothermic. The percentage desorption of U(VI) and Th(IV) from DGA-PAMAMG_3-SDB resin were determined to be ~99 % and 78 % at pH 0.1 M and 0.3 M respectively.

Xanthate Functionalized PAMAM Dendrimer (XFPD) ligand is effective in removal of various metal ions from aqueous solution by precipitation. XFPD form water insoluble complexes with copper, cobalt (representative of radioactive divalent transition metal ions) and europium (representative of lanthanides & surrogate of americium) metal ions. The pH of aqueous solution plays an important role on both complexation and settling of suspended metal-xanthates. XFPD ligand effectively removes metal ions at pH > 4 and settling of suspended metal-xanthate complexes at pH > 6 requires further addition of a coagulating agent like aluminium sulphate. The presence of alkaline earth metal ions in aqueous waste enhances removal of metal ions by coagulation process. The loading capacity of XFPD for copper, cobalt and europium metal ions are determined to be 0.355 g, 0.48 g and 0.94 g and per gram of XFPD respectively. Studies on removal of various metal ions from SNLW by xanthate process showed that except cesium, all other metal ions are effectively removed. The removal of lanthanides (Ce, Gd, La, Nd, Sm) and actinides (Th & U) are greater than 99 % and removal of Co, Ni and Zn metal ions are greater than 90 %. Transition metal ions are precipitated as metal-xanthate complex whereas lanthanides get precipitated as metal-oxo-xanthate complexes. In case of actinides, removal is due to precipitation as hydroxides as well as adsorption on metal xanthate complexes. Though alkaline earth metal ions (Ba & Sr) do not form any precipitate with XFPD ligand, their percentage removal is observed to be about 50-70 %. This could be explained by considering their role as coagulating agent. Studies with radioactive liquid waste (RLW) show that percentage removal of radionuclides are observed to be in the following order; Zr ≈ Eu ≈ Co (> 99.8) > Ce (98.84) > Sb (83.31) > Ru (79.44) > Mn (54.29) > Cs (24.02). Hence, XFPD ligand possesses potential application in decontamination of radioactive wastes.

7.2 Scope for the future study

In the present study, potential application of dendrimer based chelating agents in removal of radionuclides from wastewater is explored. Though, PAMAM dendrimer based chelating agents shows selectivity in removal of actinides from aqueous solution, their synthesis involve number of steps that is time consuming and expensive. Hence, attention shall be provided for reducing the number of steps involved in dendrimer synthesis.

Preparation of PAMAM dendron-SDB chelating resin finds application in both pre-concentration and waste volume reduction. The present study demonstrates the selective removal of uranium and thorium from SNLW by batch experiment using PAMAM-SDB chelating resin. However, the practical applicability of this chelating resin has to be evaluated by column experiments. DGA-PAMAM-SDB is able to remove uranium and thorium metal ions from both aqueous and nitric acid medium. Studies can be expanded for removal of these metal ions and other actinides such as plutonium and americium from HLW. Dendrimer based chelating agents could find potential applications for treatment of various types of liquid wastes (HLW, ILW and LLW). Therefore, studies shall be extended to examine the radiation stability of these chelating agents.

Radionuclides such as ^{137}Cs and ^{90}Sr are the major radionuclides present in LLW arising from nuclear industry. Removal of both radionuclides demands modification in dendrimer terminal with suitable chelating groups. Removal of these metal ions may be attempted by combined precipitation method by using copper/zinc ferrocyanide, calcium phosphate along XFPD precipitating agent.

Application of indigenously developed PAMAM dendrimer chelating ligand, PAMAM dendron grafted - styrene divinyl benzene (PAMAM-SDB) chelating resin, Diglycolamic acid functionalized -PAMAM dendron- styrene divinyl benzene (DGA-PAMAM-SDB) chelating resin and Xanthate Functionalized Dendrimer (XFPD) for removal of various toxic organic and inorganic compounds in drinking water shall be explored.

Functionalized PAMAM dendrimers are bio-compatible and extensively studied as a drug delivery agent. Hence, studies shall be extended by using them as radionuclide decorporation agents.

References

REFERENCES

(1) U.S. Nuclear Regulatory Commission, NUREG-1350, 25 (2013).

(2) R.B. Grover, Curr. Sci. 78 (2000) 1191-1195.

(3) R.G. Bucher, India's Baseline Plan for Nuclear Energy Self-sufficiency, ANL/NE-09/03 (2009).

(4) Classification of Radioactive Waste, IAEA Safety Standard Series, GSG-1 (2009).

(5) Actinide Separation Chemistry in Nuclear Waste Streams and Materials, NEA/NSC/DOC (97)19 (1997).

(6) D.D. Sood, A.V.R. Reddy, N. Ramamoorthy, Fundamentals of Radiochemistry, IANCAS (2004).

(7) R.O. Abdel Rahman, Planning and Implementation of Radioactive Waste Management System Radioactive Waste (2012). http://www.intechopen.com/books/radioactive-waste/planning-and-implementation-of-radioactive-wastemanagement- system

(8) G.A. Burney, 238Pu Processing at the Savannah River Plant, DP-MS-83-63 (1983).

(9) I.W. Osborne-Lee, C.W. Alexander, Californium-252: Remarkable Versatile Radioisotope, ORNL/TM-12706 (1995).

(10) A.S. Paschoa, A.T. Filho, Appl. Radiat. Isot. 46 (1995) 707-715.

(11) P.A. Baisden, G.R. Choppin, Nuclear Waste Management and the Nuclear Fuel Cycle, Radiochemistry and Nuclear chemistry (2007).

(12) K. J. Sutherland, Radioactive Wastes, Origins, Classification and Management (2008).

(13) K. Raj, K.K. Prasad, N.K. Bansal, Nucl. Eng. Des. 236 (2006) 914-930.

(14) R.O. Abdel Rahman, H.A. Ibrahium, Y.T. Hung, Water 3 (2011) 551-565.

(15) S.L.Wee, C.T. Tye, S.Bhatia, Sep. Purif. Technol. 63 (2008) 500-516.

(16) D. Rana, T. Matsuura, M.A. Kassim, A.F. Ismail, Desalination 321 (2013) 77-92.

(17) G.H. Hsiue, L.S. Pung, M.L. Chu, M.C. Shieh. Desalination 71 (1989) 35-44.

(18) S. Prabhakar, S.T. Panicker, B.M. Misra, M.P.S. Ramani, Sep. Sci. Technol. 27 (1992) 349-359.

(19) S. Prabhakar, C. Balasubramaniyan, M.S. Hanra, B.M. Misra, S.B. Roy, A.M. Meghal, T.K. Mukherjee, Sep. Sci. Technol. 31 (1996) 533-544.

(20) L. Garrett, Reverse Osmosis Applications to Low Level Radioactive Wastes. WHC-SA-0993; CONF-9010202-1 (1990).

(21) T. Leiknes, J. Environ. Sci. 21 (2009) 8-12.

(22) A.W. Zularisam, A.F. Ismail, R. Salim, Desalination 194 (2006) 211-231.

(23) A.F. Reguillon, G. Lebuzit, D. Murat, J. Foos, C. Mansour, M. Draye, Water. Res. 42 (2008) 1160-1166.

(24) O. Raff, R.D. Wilken, Desalination 122 (1999) 147-150.

(25) K.H. Choo, D. J. Kwon, K.W. Lee, S.J. Choi, Environ. Sci. Technol. 36 (2002) 1330-1336.

(26) S. Szoke, G. Patzay, L. Weiser, Desalination 175 (2005) 179-185.

(27) R.K. Singhal, R. Karpe, K.P. Muthe, A.V.R. Reddy, J. Radioanal. Nucl. Chem. 280 (2009) 141-148.

(28) Y. Gao, J. Zhao, G. Zhang, D. Zhang, W. Cheng, G. Yuan, X. Liu, B. Ma, J. Zeng, P. Gu, Sep. Purif. Technol. 40 (2004) 183-189.

(29) S.V.S. Rao, B. Paul, K.B. Lal, S.V. Narasimhan, J. Ahmed, J. Radioanal. Nucl. Chem. 246 (2000) 413-418.

(30) J.G. Cao, P. Gu, J. Zhao, D. Zhang, Y. Deng, J. Radioanal. Nucl. Chem. 285 (2010) 539-546.

(31) C.P. Zhang, P. Gu, J. Zhao, D. Zhang, Y. Deng, J. Hazard. Mater. 167 (2009) 1057-1062.

(32) A.A. Svittsov, S.B. Khubetsov, K. Volchek, Water Sci. Technol. 64 (2011) 854-860.

(33) C.S. Kedari, S.S. Pandit, S.C. Tripathi, J. Membr. Sci. 341 (2009) 122-130.

(34) E. Curcio, E. Drioli, Sep. Purif. Rev. 34 (2005) 35-86.

(35) G.Z. Trznadel, M. Harasimowicz, A.G. Chmielewski, J. Memb. Sci. 163 (1999) 257-264.

(36) G. Z. Trznadel, J. Membr. Sci. 225 (2003) 25-39.

(37) G.Z. Trznadel, M. Khayet, Membrane in Nuclear Science and Technology: Membrane modification as a tool for performance improvement, Membrane Modification: Technology and Applications, CRC Press, Boca Raton, FL, ch.1 (2012) 1-19.

(38) N.N. Saucer, S.D. Ehler, B.L. Duran, J. Environ. Engine. 130 (2004) 585-588.

(39) G.Z. Trznadel, M. Harasimowicz, Desalination 144 (2002) 207-212.

(40) B.F. Smith, R.R. Gibson, G.D. Jarvinen, T.W. Robinson, N.C. Schroeder, N.D. Stalnaker J. Radioanal. Nucl. Chem 234 (1998) 225-229.

(41) A.P. Novikov, V.M. Shkinev, B.Y. Spivakov, B.F. Myasoedov, K.E. Geckeler, E. Bayer, Radiochim. Acta 46 (1989) 35-37.

(42) A. Novikov, S. Korpusov, R. Zhou, K.E. Geckeler, Chem. Tech. 45 (1993) 464.

(43) S.G. Korpusov, A.P. Novikov, V.M. Shkinev, Radiochem. 34 (1992) 1-135.

(44) K.E. Geckeler, K. Volchek, Environm. Sci. Technol. 30 (1996) 725-734.

(45) K.E. Geckeler, V.M. Shkinev, B.Y. Spivakov, Sep. Purif. Methods. 17 (1988) 105- 140.

(46) W. Bisset, H. Jacobs, N. Koshti, P. Stark, A. Gopalan, React. Funct. Polym. 55 (2003) 109-119.

(47) I.M. Villoslada, B.L. Rivas, J. Membr. Sci. 215 (2003) 195-202.

(48) U.C. Gerstmann, C. Lierse, K.E. Geckeler, Radiochim. Acta. 89 (2001) 377-385.

(49) L. Dambies, A. Jaworska, G.Z. Trznadel, B.J. Sartowska, J. Hazard. Mater. 178 (2010) 988-993.

(50) A.G. Chmielewski, M. Harasimowicz, Separ. Sci. Tech. 30 (1995) 1779-1789.

(51) V. Ramachandhran, S.K. Samanta, B.M. Misra, J. Radioanal. Nucl. Chem. Letter 237 (1998) 121-124.

(52) M.K. Sureshkumar, D. Das, M.B. Mallia, P.C. Gupta, J. Hazard. Mater. 184 (2010) 65-72.

(53) X. Sun, X. Huang, X.P. Liao, Bi Shi, J. Hazard. Mater. 179 (2010) 295-302.

(54) F.L. Fan , Z. Qin, J. Bai , W.D. Rong , F.Y. Fan , W. Tian , X.L. Wu, Y. Wang , L. Zhao, J. Environ. Radioactiv. 106 (2012) 40-46.

(55) A. Kilislioglu, B. Bilgin, Radiochim. Acta. 90 (2002) 155-160.

(56) Z.J. Guo, H.Y. Su, W.S. Wu, Radiochim. Acta. 97 (2009)133-140.

(57) S. Li , H. Bai, J. Wang , X. Jing , Q. Liu , M. Zhang , R. Chen, L. Liu , C. Jiao , Chem. Eng. J. 193–194 (2012) 372–380.

(58) M. Ghasemi, A.R. Keshtkar, R. Dabbagh, S.J. Safdari, J. Hazard. Mater. 189 (2011) 141-149.

(59) B. Gao, Y. Gao, Y. Li, Chem. Eng. J. 158 (2010) 542-549.

(60) A.M. Starvin, T.P. Rao, Talanta 63 (2004) 225-232.

(61) A.K. Singha Deb, P. Ilaiyaraja, D. Ponraju, B. Venkatraman, J. Radioanal. Nucl. Chem. 291 (2012) 877–883.

(62) N. Demirel, M. Merdivan, N. Pirinccioglu, C. Hamanci, Anal. Chim. Acta 485 (2003) 213-219.

(63) R. Pathak, G.N. Rao, Anal. Chim. Acta. 335 (1996) 283-290.

(64) V.K. Jain, A. Handa, S.S. Sait, P. Shrivastav, Y.K. Agrawal, Anal. Chim. Acta 429 (2001) 237-246.

(65) K. Dev, R. Pathak, G.N. Rao, Talanta 48 (1999) 579-584.

(66) T. Kimura, J. Radioanal. Nucl. Chem. 141 (1990) 295-306.

(67) K. Alcock, G.F. Best, E. Hesford, H.A.C. McKay. J. Inorg. Nucl. Chem. 6 (1958) 328-333.

(68) T. Kimura, J. Radioanal. Nucl. Chem. 141 (1990) 307-316.

(69) M. Yamaura, H.T. Matsuda, J. Radioanal. Nucl. Chem. 224 (1997) 83-87.

(70) J. N. Mathur, M. S. Murali, R. H. Iyer, A. Ramanujam, P.S. Dhami, V. Gopalakrishnan, L.P. Badheka, A. Banerji, Nucl. Technol. 109 (1995) 216-225.

(71) Y. Wei, M. Kumagai, Y. Takashima, G. Modolo, R. Odoj, Nucl. Technol. 132 (2000) 413-423.

(72) M. Yamaura, H.T. Matsuda, J. Radioanal. Nucl. Chem. 241(1999) 277-280.

(73) M.A. Maheswari, M.S. Subramanian, Talanta 65 (2005) 735-742.

(74) D. Prabhakaran, M.S. Subramanian, Anal. Bioanal. Chem. 379 (2004) 519-525.

(75) Ch.S.K. Raju, M.S. Subramanian, Talanta 67 (2005) 81-89.

(76) Ch.S.K. Raju, M.S. Subramanian, J. Hazard. Mater. 145 (2007) 315-322.

(77) S.A. Ansari, P.K. Mohapatra, V.K. Manchanda, J. Hazard. Mater. 161 (2009) 1323-1329.

(78) S.A. Ansari, P.K. Mohapatra, V.K. Manchanda, Talanta 73 (2007) 878-885.

(79) D. Prabhakaran, Subramanian. Talanta 65 (2005) 179-184.

(80) D. Prabhakaran, M.S. Subramanian, Anal. Lett. 36 (2003) 2277-2289.

(81) J.M. Gladis, T.P. Rao, Anal. Lett. 36 (2003) 2107-2121.

(82) R.S. Praveen, P. Metilda, S. Daniel, T. Prasada Rao, Talanta 67 (2005) 960-967.

(83) V.K. Jain, A. Handa, R. Pandya, P. Shrivastav, Y.K. Agrawal, React. Funct. Polym. 51 (2002) 101-110.

(84) E.P. Horwitz, M.L. Dietz, D.M. Nelson, J.J. Larosa, W.D. Fairman, Anal. Chim. Acta 28 (1990) 263-271.

(85) E.P. Horwitz, M.L. Dietz, R. Chiarizia, H. Diamond, S.L. Maxwell, M.R. Nelson. Anal. Chim. Acta 310 (1995) 63-78.

(86) E.P. Horwitz, R. Chiarizia, M. L. Dietz, H. Diamond, Anal. Chim. Acta 281 (1993) 361-372.

(87) G.J. Lumetta, D.W. Wester, J.R. Morrey, M.J. Wagner, Solvent Extr. Ion Exch. 11 (1993) 663-682.

(88) C. Pin, S. Joannon, J. Anal. At. Spectrom. 16 (2001) 739-743.

(89) L.L. Smith, J.S. Crain, J.S. Yaeger, E.P. Horwitz, H. Diamond, R. Chiarizia, J. Radioanal. Nucl. Chem. 194 (1995)151-156.

(90) V. Hecke, K.G. Modolo, J. Radioanal. Nucl. Chem. 261 (2004) 269-275.

(91) E.P. Horwitz, D.R. McAlister, A.H. Bond, R.E. Barrans Jr., Solvent Extr. Ion Exch. 23 (2005) 319-344.

(92) U.V. Trivedi, S.K. Menon, Y.K. Agrawal, React. Funct. Polym. 50 (2002) 205-216.

(93) J.P. Glatz, H. Bokelund, S. Valkiers, Inorg. Chim. Acta. 94 (1984) 129-131.

(94) Chemical Precipitation of Processes for the Treatment of Aqueous Radioactive Waste, IAEA TRS No. 337 (1992).

(95) Advances in Technologies for the Treatment of Low and Intermediate level Radioactive Liquid Wastes, IAEA TRS No. 370 (1994).

(96) K.W. Carley Macauly, R.G. Gutman, E.W. Hooper, J.A. Jenkins, A.D. Turner, P.F. Wace, P. Cnauvet, J.P. Gauchon, T. Dippel, Radioactive Waste: Advanced Management Methods for Medium Active Liquid Waste ISSN: 0275- 7273, 1 (1981).

(97) G.R. Choppin, J. Nucl. Radiochemic.sci. 6 (2005) 1-5.

(98) J. Wang, Y. Cheng, T. Xu, Recent Patents on Chemical engineering 1 (2008) 41-51.

(99) H.M. Scott, M. E. H. El-Sayed, Chem. Rev. 109 (2009) 3141-3157.

(100) D.A. Tomalia, H. Baker, J. Dewald, M. Hall, G. Kallos, S. Martin, J. Roeck, J. Ryder, P. Smith, Polymer Journal 17 (1985) 117-132.

(101) J.F. Kukowska-Latallo, A.U. Bielinska, J. Johnson, R. Spindler, D.A. Tomalia, J.R. Baker, Proc. Natl. Acad. Sci. U.S.A 93 (1996) 4897-4902.

(102) Elizabeth R. Gillies, Jean M.J. Fréchet, Drug Discov. Today 10 (2005) 35-43.

(103) S. E. Stiriba, H. F. P. Doz, R. Haag, Angew. Chem. 41 (2002) 1329-1334.

(104) A. R. Menjoge, R. M. Kannan, D. A. Tomalia, Drug Discov.Today 15 (2010) 171-185.

(105) Y.-M. Chung, H.-K. Rhee, Catalysis Letters. 85 (2003) 159-164.

(106) S.M. Cohen, S. Petoud, K. N Raymond, Chem. Eur. J. 7 (2001) 272-279.

(107) Diallo M.S: US2006021938 (2006).

(108) A. Rether, M. Schuster, React. Funct. Polym. 57 (2003) 13-21.

(109) M.S. Diallo, W. Arasho, J.H Johnson, W.A Goddard, Environ. Sci. Technol. 42 (2008) 1572-1579.

(110) M. Arkas, D.Tsiourvas, C.M. Paleos, Chem. Mater. 15 (2003) 2844-2847.

(111) Sonke Svenson, Eur. J. Pharm. Biopharm. 71 (2009) 445-462.

(112) J. Peterson, A. Ebber, V. Allikmaa, M. Lopp, Proc. Estonian Acad. Sci. Chem. 50 (2001) 153-166.

(113) S. Xiangyang, B. Xiangdong, T. R. Ganser, S. Hong, L.A. Myc, A. Desai, M.M.B. Holl, J.R. Baker, Analyst 131 (2006) 842-848.

(114) J. Peterson, V. Allikmaa, J. Subbi, T. Pehk, M. Lopp, European Polymer Journal 39, (2003) 33-42.

(115) S.B. Savvin, Talanta 8 (1961) 673-685.

(116) L. Meites, Handbook of Analytical Chemistry, Mcgraw-Hill Classic Handbook. Reissue, First edition, (1963).

(117) D.A. Tomalia, Aldrichchim. Acta 37 (2004) 39-57.

(118) X. Shi, W. Lesniak, M.T. Islam, M.C. Muniz, L.P. Balogh, J.R. Baker, Colloids Surf.

A: Physicochem.Eng. Aspects 272 (2006) 139-150.

(119) Y. Kim, A. M. Klutz, K. A. Jacobson, Bioconjug Chem. 19 (2008) 1660-1672.

(120) G.R. Killat, D.A. Tomalia, US Patent 4871779 (1989).

(121) M. J. Frechet and Donald A. Tomalia, Dendrimers and other Dendritic Polymers, ISBNs: 0-471-63850-1 (2001).

(122) H.P.S. Chauhan, A. Bakshi, J. Thermal Anal. Calorim. 105 (2011) 937-946.

(123) H.D. Yin, J. Zhai, Y.Y. Sun, D. Q. Wang, Polyhedron 27 (2008) 663-670.

(124) L Liu, J. Wu, X Li, Y Ling, Sep. Purif. Tech.103 (2013) 92-100.

(125) A.K. Pabby, Membr. Technol. 11 (2008) 9-13.

(126) N. Savage and M. S. Diallo, J. Nanopart. Res. 7 (2005) 331-342.

(127) M.S. Diallo, S. Christie, P. Swaminathan, L. Balogh, X. Shi, W. Um, C. Papelis, W.A. Goddard, J.H Johnson, Langmuir 20 (2004) 2640-2651.

(128) M.S. Diallo, S. Christie, P. Swaminathan, J.H. Johnson, W.A. Goddard, Environ. Sci. Technol. 39 (2005) 1366-1377.

(129) M.J. Kang, B.E. Han and P.S. Hahn, Environ. Eng. Res. 7 (2002) 149-157.

(130) A. Scierz, H. Zanker, Environ. Pollut. 157 (2009) 1088-1094.

(131) Y. Khazaei, H. Faghihian, M. Kamali, J. Radioanal. Nucl. Chem 289 (2011) 529-536.

(132) T.S. Anirudhan, S.R. Rejeena, Ind. Eng. Chem. Res. 50 (2011) 13288-13298.

(133) M. Giblin, B.D. Batts, D.J. Swaine, Geochim. Cosmochim. Acta. 45 (1981) 699-709.

(134) R. Neetika, Thermodynamics of complexation of actinides and lanthanides with ligand revalent to environmental and separation science, Ph.D Thesis (2011).

(135) G. Meinrath, J. Radioanal. Nucl. Chem. 224 (1997) 119-226.

(136) Y. Kato, G. Meinrath, T. Kimura and Z. Yoshida, Radiochimica Acta 64 (1994) 107-111.

(137) L. Zavodska, E. Kosorinova, L. Scerbakova, J. Lesny Environmental chemistry of

uranium. HV ISSN 1418-7108: HEJ Manuscript No: ENV-081221-A (2008) 1-18.

(138) R.G. Skirrow, S. Jaireth, D.L Huston, E.N. Bastrakov, A. Schofield, S.E van der Wielen, A.C Barnicoat, Uranium mineral systems: processes, exploration criteria and a new deposit framework. Geoscience Australia Record 20 (2009).

(139) G. Plancque, V. Moulin, P. Toulhoat, and C. Moulin, Anal. Chim. Acta 478 (2003) 11-22.

(140) R.N. Collins, A.S. Kinsela, Chemosphere 79 (2010) 763-771.

(141) V. Swali, N.J. Wells, G.J. Langley and M. Bradley, J. Org. Chem. 62 (1997) 4902-4903.

(142) R. Qu, Y. Niu, C. Sun, C. Ji, C. Wang, G. Cheng, Micropor. Mesopor. Mat. 97 (2006) 58-65.

(143) C.C. Chu, N. Ueno and T. Imae, Chem. Mater. 20 (2008) 2669-2676.

(144) H. Wang, L. Ma, K. Cao, J. Geng, J. Liu, Q. Song, X. Yang, S. Li, J. Hazard. Mater. 229-230 (2012) 321-330.

(145) S.H. Chien, W.R. Clayton, Soil Sci. Soc. Am. J. 44 (1980) 265-268.

(146) O. Hamdaoui, E. Naffre choax, J. Hazard. Mater. 147 (2007) 381-394.

(147) C.L. Chen, X.L. Li, X.L. Wang, Radiochim. Acta 95 (2007) 261-266.

(148) Y. Liu, L. Yuan, Y. Yuan, J. Lan, Z. Li, Y. Feng, Y. Zhao, Z. Chai, W. Shi, J. Radioanal. Nucl. Chem. 292 (2012) 803-810.

(149) K. Li, Z. Liu, T. Wen, L. Chen, Y. Dong, J. Radioanal. Nucl. Chem. 292 (2012) 269-276.

(150) D.L. Zhao, S.J. Feng, C.L. Chen, S.H. Chen, D. Xu, X.K. Wang, Appl. Clay. Sci. 41(2008) 17-23.

(151) S.A. Ansari, P. Pathak, P.K. Mohapatra, V.K. Manchanda, Chem. Rev. 112 (2012) 1751-1772.

(152) A.S. Suneesh, R. Kumaresan, S. Rajeswari, P.K. Nayak, K.V. Syamala, K.A. Venkatesan, M.P. Antony, P.R. Vasudeva Rao, Sep. Sci. Technol. 48 (2013) 1998-2006.

(153) K. Shimoji, H. Naganawa, J. Noro, F. Kubota, M. Goto, Anal. Sci. 23 (2007) 1427-1430.

(154) Robert W. Peters and Linda Shem, Separation of heavy metal: Removal from Industrial waste waters and contaminated, ANL-report 1993.

(155) M. Reyes, F. Patino, F.J. Tavera, R. Escudero, I. Rivera, M. Perez, J. Mex. Chem. Soc. 53 (2009) 15-22.

(156) Q. Chang, X. Hao, L. Duan, J. Hazard. Mater. 159 (2008) 548-553.

(157) S. Liang, X. Guo, N. Feng, Q. Tian, J. Hazard. Mater. 170 (2009) 425-429.

(158) W. Lu-Feng, D. Jia-Cai, M. Wen-Hua, Z. Ruo-Jie, S.Y. Pan, X. Xiao-Yun, J. Hazard. Mater.186 (2011) 1681-1686.

(159) P.D. Beer, A.R. Cowley, J.C. Jeffery, R.L. Paul, W.H. Wong, Polyhedron 22 (2003) 795-801.

(160) X.H. Jiang, W.G. Zhang, Y. Zhong, S.L. Wang, Molecules 7 (2002) 549-553.

(161) A. Singhal, P. Dutta, A.K. Tyagi, S.M. Mobin, P. Mathur, I. Lieberwirth, J. Organo. Chem. 692 (2007) 5285-5294.

(162) Y.K. Chang, P.H. Shih, L.C. Chiang, T.C. Chen, H.C. Lu, J.E. Chang Envcopper. Inform. Arch. 5 (2007) 684-689.

(163) L. Sha, G. Xue-yi, F. Ning-chuan, T.Qing-hua Trans. Nonferrous Met. Soc. China. 20 (2010) 187-191.

(164) P.L. Homagai, K.N. Ghimire, K. Inoue Biores. Technol. 101 (2010) 2067-2069.

(165) S.S. Garje, V.K. Jain, Coord. Chem. Rev. 236 (2003) 35-56.

(166) Y.K. Chang, J.E. Chang, T.T. Lin, Y.M. Hsu, J. Hazard. Mater. B94 (2002) 89-99.

(167) Fenglian Fu, Haiyan Zeng, Qinhong Cai, Rongliang Qiu, Jimmy Yu, Ya Xiong Chemosphere 69 (2007) 1783-1789.

(168) Q. Chang, G. wang, Chem. Eng. Sci. 62 (2007) 4636-4643.

(169) S. Tiwari, A. Bajpai, React. Funct. Polym. 64 (2005) 47-54.

(170) J. S. Casas, A. Castineiras, I. Haiduc, A. Sanchez, R. F. Semeniucb, J. Sordo, J. Mol. Struct. 656 (2003) 225-230.

(171) N. Davison, W. R. Mcwhinnie, A. Hooper, Clay and Clay minerals 39 (1991) 22-27.

(172) H.G. Liu, S. Park, K.Jang, W.S. Zhang, H.J. Seo, Y.I. Lee, Mater. Chem. Phys. 82 (2003) 84-92.

(173) F. Mercier, C. Alliot, L. Bion, N. Thromat, P. Toulhoat, J. Electron Spectrosc. Relat.Phenom.150 (2006) 21-26.